

Effect of a Short Term High Fat Diet on
Kidney Morphology and Function

by

Catherine Crinigan

A Thesis Presented in Partial Fulfillment
of the Requirements for the Degree
Master of Science

Approved November 2014 by the
Graduate Supervisory Committee:

Karen Sweazea, Chair
Carol Johnston
Sandra Mayol-Kreiser

ARIZONA STATE UNIVERSITY

May 2015

ABSTRACT

Long term high fat diets (HFD) are correlated with the development of diabetes and kidney disease. However, the impact of short term high fat intake on the etiology of kidney disease has not been well-studied. Therefore, this study examined the impact of a six week HFD (60% fat) on kidney structure and function in young male Sprague-Dawley rats. Previous studies have shown that these animals develop indices of diabetes compared to rats fed a standard rodent chow (5% fat) for six weeks. The hypothesis of this study is that six weeks of HFD will lead to early stages of kidney disease as evidenced by morphological and functional changes in the kidney. Alterations in morphology were determined by measuring structural changes in the kidneys (changes in mass, fatty acid infiltration, and structural damage). Alterations in kidney function were measured by analyzing urinary biomarkers of oxidative RNA/DNA damage, renal tissue lipid peroxidation, urinary markers of impaired kidney function (urinary protein, creatinine, and hydrogen peroxide (H_2O_2)), markers of inflammation (tumor necrosis factor alpha ($TNF\alpha$) and interleukin 6 (IL-6)), as well as cystatin C, a plasma biomarker of kidney function. The results of these studies determined that short term HFD intake is not sufficient to induce early stage kidney disease. Beyond increases in renal mass, there were no significant differences between the markers of renal structure and function in the HFD and standard rodent chow-fed rats.

ACKNOWLEDGMENTS

I would like to thank my committee members Dr. Johnston and Dr. Mayol-Kreiser for their support and feedback throughout my thesis project. I would like to express the deepest gratitude to my mentor Dr. Sweazea for her support, encouragement, and impressive ability to be answer every question I had. I have grown as a person and as a researcher thanks to her guidance; I could not have asked for a better mentor.

This thesis was accomplished with supporting funds from the Graduate Research Support Program and from Sigma Xi of Arizona State University.

Finally, I would like to thank Derek Juengel, my family, the students in Dr. Sweazea's laboratory, and my friends. I could not have completed this thesis without their unwavering love and patience and will be eternally grateful.

TABLE OF CONTENTS

	Page
LIST OF TABLES	vi
LIST OF FIGURES.....	vii
CHAPTER	
1 INTRODUCTION	1
Overview.....	1
Purpose of the Study.....	2
Research Aim and Hypothesis	2
Definition of Terms	3
Delimitations.....	5
Limitations.....	5
2 REVIEW OF LITERATURE	6
Introduction: Pre-diabetes, Obesity and Renal Disease.....	6
Visceral Adiposity	12
Obesity and High Fat Diets (HFD) on Renal Function	15
Markers of Morphological Changes from Renal Disease	17
Renin-Angiotenin-Aldosterone System (RAAS) Activation.....	19
Oxidative Stress and Renal Disease.....	20
Cystatin C	23
Hydrogen Peroxide.....	24
Biomarkers of Inflammation: TNF α and IL-6.....	25
Rats as a Model of Metabolic Syndrome	31

CHAPTER	Page
Conclusion	33
3 MATERIALS AND METHODS	36
Animal Models	36
Study Design.....	36
Laboratory Analysis	39
Variables	44
Statistical Analysis	46
4 RESULTS	47
Structural Changes.....	47
Biomarkers of Function.....	48
Inflammatory Markers.....	48
Oxidative Stress Markers	49
Cumulative Information	49
5 DISCUSSION	66
REFERENCES.....	72
APPENDIX	
A HIGH FAT DIET COMPONENTS – D12492	80
B STANDARD RODENT CHOW DIET COMPONENTS	84
C HEMATOXYLIN AND EOSIN STAIN PROTOCOL	86
D OIL RED O STAIN PROTOCOL.....	88
E CREATININE PROTOCOL	90
F CYSTATIN C PROTOCOL	95

	Page
G HYDROGEN PEROXIDE PROTOCOL	101
H IL-6 ANTIBODY	107
I TNF α ANTIBODY	110
J BETA-ACTIN ANTIBODY	113
K TNF α ELISA PROTOCOL.....	117
L TBARS PROTOCOL	124
M OXIDATIVE DNA/RNA PROTOCOL.....	127

LIST OF TABLES

Table	Page
1. Summary of Animal Subsets.....	38
2. Summary of Descriptive Statistics.....	65

LIST OF FIGURES

Figure	Page
1. Nephron Structure	8
2. Truncal Obesity, Insulin Resistance, and CKD	12
3. Overview of Major Adipokines and Their Role in CKD	14
4. Inflammatory Pathways That Induce Oxidative Stress in Obesity	21
5. Muscular IL-6 Secretion and Effects on Metabolism	28
6. Biological Role of Contraction Induced IL-6	29
7. Body Mass of Chow and HFD Rats	50
8. Epididymal Fat Pad Mass of Chow and HFD-Fed Rats	51
9. Waist Circumference of Chow and HFD Rats	52
10. Tail Lengths of Chow and HFD Animals	53
11. Renal Mass of Chow and HFD Rats	54
12. Hematoxylin and Eosin Staining of Kidneys for Morphology	55
13. Oil Red O Staining of Kidneys	56
14. Urine Protein:Creatinine Ratios of Chow-Fed and HFD-Fed Rats	57
15. Urine Creatinine in Chow-Fed and HFD-Fed Rats	58
16. Plasma Cystatin C in Chow and HFD Rats	59
17. Urinary Hydrogen Peroxide:Creatinine Ratio in Chow and HFD Rats	60
18. Renal Tissue TNF α Protein Expression in Chow and HFD Rats	61
19. Renal Tissue IL-6 Protein Expression in Chow and HFD Rats	62
20. Renal Tissue TBARS in Chow and HFD rats	63
21. Oxidative DNA Damage in the Plasma of Chow and HFD-Fed rats	64

CHAPTER 1

INTRODUCTION

Overview

According to the 2011 National Diabetes Fact Sheet, 25.8 million children and adults living in the United States are diabetic. Major complications of diabetes include cardiovascular disease and kidney disease [1]. The 2014 National Chronic Kidney Disease (CKD) Fact Sheet states that more than 33% of adults who have diabetes also have CKD, making diabetes the leading cause of renal failure in the United States [1,2]. However, the impact of poor nutrition on the development of kidney disease has been not been well-studied, despite the major contribution of poor dietary habits to the development of diabetes. According to a paper by Deji et al. (2009), the mechanisms leading to the development of CKD in subjects with metabolic syndrome are not well-understood [3]. Deji et al. (2009) fed 1.5 month old mice a high fat diet (HFD) (60% fat) for 12 weeks. The mice were found to develop hypertension and elevated plasma insulin and glucose concentrations. Moreover, the animals showed evidence of kidney disease as they had increased proteinuria, changes in kidney morphology, and renal steatosis as evidenced by microscopy [3]. Similarly, Altunkaynak et al. (2008) demonstrated that feeding adult female Sprague-Dawley rats a moderate fat diet (30% fat) for 12 weeks caused the animals to become overweight and to develop increased kidney mass with significant morphological changes indicative of renal disease [4]. Additionally, others have shown that feeding spontaneously hypertensive rats a high fat diet (58% fat) results in hypertension, lipid infiltration and increased markers of inflammation in the kidneys [5].

Studies of the effects of shorter term feeding protocols to mimic early onset pathological changes with high fat feeding are not evident in the literature. For this reason, the effects of feeding rats a HFD (60% fat) for six weeks will be studied to determine the effects of a shorter term feeding protocol on the morphology of the kidney and renal biomarkers of function. Prior studies by the Sweazea laboratory have shown that young (1.5 month old) male Sprague-Dawley rats fed a HFD (60% kcal from fat) for six weeks develop indices of diabetes and cardiovascular disease: increased body fat, high blood glucose concentrations, impaired glucose tolerance and hypertension [6,7]. Unpublished observations from the Sweazea laboratory also demonstrate that these animals develop hepatic steatosis. However, these prior studies did not examine kidney morphology or function. Examining the effect of the short term HFD on the kidney fills a gap in the literature and allows for a better understanding of the early pathological changes that occur from consuming a HFD even for a short period.

Purpose of Study

The purpose of the study was to examine the effects of a short term (six week) HFD (60% fat) on kidney morphology and function in male Sprague-Dawley rats. The HFD-fed rats were compared with rats fed a standard rodent chow diet containing 5% fat.

Research Aim and Hypothesis

Research Aim

The aim of this study was to examine the implications of a HFD consumed over a short period of time on kidney structure and function in rats.

Hypothesis

Six weeks of HFD (60% fat) will lead to early stages of renal disease in 1.5 month old Sprague-Dawley rats, as evidenced by morphological and functional changes in the kidney, compared to control group of rats on 5% fat diet.

Definition of Terms

8-hydroxy-2'-deoxyguanosine (8-OHdG): Biomarker of oxidative damage.

Advanced glycation end products: End productions produced by glycation reactions that are implicated in multiple disease states.

Chronic kidney disease (CKD): Gradual loss of renal function over time, during which the kidneys lose the ability to adequately filter blood and remove waste products.

Cystatin C: Biomarker of renal function.

Diabetic kidney disease (DKD): Kidney disease caused by uncontrolled diabetes.

Glomerular filtration rate (GFR): Estimation of the per minute filtration rate of glomeruli.

Glomerulosclerosis: The scarring or hardening of the glomeruli.

Glomerulomegaly: Abnormal glomerular enlargement.

High fat diet (HFD): Rodent diet consisting of 20% kcal from protein, 20% kcal from carbohydrates, and 60% kcal from fat (Appendix A).

Hydrogen Peroxide (H₂O₂): Biomarker of inflammation, oxidative stress, and early renal dysfunction.

Hyperglycemia: High blood glucose levels.

Interleukin 6 (IL-6): Biomarker of inflammation; pro-inflammatory cytokine.

Metabolic syndrome: A clustering of risk factors such as hypertension, hyperglycemia, high cholesterol and abdominal fat that increase the risk of developing cardiovascular disease.

Oxidative stress: An imbalance between antioxidant defenses and radical oxygen species.

Proteinuria: Urinary protein excretion, an indication of renal dysfunction.

Renin-angiotensin-aldosterone system (RAAS): Hormonal system that regulates fluid and blood pressure balance.

Reactive Oxygen Species (ROS): Oxygen molecules containing an unpaired electron that are able to oxidize nucleic acids, lipids and proteins, causing a chain reaction of damage to tissues and oxidative stress.

Renal failure: Medical condition in which the kidneys are not able to adequately filter blood and remove waste products; can be chronic or acute in nature.

Short term diet: Six weeks of feeding.

Standard rodent chow: Rodent chow consisting of: 18.9% kcal from protein, 57.33% kcal from carbohydrates, and 5% fat (Appendix B).

Tubular reabsorption: The flow of glomerular fluid from the proximal convoluted tubule into the peritubular capillaries, which allows for specific substrates to be reabsorbed into the blood.

Tubular secretion: Transfer of substrates from the blood into the glomerular fluid for excretion.

Tumor necrosis factor alpha (TNF α): Biomarker of inflammation; pro-inflammatory cytokine.

Delimitations

The rats used in the study are male 1.5 month old Sprague-Dawley rats. The effects of a diet consisting of 60% fat for six weeks on renal morphology and structure were examined.

Limitations

Limitations include the assumption that metabolic syndrome caused by HFD damaged renal function to the point of significant structural damage and altered functional biomarkers. The samples that were used for this study (plasma, urine and kidneys) were collected in prior studies and stored at -80°C for up to three years prior to analysis.

CHAPTER 2

REVIEW OF LITERATURE

Introduction: Pre-Diabetes, Obesity and Renal Disease

According to the 2011 National Diabetes Fact Sheet, 25.8 million children and adults living in the United States are diabetic; major complications of which include cardiovascular disease and kidney disease [1]. Furthermore, the 2014 National Chronic Kidney Disease (CKD) Fact Sheet states that one in three adults over the age of 20 who have diabetes also have CKD, making diabetes the leading cause of renal failure in the United States [1,2]. The average annual growth of incidences of diabetes worldwide is nearly double the growth of the global population [8]. Research has shown a clear connection between poorly controlled diabetes and renal dysfunction.

Fully functioning kidneys filter 150 quarts of blood and produce two quarts of urine daily. The basic filtering unit of the kidney is the nephron and roughly one million are contained in a human kidney. Each nephron filters a small amount of blood and consists of a renal corpuscle and renal tubule. The renal corpuscle is made up of the Bowman's capsule, which is an epithelial cup that surrounds the glomerulus. The glomerulus contains capillaries that join the afferent arteriole (which brings blood into the glomerulus) and the efferent arteriole (which removes blood from the glomerulus). The smaller diameter of the efferent arteriole in comparison to the afferent arteriole increases the blood pressure within the glomerulus. The Bowman's capsule has two walls; the inner wall adheres to the outer wall of the glomerulus and forms a filtration membrane. The increased blood pressure created by the differing diameters of the two arterioles facilitates the passage of excess fluid and solutes from the glomerulus into the Bowman's

capsule. This process along with the presence of specialized cells prevents erythrocytes, proteins, and other large molecules from entering the urine. Glomerular filtration rate (GFR) is an estimation of the per minute filtration speed of the glomeruli and is considered the gold standard marker of kidney function [9].

The glomerular filtrate then travels from the Bowman's capsule to the proximal convoluted tubule where tubular reabsorption and tubular secretion occur. At this point, water and solutes (i.e. sodium, chloride, bicarbonate, potassium, glucose, calcium, etc) are removed from the filtrate and reabsorbed by the blood while other solutes, such as uric acid, are secreted into the tubular fluid. The fluid then continues into the Loop of Henle, through which it enters the renal medulla and subsequently returns to the renal cortex. As the glomerular fluid enters the distal convoluted tubule, additional sodium, calcium, bicarbonate, hydrogen, chloride and water are reabsorbed into the blood while potassium, urea, hydrogen ions and wastes are secreted into the tubular fluid. Finally, any excess water still in the tubular fluid is reabsorbed into the blood and the final tubular product, urine, is excreted via the bladder [10]. Urine creatinine clearance is a useful marker of the glomerular filtration rate as it is negligibly reabsorbed or secreted after filtration. Figure 1 illustrates the structure of the nephron.

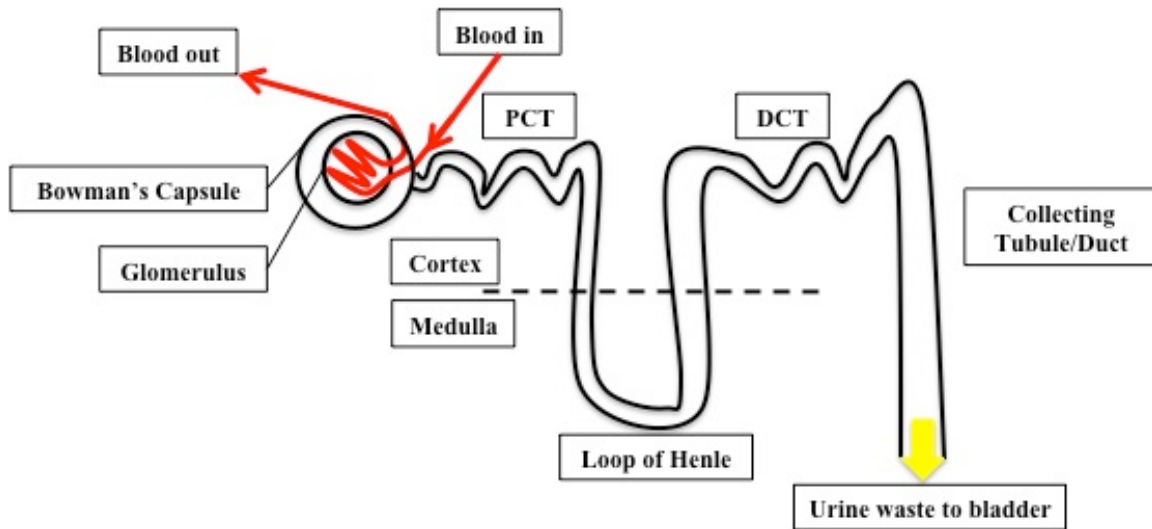


Figure 1 – Nephron structure.

Blood is initially filtered through the glomerulus. Excess fluids and solutes pass through the Bowman's capsule and into the proximal convoluted tubule (PCT) where the majority of reabsorption occurs. From there the filtrate enters the loop of Henle and then the distal convoluted tubule (DCT) where the majority of secretion occurs. The urine then enters the collecting duct where urine is either concentrated to conserve water or diluted to rid the body of excess water. The urine then collects in the bladder and can be excreted from the body through the ureters and urethra.

Increased plasma glucose concentrations (i.e. hyperglycemia), a risk factor of both CKD and cardiovascular disease, have been shown to damage the filtering ability of the kidneys. Hyperglycemia may initiate hypertrophy and proliferation of the mesangial cells, which are responsible for maintaining the structure of glomerular capillaries and modulating glomerular filtration. Additionally, hyperglycemia is positively associated with glomerular basement membrane thickening and increases in mesangial matrix production and mesangial cell apoptosis [11,12]. Three mechanisms believed to explain the harmful effects of hyperglycemia on glomerular filtration are: the production of advanced glycation end products via the glycosylation of free amino acids; the activation of protein kinase C, which instigates the secretion of vasodilatory prostanoids and

glomerular hyperfiltration; and the acceleration of the aldose reductase pathway [13-15]. The stressing of glomerular filtration eventually contributes to the leakage of proteins such as albumin, which are then excreted in the urine. The presence of albumin in the urine is called albuminuria and proteinuria is defined as an excess of proteins found in urine. Therefore, albuminuria and proteinuria are common markers used to assess renal function [8,16,17]. Fully functioning kidneys excrete little to no protein and the presence of urinary protein indicates a decline in renal filtering abilities and the pathogenesis of CKD.

Microalbuminuria and macroalbuminuria are used as assessment tools in the diagnosis of renal dysfunction. Emerging research has shown the humans can progress to end-stage renal disease without exhibiting signs of microalbuminuria or macroalbuminuria [8]. Albumin is a protein; however the specificity of testing for only one protein can be limiting. Testing for the excretion of total proteins in the urine, proteinuria, is therefore also a common practice and a useful marker of renal function [5,16,17]. Multiple studies have found a stronger association between proteinuria and renal disease outcomes than any other tested factors [17]. Proteinuria is used not only as a marker of kidney damage, but also as a risk factor for disease progression, a hypothesized marker of endothelial dysfunction, and a surrogate outcome for the progression of kidney disease [17]. In fact, clinical studies on humans have identified proteinuria as the first clinical symptom of kidney damage that can appear years before the GFR declines [18]. Cellular damage caused injury, pathogens, or allergies promotes a bodily defense known as inflammation. Inflammation may be the initial indication of renal damage; however, it cannot be examined in human kidneys *in vivo*, whereas it may be readily examined in

animal models. Chronic inflammation is a prolonged, maladapted response that pathologically consists of both the repair and destruction of tissues [19].

Kidney failure is the final stage of CKD. In humans, CKD is diagnosed in individuals who demonstrate renal damage through albuminuria or decreased renal function (GFR of less than 60 mL/min) for at least three months. Renal failure is categorized as a GFR of less than 15 mL/min. As the incidence of diabetes continues to increase throughout the world, rates of albuminuria and diabetic kidney disease (DKD) are also increasing [8]. However, signs of renal impairment, such as tubular atrophy and interstitial fibrosis, can be found even when an individual is in the pre-diabetic state of metabolic syndrome [20].

Metabolic syndrome is diagnosed in individuals with at least three of the following risk factors: hyperglycemia, hypertension, high levels of plasma triglycerides, high cholesterol, low plasma HDL concentrations, atherosclerosis, non-alcoholic fatty liver disease, abdominal obesity, and endothelial dysfunction [21]. These characteristics of metabolic syndrome also increase the risk of developing cardiovascular disease and type II diabetes, which then increase the risk of renal dysfunction and subsequent failure. According to a study by Deji et al. (2009), the mechanisms leading to the development of CKD in subjects with metabolic syndrome are not well-understood [3]. A multitude of mechanisms have been proposed as being both causes and symptoms of renal damage: inappropriate activation of the intrarenal renin-angiotensin-aldosterone system (RAAS), hyperglycemia, decreased GFR, visceral adiposity, hypertension, impaired endothelial function, insulin resistance, proteinuria, oxidative stress, and advanced glycation end

products [9,17,18,22,23]. Many of these changes to normal bodily functions are also risk factors for cardiovascular disease and diabetes.

Oxidative stress is defined as a systemic imbalance between radical oxygen species (ROS) and the antioxidants that prevent the ROS from causing cellular damage. Chronic inflammation and oxidative stress are understood to exacerbate each other, leading to systemic damage [19].

Hyperglycemia also initiates multiple pathways that lead to the accumulation of extracellular matrix proteins and fibrosis. As fibrosis severity increases, so does nephron necrosis, resulting in interstitial scarring that impairs renal function [24]. Being able to detect signs of renal disease before DKD, CKD, or diabetic nephropathies develop fully is vital to the future health of individuals worldwide.

Rats are often used as a model of obesity and metabolic syndrome due to similarities and homology between the genomes of rats and humans; rats have also been shown to readily gain weight when fed a HFD. Prior studies completed in the Sweazea laboratory and by others have shown that a model of metabolic syndrome can be developed by feeding rats a HFD for as few as six weeks [7,25]. Figure 2, adapted from Chalmers, Kaskel, and Bambgola (2006), illustrates the relationship between metabolic syndrome, insulin resistance, and CKD [26].

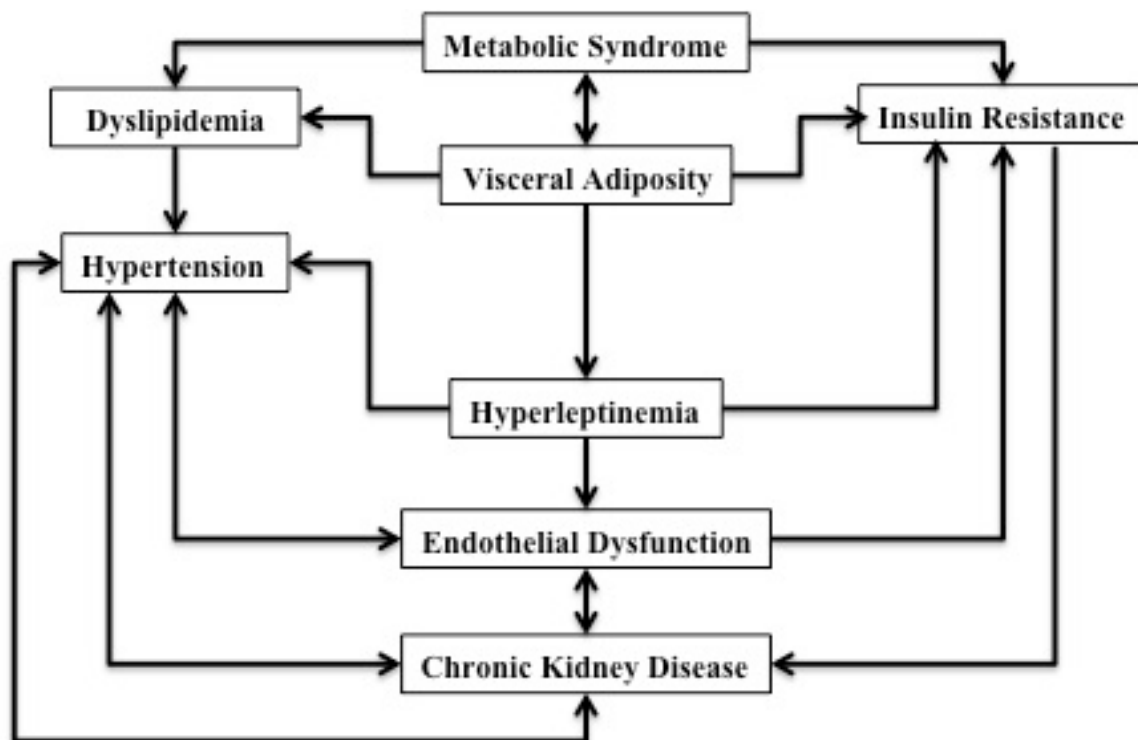


Figure 2 – Metabolic syndrome, insulin resistance, and CKD.

The increased visceral adipose tissue associated with metabolic syndrome promotes a variety of pathologies including insulin resistance, dyslipidemia, and endothelial dysfunction, which contribute to hypertension and chronic kidney disease [26].

Visceral Adiposity

Adipose tissue is a highly active endocrine organ. Adipose cells secrete adipokines, which can act as both pro-inflammatory and anti-inflammatory factors. Visceral adipose cells are more resistant to leptin, more sensitive to lipolytic hormones, contain a higher triglyceride content than peripheral fat stores and are more lipolytically active than subcutaneous fat [27]. The lipolysis of triglycerides in visceral adipose tissue releases free fatty acids into the portal vein where they are then transported to the liver [28]. Insulin acts to suppress glucose production in two ways: via direct action upon the liver or indirectly through free fatty acids. Hyperinsulinemia, high blood insulin

concentrations, normally represses lipolysis and the release of free fatty acids; however, visceral adiposity has shown resistance to the antilipolytic effects of insulin. Therefore, when excess free fatty acids reach the liver through the portal circulation, they interfere with the mechanism by which insulin normally inhibits hepatic glucose output [29]. An excess of free fatty acids from obesity and increased visceral fat stores negatively impacts insulin-glucose balance within the body.

Upregulation of fatty acid synthase with CKD increases triglyceride synthesis, which, due to impaired triglyceride transportation, leads to fat accumulation in the liver, (i.e. hepatic steatosis or non-alcoholic fatty liver disease), a co-morbidity of diabetes. Similarly, renal steatosis has also been associated with high levels of visceral adiposity [30]. Steatosis of these organs and the adipokines released by the infiltrating macrophages can lead to liver and renal dysfunction. Leptin, resistin, visfatin, tumor necrosis factor alpha (TNF α), interleukin 6 (IL-6), angiotensin II, and adiponectin are common adipokines released by adipose tissue. In a healthy state, adiponectin (an anti-inflammatory and anti-proteinuric adipokine) expression is balanced with TNF α and angiotensin II (pro-inflammatory adipokines) levels [18,27,31]. The increased macrophage infiltration of adipose cells can disrupt this balance, leading to increased secretion of pro-inflammatory factors (i.e. TNF α and angiotensin II) and the promotion of inflammation, oxidative stress, endothelial dysfunction, and ultimately CKD [32,33].

Chronic inflammation is often associated with multiple disease states and has been hypothesized to contribute to both morbidity and mortality in CKD patients [33]. Studies on animals fed HFDs have found lipid accumulation in the glomeruli and proximal tubules of kidneys along with increased expression of inflammatory markers,

particularly $\text{TNF}\alpha$ and IL-6 [3,27]. Figure 3, adapted from Ruster and Wolf (2013), exemplifies this relationship.

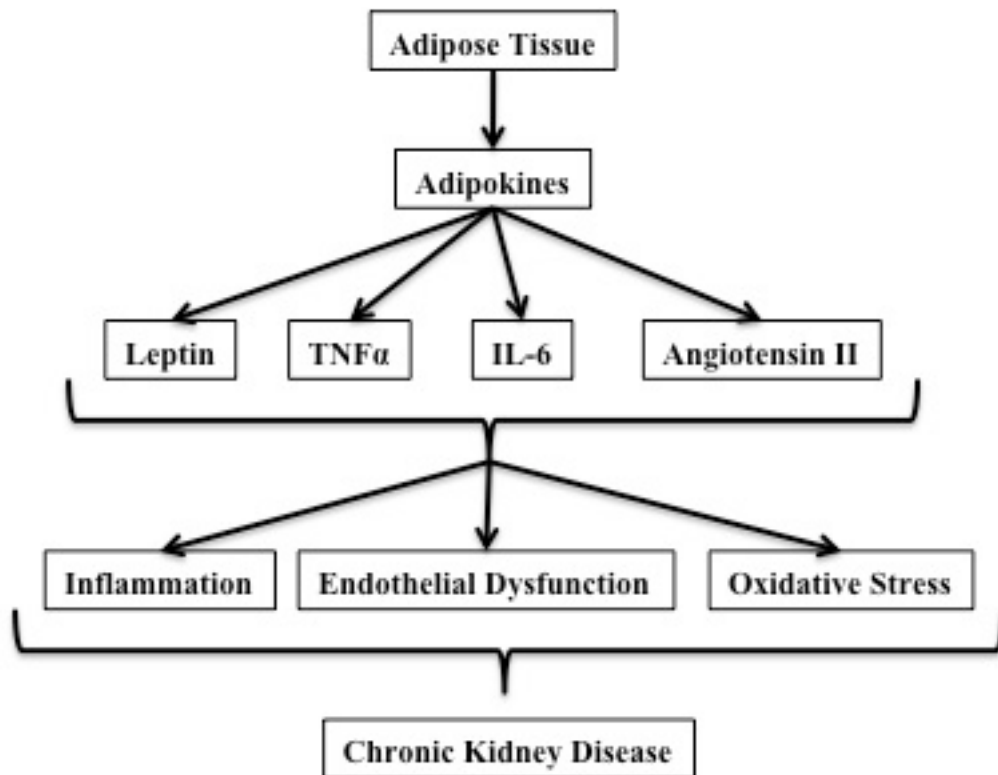


Figure 3 – Relationship between major adipokines and CKD.

Adipokines secreted by adipose tissue include leptin, tumor necrosis factor alpha ($\text{TNF}\alpha$), interleukin-6 (IL-6), and angiotensin II, all of which can initiate and promote inflammation, endothelial dysfunction and oxidative stress. These factors promote chronic kidney disease. [27].

Foster et al. (2011) conducted a study on participants from the Framingham Heart Study (n = 2923) that examined the relationship between renal fat accumulation, hypertension and CKD. Participants were assessed for renal fat by computed tomography. Their results indicated positive associations between fatty kidney and hypertension and between fatty kidney and CKD. After adjusting for visceral adipose tissue, no association was found between fat infiltration in the kidney and diabetes. These

data indicate that there may be an independent association between hypertension, renal fat accumulation, and CKD [23]. Ectopic fat accumulation in the kidneys may constrict the renal vein and artery and thereby cause hypertension. Both human and animal studies have shown renal fat accumulation caused by HFDs [34-36].

Sweazea et al. (2010) have demonstrated that a HFD (60% fat) for six weeks created a model of metabolic syndrome in young male Sprague-Dawley rats. The HFD rats show signs of significant visceral adiposity as well as increased plasma TNF α and lipid peroxidation. As discussed, other studies have shown that increased visceral adiposity, endothelial dysfunction, hypertension, inflammation and oxidative stress (characteristics shared by these animals) increase blood pressure in the kidneys and promote renal damage, although this has yet to be examined in the six week HFD rat model.

Obesity and High Fat Diets (HFDs) on Renal Function

Many studies that have shown that HFDs induce obesity in rats [4,23,30,37]. Altunkaynak et al. (2008) found that feeding adult female Sprague-Dawley rats a HFD (30% fat) for twelve weeks caused the rats to become overweight [4]. These rats then developed increased kidney mass, along with significant morphological changes indicative of renal disease. Others have shown that feeding spontaneously hypertensive rats a HFD (58% fat) results in hypertension, lipid infiltration and increased markers of inflammation in the kidneys [5].

Aside from the damaging effects of hyperglycemia, endothelial dysfunction, and hypertension associated with metabolic syndrome, obesity itself has been shown to

increase the risk of developing CKD 3-4-fold [38]. HFDs can disrupt the balance between lipogenesis and lipolysis in the kidney, thereby leading to increased renal lipid accumulation and lipid peroxidation [23,37]. The fat accumulation caused by the HFD can then lead to endothelial dysfunction and over-expression of inflammatory factors, fibrosis, hypertension, and oxidative stress [27].

Deji et al. (2009) conducted a study in which 1.5 month old mice were fed a HFD (60% fat) for twelve weeks. The mice developed hypertension, elevated plasma insulin and glucose concentrations, proteinuria, changes in kidney morphology, and renal steatosis as evidenced by microscopy [3]. The mice had increased renal mRNA expression of renin, ACE, and angiotensin, which may lead to dysfunction of the RAAS. Additionally, Deji et al. (2009) discovered evidence that obesity induced by the HFD, as opposed to the consumption of a HFD itself, may cause a majority of the renal damage. This evidence is interesting, as being overweight has been correlated with increased risk of developing CKD; perhaps it is the increased adiposity along with the associated increase in adipokines specifically, as opposed to the weight itself, that increases CKD risk [38].

Kume et al. (2007) found that mice fed a HFD (45% fat) developed insulin resistance at four weeks, renal steatosis at eight weeks, and renal injury at sixteen weeks of diet consumption [37]. Unsurprisingly, the damage to the kidneys increased with continued stress and insulin resistance. It is important to note that changes to normal renal function began with insulin resistance after only four weeks of the HFD.

Borst and Conover (2005) fed young Wistar rats a diet of 50% total calories from fat for 39 days and found that the rats doubled their visceral and subcutaneous fat content

without significantly altering their body weight, muscle mass, or serum free fatty acid content [32]. They further found a correlation between insulin resistance in the HFD rats and increased expression of the pro-inflammatory cytokine TNF α in muscle, liver and fat tissues. Again, these findings suggest that increased adipose tissue may be of more importance in creating a pro-inflammatory environment than body mass itself.

Stemmer et al. (2012) compared lean chow-fed Wistar rats with HFD-fed rats that were classified as either sensitive or partially resistant to diet induced obesity after eleven months of the HFD (40% fat). A positive correlation was established between levels of adiposity and the severity of renal damage. Their results indicate that lipotoxicity is not a strong contributor to renal dysfunction as they found plasma triglyceride and free fatty acid as well as renal triglyceride levels did not differ significantly between the treatment and control groups [30]. Rather, they discovered hyperleptinemia, monocyte infiltration, augmented expression of inflammatory cytokines in adipocytes (particularly IL-6 and TNF α), and increased expression of pathways leading to renal carcinogenesis [30].

Markers of Morphological Changes from Renal Disease

High fat intake has been shown in multiple studies to induce an overweight/obese, pre-diabetic state leading to impaired renal function in animal models. Morphological changes found in studies include glomerular lesions, accumulation of extracellular matrix proteins, dilation of glomerular capillaries, enlarged lumens in the tubules and Bowman's space, mononuclear cell infiltration in the renal cortex, nephron degradation and basal membrane thickening of the glomeruli and tubules [3,4]. Specifically in cases of obesity-induced kidney damage, both focal and segmental

glomerulosclerosis (the scarring or hardening of the glomeruli) and glomerulomegaly (abnormal glomerular enlargement) are found [18]. Additionally, the necrosis of renal interstitial cells and tubules, shortened epithelium of the tubules, and increased renal mass have been observed as markers of damage [3,4].

Increased adipose and macrophage infiltration and renal hypertrophy are likely responsible for the increased mass of damaged kidneys [4,23,30]. The kidneys of diabetic Sprague-Dawley rats have been found to double in size only four weeks after induced diabetes [39]. The increases in renal volumes of HFD-consuming rats have been attributed to inflammation, vasodilatation and connective tissue enlargement initiated by the HFD. Edema caused by mononuclear cell infiltrations of the renal tubules may also be responsible for volumetric increases in kidney mass [4]. The infiltration of adipocytes promotes the secretion of proinflammatory cytokines such as $TNF\alpha$, which can also be measured as a marker of renal damage [40].

Altunkaynak et al. (2008) used stereology to calculate the volume of the cortex, medulla, glomeruli, and tubules of adult female Sprague-Dawley rats fed a HFD (30% fat) for 12 weeks. This study was unique in that it used the relatively new technology of stereology in order to quantify renal morphology in terms of kidney volume, surface area, cortex volume, number and length of glomeruli, and surface area and number of glomerular capillaries [4]. These stereological techniques indicated that morphological damage was caused by the HFD. They also found inflammation, increased connective tissue within the kidneys, dilatation of glomerular capillaries, and tubular defects causing renal deformities [4].

Renin-Angiotensin-Aldosterone System (RAAS) Activation

Renal dysfunction may be related to the abnormal regulation of RAAS, components of which can be found throughout the kidney [3,5,17,18,21,27]. Angiotensin II, however, is found only in limited kidney regions and is responsible for increasing blood pressure through vasoconstriction. Intrarenal RAAS is regulated by mechanisms distinct from those that control circulatory RAAS, as indicated by the higher concentrations of RAAS components and angiotensin II in the kidneys compared to plasma concentrations. HFD has been shown to significantly increase the mRNA expression of renin, ACE, and angiotensin in the kidneys of mice, which activates the RAAS system, and can be a mechanism for both renal injury and hypertension [3].

Additionally, hyperglycemia and overt levels of albuminuria have been shown to upregulate intrarenal RAAS; these factors may be an aspect of the pathogenesis of both hypertension and renal dysfunction [5]. Angiotensin II in particular has been related to obesity and can be linked to hypertension, dyslipidemia, and insulin resistance, which together, cause obesity-related kidney disease [22]. Angiotensin II is the final effector of the RAAS and can act as both a profibrogenic and pro-inflammatory cytokine; therefore, inappropriate levels of angiotensin II can cause renal damage [22,27].

Prior studies in the Sweazea laboratory have shown that six weeks of HFD leads to impaired endothelium-mediated vasodilation [6]. Since upregulation of the RAAS may contribute to endothelial dysfunction it is reasonable to suspect that the rats fed a HFD may have evidence of renal disease [41].

Oxidative Stress and Renal Disease

Oxidative stress is caused by an imbalance between ROS and the antioxidants that scavenge them. ROS, which include singlet oxygen, hydroxyl radicals, superoxide anion radicals, and hydrogen peroxides, are able to oxidize nucleic acids, lipids and proteins causing a chain reaction of damage [42,43]. Normal intracellular metabolic processes, such as cellular respiration, constantly produce ROS as by-products [42,44]. Under normal physiological conditions, a balance between ROS and cellular defense mechanisms (such as antioxidants) maintains homeostasis and prevents oxidative damage. External factors, such as smoking, radiation, and alcohol intake, as well as diseases such as diabetes, metabolic syndrome, and hypertension can lead to overproduction of ROS or underproduction of antioxidants, ultimately resulting in damage to cells, tissues, and even DNA. Kidneys are especially susceptible to oxidative stress due to a high concentration of long-chain polyunsaturated fatty acids, which easily undergo lipid peroxidation when exposed to ROS [43].

Oxidative stress and overproduction of ROS are initiated through multiple pathways that can be related to the model of increased adiposity created in the Sweazea laboratory. Obesity-initiated sources of oxidative stress include: hyperglycemia, tissue lipid accumulation, insufficient antioxidants, overproduction of ROS and chronic inflammation [45]. Adiposity and pro-inflammatory markers are specifically associated with oxidative stress across disease states [27]. HFD-induced obesity increases oxidative stress in hepatic, cardiac, and renal tissues by decreasing the enzyme activities of antioxidants such as glutathione, as shown by increased lipid peroxidation [45]. Renal injury has also been increased by macrophage infiltration and the release of cytokines

such as TNF α [43]. Oxidative stress is a key regulator in the pathway of hypertension to renal failure. The genetic damage caused by oxidative stress has been proposed by Stayanova et al. (2010) as a mechanism of renal damage in human patients with chronic renal failure [46]. Advanced glycation end products also increase during end-stage renal failure and induce oxidative stress. Additionally, hyperglycemia produces ketoimine and ketoamine adducts during glycooxidation and glycosylation, which then produce ROS [47]. Figure 4 below was adapted from Vincent and Taylor (2006) and illustrates the relationships between obesity and oxidative stress [48].

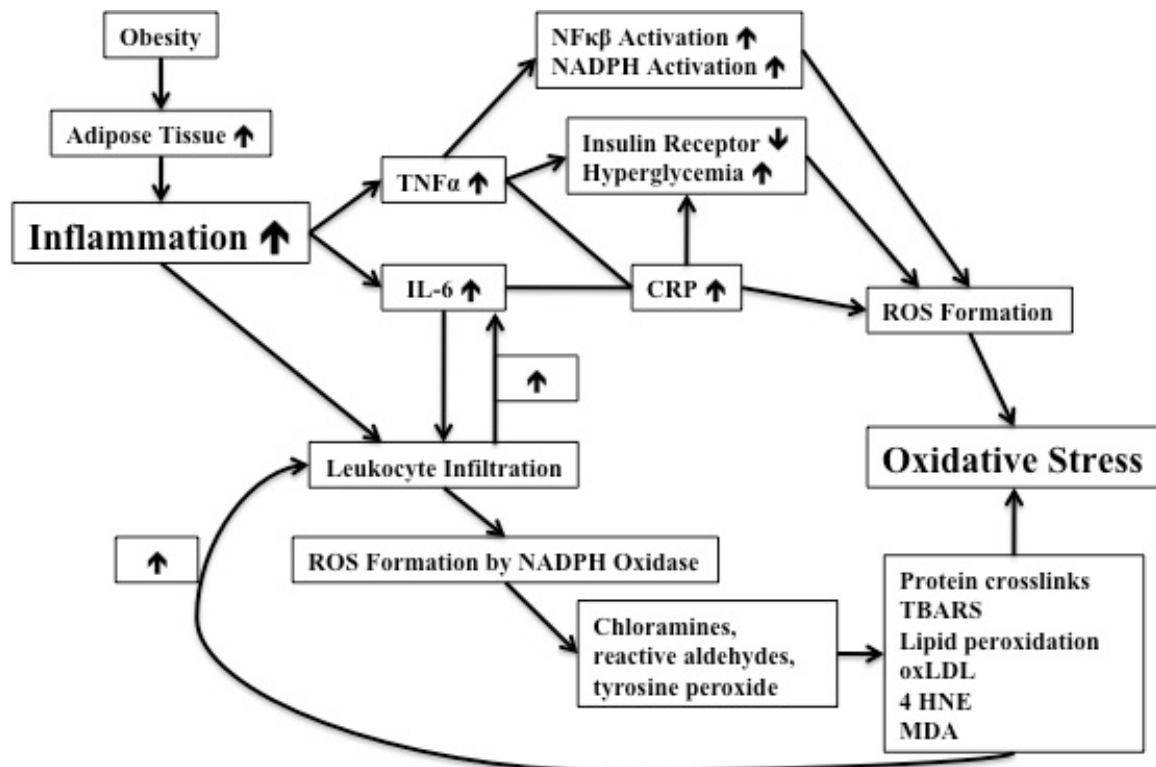


Figure 4 - Inflammatory pathways that induce oxidative stress during obesity.

Adipose tissue associated with obesity induces inflammation, which increases adipokine concentrations and the infiltration of leukocytes leading to reactive oxygen species (ROS) formation. The product of inflammation is ultimately oxidative damage and ROS formation. TNF α = tumor necrosis factor alpha; IL-6 = interleukin-6; CRP = C-reactive protein; oxLDL = oxidized low-density lipoprotein; 4 HNE = 4-hydroxynonenal; MDA = malondialdehyde [48].

Markers of Oxidative Stress

ROS production cannot be directly measured in organs *in vivo* and surrogate markers are therefore used to assess oxidative stress. 8-hydroxy-2'-deoxyguanosine (8-OHdG) is a sensitive biomarker of oxidative stress in tissue and body fluids and is a major product of damage caused by oxidative stress to DNA. 8-OHdG is produced by enzymatic cleavage of the guanine base, the base most prone to oxidation. Oxidative stress damages both DNA and RNA and other oxidized guanine species, in addition to 8-OHdG, which are excreted in the urine. Other species commonly excreted include 8-oxo-guanine, 8-hydroxyguanine, 8-oxo-deoxyguanosine, 8-hydroxyguanosine, and 8-oxo-deoxyguanosine. Emerging research demonstrates the importance of measuring multiple markers of oxidative stress in body fluids in order to gain a full understanding of oxidative damage. Urinary excretion of oxidative stress markers presents a measure of oxidative stress throughout the body while plasma oxidative stress measures can indicate the functional status of the kidneys themselves [42].

Lipid peroxidation is also used as a measure of oxidative stress in tissues. Hyperglycemia increases the bioavailability of free fatty acids, which are then prone to lipid peroxidation. TNF α generates ROS in tissues, which also increases lipid peroxidation, particularly with the polyunsaturated fatty acids in the kidney. Lipid peroxidation forms malondialdehyde as an end product, which can then be detected via a thiobarbituric acid reactive substance (TBARS) assay, a marker of oxidative damage to specific organ tissues that is often examined. Plasma 8-OHdG in male rats has been found to have a strong positive correlation with plasma malondialdehyde, indicating the connection between DNA oxidation and lipid peroxidation [49,50]. Examining both renal

lipid peroxidation and plasma oxidative stress markers will provide a complete analysis of oxidative stress in the metabolic-syndrome-like phenotype created by the Sweazea laboratory via HFD. Prior studies using the Sweazea laboratory rats used in this study have shown significant elevations in plasma TBARS and TNF α following high fat intake [6,7].

Cystatin C

Cystatin C is an amino acid inhibitor of cysteine proteinase and is found in serum, urine, synovial fluid, seminal fluid, cerebrospinal fluid, and in all cells of the body [51]. Serum cystatin C is filtered through the glomerulus freely and subsequently reabsorbed and catabolized by the proximal tubular cells without returning to the blood [52]. Urinary changes in cystatin C can be used as markers of acute renal injury, although not often used in CKD assessment [53]. Serum creatinine levels are often assessed as a marker of renal function, however, more recent studies indicate that serum or plasma cystatin C is a stronger, and more consistent, indicator of GFR and renal function [51,54-58]. While serum creatinine levels can be affected by sex, age, diet, muscle mass, and body mass, cystatin C levels are independent of gender, muscle mass, and malignancy [58]. A meta-analysis of 54 studies found that serum cystatin C is superior to serum creatinine levels with respect to GFR estimation [56]. Moreover, plasma cystatin C has been shown to detect early signs of renal dysfunction and is more sensitive in the detection of renal function decline [8,51,54,57]. Cystatin C increases during renal disease, even during the early stages, and is therefore a highly used biomarker in the early detection of kidney disease.

Hydrogen Peroxide

Hydrogen peroxide (H_2O_2) is used as a marker of both inflammation and oxidative stress and is extremely toxic *in vivo* [59,60]. The toxicity of H_2O_2 encourages the rapid elimination of H_2O_2 from the body via urinary excretion or the action of glutathione peroxidase, an antioxidant [61]. Urinary and tissue H_2O_2 levels are often examined in studies of renal function. The increased renal perfusion pressure that is associated with hypertension has been found to elevate H_2O_2 excretion [62]. H_2O_2 has also been related to obesity-induced hypertension by studies that have shown that activation of the RAAS and secretions of angiotensin II lead to increased H_2O_2 production [63].

H_2O_2 is a valuable marker of early renal damage not only because it is used to signify inflammation and oxidative stress but also because it has been consistently shown to precede proteinuria in the timeline of functional renal damage. Infusing H_2O_2 directly into the renal arteries of Munich-Wistar rats resulted in dose-dependent increases in proteinuria, with the excreted proteins originating from the glomeruli [64]. Although proteinuria levels were significantly elevated by the H_2O_2 , there were no changes to GFR. GFR is considered the gold standard measurement of kidney failure and the understanding that H_2O_2 increases prior to both GFR decline and proteinuria, another often-used marker of renal dysfunction, increases the importance of H_2O_2 as an indicator of the initiation of renal pathology [64].

HFDs have been shown to increase urinary H_2O_2 excretion after only one week in C57BL/6 mice fed a 60% fat diet. H_2O_2 levels remained elevated in both 12 and 36 week feeding protocols [59,65]. In HFD-fed mice, H_2O_2 was also shown to increase prior to a

more robust inflammatory and fibrotic response as well as urinary protein excretion. Because increasing H₂O₂ concentrations have been consistently shown to precede more vigorous responses to HFD-induced renal damage and inflammation, it is an important tool to assess indications of future risk for worsening damage.

Biomarkers of Inflammation: TNF α and IL-6

The two most commonly studied markers of inflammation are TNF α and IL-6, pro-inflammatory cytokines produced by adipocytes and macrophages. HFDs and obesity often lead to the infiltration of adipocytes and macrophages into the kidneys where they release these cytokines. The presence of both inflammatory markers in HFD-induced obesity allows for the classification of obesity as a low-grade inflammatory disease [66]. Chronic low-grade inflammation is defined as a 2-3-fold increase in the systemic concentrations of both pro-inflammatory and anti-inflammatory cytokines and cytokine inhibitors. Initially, cytokines appear in the following order: TNF α , interleukin-1 beta (IL-1 β), IL-6, interleukin-1 receptor antagonist (IL-1ra), soluble TNF- α -receptors (sTNF-R), and interleukin-10 (IL-10) [67]. The secretion of IL-6 is initiated by many of the same pathways as TNF α and the two biomarkers are often studied in tandem. TNF α and IL-6, in addition to other pro-inflammatory cytokines, are understood to promote a state of chronic inflammation, which often positively correlates with both increased morbidity and mortality in patients with renal disease, although IL-6 is distinct from TNF α [33,68-70].

Angiotensin II, advanced glycation end products, and oxidized low-density lipoproteins (LDL) can stimulate TNF α synthesis [71]. Several animal studies have

shown that the presence of TNF α can increase insulin resistance [32]. TNF α is therefore not only a pro-inflammatory cytokine, but also a contributor to CKD by increasing insulin resistance, damaging the filtration ability of the kidneys by increasing hyperglycemia, and by increasing oxidative stress [32]. As previously mentioned, hyperglycemia eventually damages the kidneys resulting in proteinuria, and both proteinuria and hyperglycemia have been indicated in the mechanism of inappropriate activation of the intrarenal RAAS. Additionally angiotensin II, a component of the RAAS, stimulates the secretion of TNF α furthering the cycle of renal damage [3,5,18,22]. Reunguli et al. (2008) found that as renal damage in male Sprague-Dawley rats increased, so did renal oxidative stress and TNF α levels [72].

It is important to test for TNF α in tissues as opposed to, or in addition to, serum because it has been shown that although TNF α expression can be markedly increased in both skeletal muscle and visceral adipose tissue; serum TNF α expression may be unaffected [32]. Borst and Conover (2005) demonstrated that feeding young Wistar rats a HFD of 50% fat for 39 days led to increased adiposity, insulin resistance, and increased tissue expression of TNF α , while serum TNF α levels remained unchanged. Prior studies in the Sweazea laboratory's model of metabolic syndrome created by HFD-feeding of male Sprague-Dawley rats (60% fat for six weeks) demonstrates that plasma TNF α as well as vascular and plasma oxidative stress were elevated with the short term feeding protocol [6,7]. Therefore renal TNF α expression is anticipated to be elevated as well in these animals.

IL-6 acts as both a pro-inflammatory cytokine and an anti-inflammatory myokine; its role in inflammation has therefore been considered controversial due to its paradoxical

relationship to inflammation. In a pro-inflammatory state, IL-6 is secreted by macrophages via nuclear factor kappa beta, a TNF α -involved pathway. However, emerging research challenges the role of IL-6 as a pro-inflammatory cytokine with evidence that as skeletal muscles contract during physical activity, myocytes produce and release IL-6 into circulation, independent of any preceding TNF α release. Both the upstream as well as the downstream signaling pathways for IL-6 production differ between IL-6 production in macrophages and myocytes [70]. Pederson and Febbraio (2008) have found that monocytes specifically are not responsible for the increase in plasma IL-6 that has been consistently observed during and post-exercise [68].

Differences between IL-6 and TNF α are important in understanding their effects on metabolism. For example, although both IL-6 and TNF α induce lipolysis, only IL-6 stimulates fat oxidation. Adipocyte lipolysis induced by TNF α increases circulating free fatty acids and forms a direct link between TNF α and insulin resistance, supporting the increasing research interest in the hypothesis that TNF α can be directly implicated as having a pathogenic role in glucose metabolism contributing to diabetes [68,70,73]. Although insulin resistance induced by TNF α has been carefully examined, the part that IL-6 plays in the etiology of obesity-induced insulin resistance and hyperglycemia has not been elucidated. Figures 5 and 6 diagram the anti-inflammatory effects of IL-6 and the pathways by which it increases lipolysis and fat oxidation, stimulates glucose production by the liver, and decreases pro-inflammatory TNF α by increasing anti-inflammation cytokine concentrations. Although TNF α is implicated in the downstream signaling pathway of IL-6 production by adipocytes and macrophages, IL-6 has an inhibitory effect on TNF α production, leading to speculation that IL-6 may function as a

defense mechanism against $\text{TNF}\alpha$ or as a compensatory mechanism in cases of insulin resistance [68]. A third theory that may explain the paradoxical associations with IL-6 and both the enhanced insulin action during post-exercise periods and with its association with obesity-induced insulin resistance is that there are significant differences between the acute elevation post-exercise and the chronic elevation that occurs with obesity. Chronic increased IL-6 levels are an indication of continued $\text{TNF}\alpha$ production and activation of inflammatory pathways.

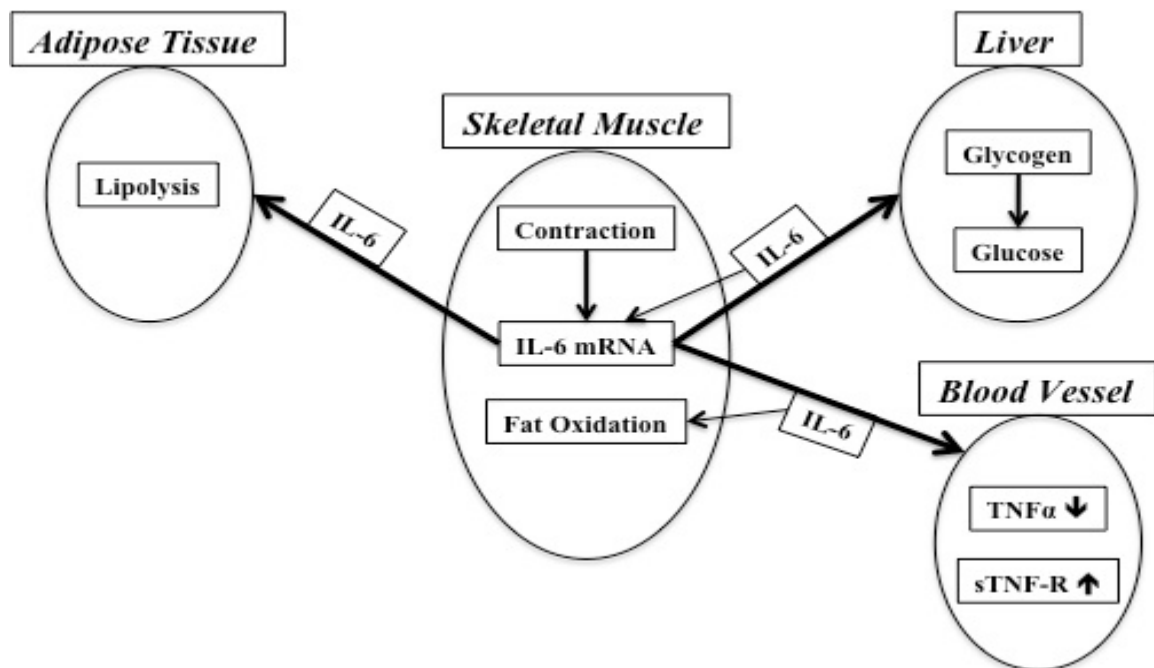


Figure 5 - Muscular IL-6 secretion and effects on metabolism.

Interleukin 6 (IL-6) secreted by muscular contraction during exercise induces fat oxidation and lipolysis while influencing glucose homeostasis. IL-6 also acts as an anti-inflammatory cytokines by inhibiting tumor necrosis factor alpha ($\text{TNF}\alpha$) and stimulating the soluble tumor necrosis factor receptor (sTNF-R) [69].

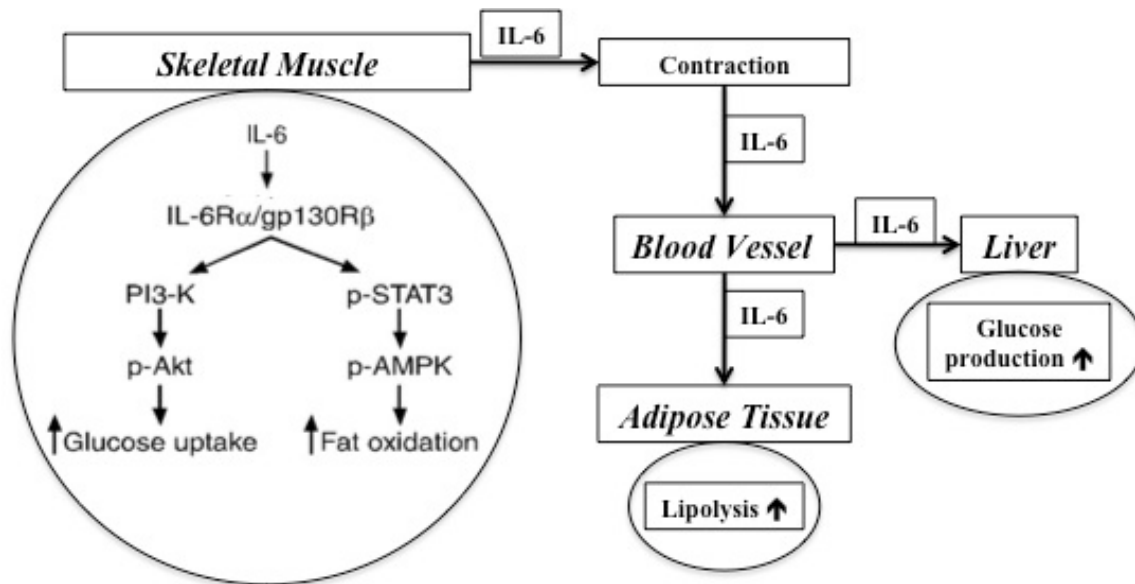


Figure 6 - Biological role of contraction-induced IL-6.

Exercise causes myokines, such as interleukin 6 (IL-6), to be secreted and released into circulation. Blood vessels transport IL-6 to adipose tissue and the liver, where it initiates lipolysis and glucose production. Within skeletal muscle, IL-6 signals a gp130Rβ/IL-6Rα homodimer that activates AMP-kinase and/or phosphatidylinositol 3-kinase and increases glucose uptake and fat oxidation. IL-6Rα/gp130Rβ = interleukin-6 homodimer; PI3-K = phosphatidylinositol 3-kinase; p-Akt = phosphorylated protein kinase B; p-STAT3 = phosphorylated signal transducer and activator of transcription 3; p-AMPK = phosphorylated AMP-kinase [68].

Despite the controversy regarding the differing effects of IL-6 as a cytokine and as a myokine, it continues to be studied as a marker of inflammation in HFD-induced obesity. The research conducted on the model of visceral adiposity created in the Sweazea laboratory investigates the effect of a HFD without exercise and therefore the anti-inflammatory properties of IL-6 as a myokine are not of major concern. Studies on both overweight and obese women have found that serum TNFα and IL-6 levels were positively correlated while Ozay et al. (2014) found that HFD-induced obesity in male Wistar albino rats (26% fat for 12 weeks) increased plasma TNFα without altering

plasma IL-6, supporting the role of TNF α as a predecessor to IL-6 expression [19,74]. Conversely, Kern et al. (2001) found that IL-6 levels in obese human subjects were higher in both plasma and adipose tissue compared to TNF α [73]. Additionally, Kern et al. (2001) found no relationship between the plasma levels of IL-6 and TNF α while there was a strong linear relationship between the expressions of these cytokines in adipose tissue. The local effects that TNF α exhibits in a paracrine capacity explain these findings; IL-6 in plasma may be of more importance systemically [73]. Stemmer et al. (2012) examined the effect of a HFD (40% fat for 11 months) on male Wistar rats and the creation of an inflammatory renal environment. Their results indicate an increase of IL-6 and TNF α in retroperitoneal fat and in the kidneys, while there was no increase in circulating IL-6. Aside from the research being conducted in this thesis, Stemmer et al. (2012) constitute the sole researchers who have investigated the effects of HFD-induced obesity on renal tissue inflammation. This thesis investigates both IL-6 and TNF α protein expression via Western Blot analysis whilst Stemmer et al. (2012) utilized real time polymerase chain reaction (RT-PCR) to determine mRNA expression. A limitation of their methodology is that even with increased mRNA expression, post-transcriptional modifications can prevent protein expression in tissues.

Regulation of inflammatory markers varies across tissue types, as demonstrated by Lamas et al. (2004), who fed young male Wistar rats a cafeteria diet consisting of 62% fat, including paté, chips, bacon, chocolate, and biscuits for five weeks. In just five weeks, the HFD rats had significant differences in body weight, serum triglycerides, free fatty acids, and total cholesterol while serum glucose, total proteins, and insulin remained the same across diet groups [75]. This study found that despite the significant effects of

the HFD on the aforementioned markers, there was decreased splenic mRNA expression of IL-6 and TNF α , a negative correlation between splenic TNF α mRNA and total fat pad mass, and no correlation between splenic IL-6 mRNA and total fat pad mass [75]. The decreased mRNA expression of both TNF α and IL-6 is contrary to most other HFD studies in rats but demonstrates that inflammatory markers can vary widely in different tissues.

Rats as a Model of Metabolic Syndrome

Researching the effects of metabolic syndrome on renal function using an animal model requires determining the most appropriate model. There is a wide variety of research concerning both metabolic syndrome and renal function in rats, with the research varying in terms of diet composition and administration, duration of treatment, as well as rodent model, sex, and age.

Variations in the type of fat used and the duration of feeding in HFD-rodent studies change the resulting model of metabolic syndrome and obesity. Buettner et al. (2006) examined the effect of the varying fatty acids on 1.5 month old male Wistar rats. Rats were randomly assigned to coconut oil (saturated fatty acids), olive oil (monounsaturated fatty acids), lard (comparable amounts of saturated fatty acids and monounsaturated fatty acids), or fish oil (polyunsaturated fatty acids) and examined for morphometric and physiologic differences after twelve weeks. Hematoxylin and eosin staining revealed hepatic microvesicular fat deposits and increased liver triglycerides in the lard, coconut oil, and olive oil groups but no liver inflammation or fibrosis [76]. Sweazea et al. (unpublished observations) similarly found hepatic steatosis after feeding

male Sprague-Dawley rats a HFD of 60% lard for six weeks. The lard group in Buettner et al.'s (2006) study showed increased plasma insulin and glucagon, increased whole body insulin resistance, and decreased plasma adiponectin, making the lard diet a good model of insulin resistance. Further supporting the justification for using a HFD consisting of a saturated fat such as lard to create a model of metabolic syndrome, Buettner et al. (2006) established that lipid synthesis genes, such as fatty acid synthase, were upregulated in the lard group while fatty acid oxidation enzymes, such as carnitine palmitoyltransferase, were downregulated. Although plasma creatinine was examined as a marker of renal function, no changes were found among any diet groups [76]. Stark et al. (2000) demonstrated the importance of fatty acid subtype by finding no insulin resistance or impaired glucose tolerance after feeding Sprague-Dawley rats a HFD consisting of 25% soybean oil, a polyunsaturated fatty acid, for three months [77].

In order to better classify the appropriate age-diet relationship, de Castro et al. (2013) conducted research comparing high fructose (60% total calories from fructose) and high saturated fat (40% total calories from fat) diets for 13 weeks on young (4 week old) and adult (12 week old) male Fischer rats. Their results concluded that the HFD was the most effective diet for inducing metabolic syndrome in young rats [21]. The HFD animals developed increased fasting glucose without increased hepatic glycogen, indicating that the HFD altered both glucose and hepatic metabolism. Additionally, de Castro et al. (2013) demonstrated that the young HFD-fed rats exhibited central obesity, increased blood pressure, increased heart rate, and renal inflammatory infiltrates, despite serum creatinine and urea levels remaining unchanged. De Castro et al. (2013) conducted

their research on Fischer rats in particular, however Sprague-Dawley rats have also been shown to be an equally useful animal model of metabolic syndrome [78].

Pranprawit et al. (2013) write that inducing metabolic syndrome in Sprague-Dawley rats can be inconsistent based on the type and amount of fat incorporated into the diet and the length of study protocol [78]. Although Pranprawit et al. (2013) found that eight weeks of HFD (60% total calories from fat, consisting of lard and soybean oil) did not induce glucose impairment or increase kidney mass in male Sprague-Dawley rats, Jiao et al. (2008) found that male Sprague-Dawley rats consuming a HFD (23% calories from fat, consisting of lard) developed insulin resistance in as few as three to four weeks [79]. These findings indicate the importance of saturated fat intake in diet-induced-obesity Sprague-Dawley rats.

Conclusion

HFDs have been examined in rodent models to determine dietary influences on a myriad of disease pathologies. When examining the effect of high fat feeding on renal structure and function, the majority of studies examine long term feeding protocols. Studies of the effects of shorter term feeding protocols to mimic early onset pathological changes resulting from HFDs are not evident in the literature. Research using a variety of rodent models has investigated the effects of a HFD from eight weeks to 11 months, and although kidneys have been examined at four weeks, there are no studies that have fully examined the effects of shorter term feeding protocols on renal function [3-5,30,76,78]. Renal dysfunction has been shown to be highly associated with uncontrolled diabetes and HFDs can induce the pre-diabetic state of metabolic syndrome in as short a time as six

weeks, as demonstrated by the model created in the Sweazea laboratory. The Sweazea model, and this study, are unique in that they represent the shortest feeding protocol in HFD-fed rodent renal studies.

Studies throughout the literature have examined HFDs ranging from 30% total calories from fat to 60% total calories from fat and a variety of animal models have been used to examine the effect of such diets on obesity, hypertension, metabolic syndrome, renal function, oxidative stress, and markers of inflammation. Few studies look at all of these factors together, and how the kidney is affected, after a short period of time. Prior studies by the Sweazea laboratory have shown that young (1.5 month old) male Sprague-Dawley rats fed HFD (60% total calories from fat, consisting primarily of lard) for six weeks develop metabolic syndrome: increased body fat, high blood glucose concentrations, impaired glucose tolerance, hypertension, endothelial dysfunction, oxidative stress, and inflammation [6,7]. Unpublished observations from the laboratory also demonstrate that these animals develop hepatic steatosis. The research conducted on this model of increased adiposity will examine not only a shorter term feeding protocol than other studies but will also study a wide variety of renal structural and functional markers. In order to fully assess renal status in the HFD-fed rats, animal morphometrics, renal mass, renal morphology, renal lipid infiltration, proteinuria, urinary cystatin C, urinary hydrogen peroxide, renal tissue TNF α and IL-6 protein expression, renal lipid peroxidation, and urinary markers of oxidative DNA damage were all studied. No other studies evident in the literature examine either a six week feeding protocol or such a variety of markers. This study is novel in that it presents a full picture of the effects of the relatively short term HFD feeding regime on renal function and structure. The etiology of

increased adiposity in relation to renal dysfunction is not fully understood and this study allowed for a greater understanding of the changes induced with a short feeding protocol. Additionally, only Stemmer et al. (2012) have previously studied renal tissue inflammation caused by a high fat feeding; this study protocol examined both TNF α and IL-6 and is unique for doing so.

The summation of current literature on the HFDs and renal dysfunction supports the hypothesis that even during the early stages of metabolic syndrome, the kidneys begin to develop signs of stress and damage, which can eventually lead to diabetic nephropathy, diabetic kidney disease, and ultimately end-stage renal disease. Understanding the etiology of damage related to poor nutrition is vital to the prevention and treatment of renal failure.

CHAPTER 3

MATERIALS AND METHODS

Animal Models

The animal models used in this study were male 1.5 month old Sprague-Dawley rats [140-160 g body weight, Harlan Takland Industries (Madison, WI, USA)] fed a HFD (60% kcal from fat; Research Diets Inc; Appendix A) for six weeks. These rats were already known to have developed metabolic syndrome, increased body fat, high blood glucose concentrations, endothelial dysfunction, hypertension, plasma and vascular oxidative stress and hepatic steatosis, based upon previous studies conducted in the Sweazea laboratory [6,7]. The kidneys, plasma, and urine of the rats fed the HFD were compared with 1.5 month old male Sprague-Dawley rats fed a standard rodent chow (5% fat), both of which were available from prior studies. All rats were fed either the HFD or chow diet for six weeks with the food replaced every three to four days. All rats were provided with unlimited access to food and water, housed in pairs in identical cages at the same facility and provided 12 hours of light and 12 hours of dark per day. The prior studies from which the tissues samples were obtained were approved by Arizona State University's IACUC (Protocol 09-1045R).

Study Design

The study design was a true experiment with a treatment (HFD) and control group (standard rodent chow). Rats were randomized to six weeks of either chow or HFD. At the end of the six weeks, sodium pentobarbital (200 mg/kg, i.p.) was used to euthanize all rats. Blood, urine, and kidney samples were then collected. The blood samples were

obtained via cardiac puncture and centrifuged at 13,000 rpm at 4°C for 15 minutes to separate formed elements from the plasma, which was then stored at -80°C until analyses. Urine was collected with a 25-gauge needle inserted directly into the bladder. The urine was then centrifuged at 13,000 rpm at 4°C for 10 minutes to remove debris and the supernatant was then stored at -80°C until analyses. Following a midline laparotomy, a subset of kidneys were removed and stored at -80°C until analyses while a separate subset was embedded in Optimal Cutting Temperature (OCT) compound prior to freezing.

Table 1, below, indicates the animal subsets that were used in each aspect of this study design.

Table 1 – Summary of Animal Subsets

<u>Diet/ Animal ID</u>	<u>Date of Sample Collection</u>	<u>Urine Protein (BioRad)</u>	<u>Urine Creatinine (to normalize protein)</u>	<u>Renal Morphology/ Oil Red O</u>	<u>Renal Mass</u>	<u>Body Mass, Tail Length, Waist Circumference, % Fat</u>	<u>Renal tissue TNFα and IL-6 Protein Expression</u>	<u>Plasma Cystatin C</u>	<u>Renal TBARS</u>	<u>Plasma OXDNA /RNA</u>	<u>Urine H₂O₂</u>
Chow /C1	09/08/09							X			X
Chow /C2	09/09/09									X	X
Chow /C5	09/28/09			X	X	X					
Chow /C6	09/29/09			X	X	X	X	X		X	
Chow /C7	10/12/09				X	X	X	X	X	X	
Chow /C8	10/13/09	X	X	X	X	X	X	X	X	X	
Chow /C9	10/14/09			X	X	X		X	X		X
Chow /C10	10/15/09	X	X					X		X	X
Chow /C11	11/11/09	X	X		X	X	X	X		X	
Chow /C12	11/12/09	X	X					X	X	X	
Chow /C13	11/13/09	X	X	X	X	X	X	X	X	X	
Chow /C14	12/14/09			X	X	X	X	X		X	X
Chow /C15	12/15/09	X	X		X	X	X			X	
Chow /C18	04/09/10										X
Chow /C21	04/29/10	X	X								
Chow /C22	05/06/10	X	X								
HFD /HF3	09/25/09							X			
HFD /HF4	09/24/09										X
HFD /HF5	10/07/09							X		X	
HFD /HF7	10/09/09	X	X	X				X		X	
HFD /HF8	11/02/09	X	X					X			
HFD /HF9	11/04/09			X	X	X	X	X	X	X	
HFD /HF10	11/05/09	X	X	X	X	X	X	X		X	
HFD /HF11	11/06/09	X	X	X	X	X	X	X	X	X	
HFD /HF12	11/30/09				X	X	X	X		X	X
HFD /HF13	12/01/09			X	X	X	X	X		X	X
HFD /HF14	12/07/09				X	X	X		X		
HFD /HF15	12/08/09				X	X	X	X	X		X
HFD /HF16	12/09/09	X	X		X	X	X		X	X	
HFD /HF17	04/01/10	X	X								
HFD /HF18	04/02/10	X	X								
HFD /HF21	04/30/10										X
HFD /HF22	05/04/10										X
HFD /HF24	05/10/10	X	X								

Laboratory Analysis

Kidney Morphology

Kidneys from rats fed either a standard rodent chow (5% fat) or HFD (60% fat) for six weeks were available from prior studies. Animal morphometrics (body mass, epididymal fat pad mass, waist circumference, tail length) and renal tissue masses were measured in a subset of animals (n = 9 chow and n = 8 HFD animals). Gonzales et al. (2000) have confirmed that tail length can be used as marker of overall growth in rats [80]. Waist circumferences were measured with a fabric tape measure positioned at the iliac crest.

Another subset of frozen kidneys (n = 4 chow and n = 5 HFD rats) were embedded in OCT compound and sectioned using a cryostat (Leica Biosystems CM1950; Buffalo Grove, IL). Sections of embedded tissues (14 μ m) were collected onto glass microscope slides, stained with hematoxylin and counterstained with eosin (Appendix C). Sections were viewed using a light microscope (Olympus BX50) and images collected with an Olympus DP70 camera (Melville, NY) to assess morphology. It was predicted that kidneys from HFD rats would have increased mass and morphological changes consistent with kidney disease.

In order to determine the level of fat infiltration, a subset of OCT-embedded frozen kidneys (n = 4/group) were sectioned into 14 μ m sections. Frozen sections were collected onto glass microscope slides and stained with Oil Red O using a commercially available kit (Cat. No. ORK-2-IFU; ScyTek Laboratories, Logan, UT; Appendix D). Sections were counterstained by exposure to hematoxylin. Images were collected using

the same microscope set-up as described above. It was predicted that kidneys from HFD rats would have increased fat, consistent with the development of kidney disease.

Biomarkers of Renal Function

A random set of rat urine from prior studies was used to determine urine protein concentrations (n = 8/group), which were measured using the Bradford technique (Bio-Rad, Hercules, CA). Aliquots of diluted urine (1:500) were mixed with Bradford Reagent (4:1; Bio-Rad, Hercules, CA). The mixture was loaded into a 96-well plate in duplicate and read at 595nm using a plate reader. The absorbance of the samples were compared to a bovine serum albumin standard curve (0, 20, 40, 60, 80, 100 $\mu\text{g}/\mu\text{L}$ total protein) to determine the concentration of protein in each urine sample. There is no gold standard for the measurement of proteinuria and the methods of detection have large variability.

According to the National Kidney Foundation, proteinuria should be assessed by either a 24-hour urine collection, during which creatinine content should also be measured, or by spot urine protein:creatinine ratio [16]. The same set of urine samples used to quantify urine protein were used to ascertain urine creatinine concentrations (n = 8/group) using an available kit (Cat. No. CR01; Oxford Biomedical Research, Rochester Hills, MI; Appendix E). Aliquots of urine were diluted (1:10) and prepared according to kit instructions then loaded into a 96-well plate in duplicate and read at 490nm. Creatinine concentrations were calculated from a known standard curve. It was predicted that HFD would increase urinary protein:creatinine concentrations, indicating that the filtering system of the kidney was damaged, resulting in leakage of proteins into the urine.

Plasma cystatin C, a sensitive biomarker of renal function, was measured using an available ELISA kit (Cat. No. MSCTCO; R&D Systems, Minneapolis, MN; Appendix F). Random samples of rat plasma available from prior studies (n = 10/group) were diluted 400-fold and prepared according to kit instructions in a 96-well plate in duplicate. The absorbances of the samples were read at 450nm, corrected with a reading at 540nm, then compared to a standard curve (0, 125, 250, 500, 1000, 2000, 4000, 8000 pg/mL rat cystatin C standard) to determine the plasma concentrations of cystatin C. It was predicted that HFD would increase cystatin C, indicating early renal dysfunction.

Urinary H₂O₂, a biomarker of inflammation, oxidative stress, and renal function was measured using an available kit (Cat. NO. ab102500; Abcam, Cambridge, MA; Appendix G). Random samples of rat urine (n = 6/group) were diluted (1:2 or 1:4 based on amount of available sample) and prepared according to kit instructions and loaded into a 96-well plate in duplicate. Sample absorbances were then read at 570nm and compared to a standard curve in order to quantify H₂O₂ concentrations. H₂O₂ levels were then normalized to creatinine concentrations. Urinary creatinine concentrations on the same urine samples (n = 6/group) were assessed using a kit (Cat. No. CR01; Oxford Biomedical Research, Rochester Hills, MI). Aliquots of urine were diluted (1:20 or 1:40 based on amount of available sample) and prepared according to kit instructions. Samples were then loaded into a 96-well plate in duplicate and read at 490nm and concentrations were calculated from a known standard curve. It was predicted that HFD would increase urinary H₂O₂:creatinine concentrations, indicating early renal functional damage.

Inflammatory Markers

Briefly, a subset of kidneys from both chow and HFD rats were transferred to a ground glass homogenizer containing Tris-HCl buffer [10 mM Tris (pH 7.6; Cat. No. 161-0716; Bio-Rad, Hercules, CA), 1 mM EDTA, 1% triton X-100, 0.1% Na-deoxycholate, 0.03% protease inhibitor cocktail (Cat. No. P2714; Sigma-Aldrich, St. Louis, MO), and 1 mM phenylmethanesulfonyl fluoride (PMSF)]. Samples were then centrifuged at 14,000 rpm for 10 minutes at 4°C. Total protein concentrations of the supernatants were determined using the Bradford Technique (Bio-Rad, Hercules, CA). 6 µL of 5X SDS sample buffer that includes 2% β-mercaptoethanol as a reducing agent was added to sample supernatant and boiled for 3 minutes. Supernatant (100 µg total protein/lane) was resolved using 4-15% gradient Tris-HCl SDS-PAGE gels (Cat. No. 456-1083; Bio-Rad, Hercules, CA) and transferred to PVDF membranes (Cat. No. 152-0176; Bio-Rad, Hercules, CA) for 90 minutes at 200 V. Membranes were blocked for two hours in Tris buffered saline containing Tween 20, BSA fraction VI, and 5% nonfat milk followed by an overnight incubation at 4°C in primary antibodies specific for IL-6 (1:250; Cat. No. ab6672; abcam, Cambridge, MA; Appendix H), TNFα (1:500; Cat. No. 11948; Cell Signaling, Danvers, MA; Appendix I) and beta-actin (1:2000; a loading control; Cat. No. ab8227; abcam, Cambridge, MA; Appendix J). Primary antibodies were prepared in Tris buffered saline with Tween 20 (500 µL in 1 L Tris buffered saline), Membranes were then exposed to anti-rabbit IgG secondary antibody in Tris buffered saline for one hour at room temperature (1:1000 for IL-6 and TNFα and 1:2000 for beta-actin; Cat No. 7074S; Cell Signaling Technology, Danvers, MA) followed by exposure to Pierce enhanced chemiluminescence western blotting substrate (Cat. NO 32279; Thermo

Scientific, Rockford, IL). Immunoreactive bands were visualized by exposure to x-ray film (Cat. No. 34090; Thermo Scientific, Rockford, IL) and analyzed using NIH ImageJ software. Protein expressions of IL-6 and TNF α were normalized to beta-actin to determine the level of IL-6 (n = 5 chow and 6 HFD animals) or TNF α (n = 8/group) in each sample.

An ELISA was used to quantify TNF α concentration in renal tissue supernatant (Cat. No. ER3TNFA; Thermo Scientific, Rockford, IL; Appendix K). A subset of kidneys was randomly selected and 50-100 mg of individual kidneys (n = 5/group) were homogenized with phosphate buffer saline (PBS), 1 mM pH (7.4) solution using a ground glass homogenizer. Diluted renal tissue samples (1:1) were prepared according to kit instructions, loaded into a 96-well plate in duplicate, and absorbances were read at 450nm and corrected to a reading at 550nm. Corrected absorbance readings were then compared to a standard curve (0, 31, 93, 278, 833 pg/mL rat TNF α standard) in order to establish renal TNF α concentrations.

Oxidative Stress

The same subset of samples used for the TNF α ELISA (n = 5/group) were used to evaluate renal oxidative stress via lipid peroxidation levels using a TBARS assay (Cat. No. 0801192; ZeptoMetrix Corporation, Buffalo, NY; Appendix L). Samples were prepared according to kit instructions then boiled at 95°C for one hour and subsequently put on ice for ten minutes. Samples were then centrifuged at 3,000 rpm for 15 minutes at room temperature. The supernatant was then collected and centrifuged at room temperature for 15 minutes at 3,000 rpm. The supernatant was again collected and loaded

into a 96-well plate in duplicate. The absorbance of the supernatant were read at 540nm and compared to a standard curve (0, 12.5, 25, 50, 100 nM/mol MDA) to determine renal tissue concentrations of lipid peroxidation. Lipid peroxidation levels were predicted to be elevated by HFD, indicating increased oxidative stress in the kidneys of HFD-fed rats.

Plasma 8-hydroxyguanosine, 8-OHdG, and 8-hydroxyguanine were examined as biomarkers of oxidative DNA/RNA damage using a commercially available kit, as oxidative stress has been shown to be elevated early during renal failure (Cat. No. 589320; Cayman Chemical, Ann Arbor, MI; Appendix M) [3]. Plasma samples were selected from prior studies (n = 10 chow and n = 11 HFD animals) and filtered with a 30kDa filter (Cat. No. UFC503096; EMD Millipore, Billerica, MA), diluted 1:25, prepared according to kit instructions, loaded into a 96-well plate in duplicate and absorbances were read at 410nm. Plasma oxidative DNA/RNA damage was quantified by comparing absorbances to a standard curve. Oxidative stress markers were expected to be elevated, indicating that oxidative DNA/RNA damage was initiated by the HFD.

Variables

A number of variables were used to assess the effect of HFD on kidney structure and function. The independent variable was classified as the diet each animal group consumed: either the HFD (20% kcal from protein, 20% kcal from carbohydrates, and 60% kcal from fat; Appendix A) or the standard rodent chow (18.9% kcal from protein, 57.33% kcal from carbohydrates, and 5% fat; Appendix B).

Morphometrics of the animals were available from prior studies and used to analyze the diet groups for differences in body mass, epididymal fat pad mass, waist

circumference, and tail length. This sample of animals was also used to assess renal tissue masses. Morphological changes were further evaluated by inspecting sections of kidney tissue under a light microscope for renal damage and by staining sections with Oil Red O to assess the level of fat infiltration.

Proteinuria was examined by the Bradford technique (Bio-Rad, Hercules, CA) to measure the concentrations of urinary protein and creatinine and by then normalizing protein concentrations to creatinine. The protein:creatinine ratios of the chow and HFD-fed rats were compared for mean differences. Proteinuria is considered an early marker of renal dysfunction, as it is a sign of pathologically leaky kidneys.

Plasma cystatin C is also a marker of early kidney disease and a kit was used to quantify plasma concentrations.

An available kit was used to quantify urinary H_2O_2 , which were normalized to urinary creatinine concentrations in the same animals.

Renal $TNF\alpha$ were assessed using Western blots and a commercially available ELISA in order to determine renal inflammation. Western blots were used in order to analyze IL-6 expression in renal tissue.

Plasma oxidative DNA/RNA damage and renal tissue lipid peroxidation were examined as markers of oxidative stress. Plasma oxidative DNA/RNA damage was determined using a competitive kit and renal tissue lipid peroxidation was quantified via a commercially available TBARS kit.

Together, these variables served to quantify the level of kidney damage inflicted by the short term HFD.

Statistical Analysis

Data are expressed as mean \pm SEM. Statistical analyses were computed using SigmaPlot (Systat Software Inc, Version 13.0; San Jose, CA). Data were tested for normality and were then analyzed using either Student's t-tests or Mann-Whitney U tests. Values of $p < 0.05$ were considered significant.

CHAPTER 4

RESULTS

Structural Changes

Morphometrics

Although the HFD rats tended to weigh more than the chow-fed rats, this difference was not statistically significant (Figure 7). Rats fed a HFD demonstrated significantly increased epididymal fat pad mass compared to chow-fed animals, establishing that adiposity was increased by the HFD (Figure 8). The waist circumferences of the HFD animals were significantly increased when compared to chow fed controls, indicating that the HFD caused increases in abdominal adiposity (Figure 9). The tail lengths, a marker of overall animal growth, of the HFD and chow-fed animals were not significantly different (Figure 10).

The renal masses of the HFD rats were significantly elevated compared to the renal mass of the chow group (Figure 11).

Morphological analyses using hematoxylin and eosin stained tissue sections showed no structural differences between the chow and HFD groups, indicating that although the mass of the HFD kidneys was increased, damage to the morphological structure of the kidneys was not evident (Figure 12).

Fat Infiltration

Lipid infiltration analysis using Oil Red O stained tissue sections revealed no fat infiltration of either the chow or the HFD rat kidneys, indicating that despite the HFD, there was no evidence of renal steatosis (Figure 13).

Biomarkers of Function

Proteinuria

Both urine protein concentrations and urine creatinine concentrations were assessed in order to measure renal function. The urine protein:creatinine ratios of the chow and HFD rats did not differ significantly, indicating that the filtering ability of the HFD rat kidneys were not damaged (Figure 14). There was also no difference in the urine creatinine concentrations of the two groups (Figure 15).

Plasma Cystatin C

Although HFD rat plasma cystatin C concentrations appeared higher than chow rat plasma cystatin C concentrations, the difference was not sufficient to merit statistical significance (Figure 16).

Hydrogen Peroxide

Urinary hydrogen peroxide:creatinine ratios were found to have no significant difference between chow and HFD groups (Figure 17).

Inflammatory Markers

Renal Tissue TNF α

Western blot analyses of renal tissue established no significant difference in the TNF α protein expression of the chow and HFD rat kidneys (Figure 18). Furthermore, ELISA analysis on kidney tissue supernatant revealed no significant difference in the TNF α concentrations of the HFD and chow-fed rats (data not shown).

Renal Tissue IL-6

Quantification of western blots of IL-6 expression in renal tissues showed no difference between the chow and HFD animal kidneys (Figure 19).

Oxidative Stress

Lipid Peroxidation

Renal tissue TBARS, a measure of tissue oxidative stress via lipid peroxidation, was not significantly elevated in the HFD rats (Figure 20).

Oxidative DNA/RNA Damage

Plasma levels of oxidized DNA/RNA, quantified as plasma levels of multiple oxidative stress markers, including 8-hydroxyguanosine from RNA, 8-OHdG from DNA and 8-hydroxyguanine from both DNA and RNA were examined. There were no significant differences between the chow and HFD rat groups (Figure 21).

Cumulative Information

Table 2 lists the means, standard deviations, standard errors of the means, normality testing results, equal variance testing results, and final P-values from all statistical analyses.

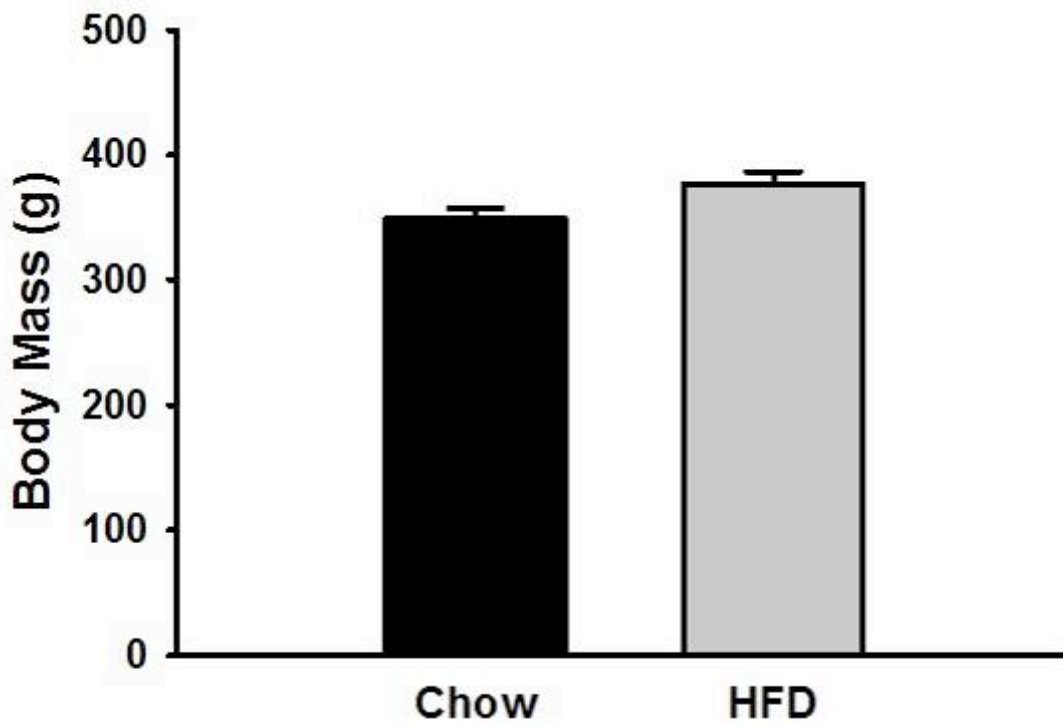


Figure 7 – Body mass of chow and HFD rats. Although the HFD-fed rats tended to weigh more than the chow-fed rats, this difference was not statistically significant (n = 9 chow and n = 8 HFD animals). Data are expressed as means \pm SEM. $p = 0.056$.

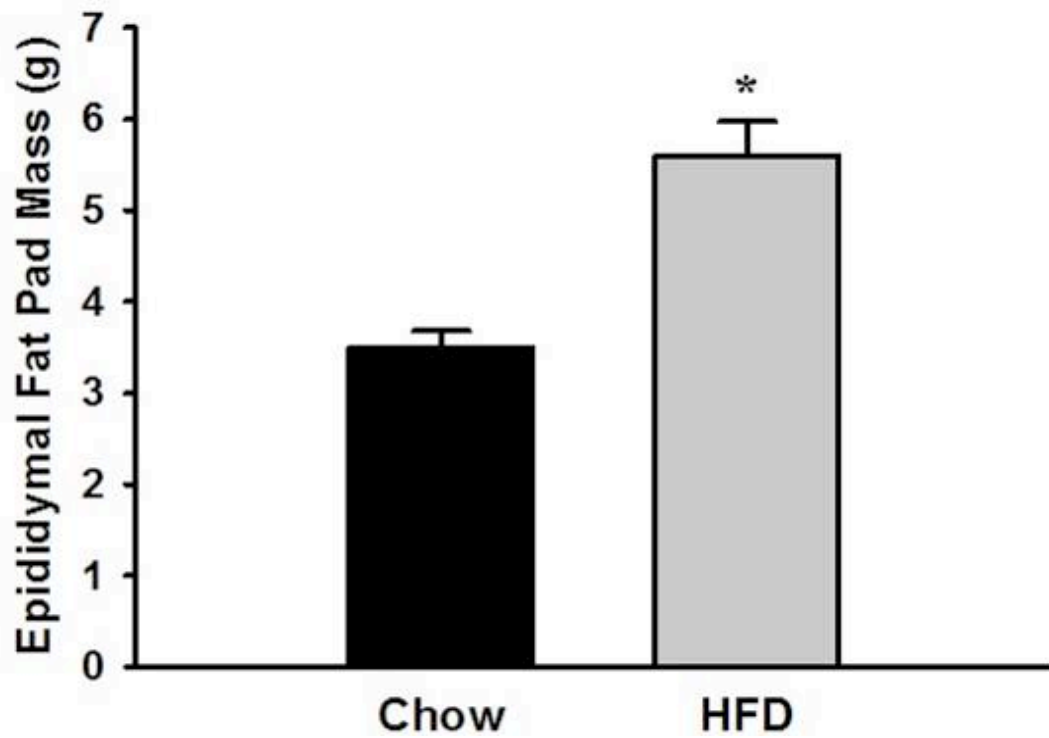


Figure 8 – Epididymal fat pad mass of chow and HFD rats. Significant differences between the fat pad masses of chow and HFD rats demonstrate that adiposity in the HFD rats increased considerably (n = 9 chow and n = 8 HFD animals). Data are expressed as means \pm SEM. *p < 0.001.

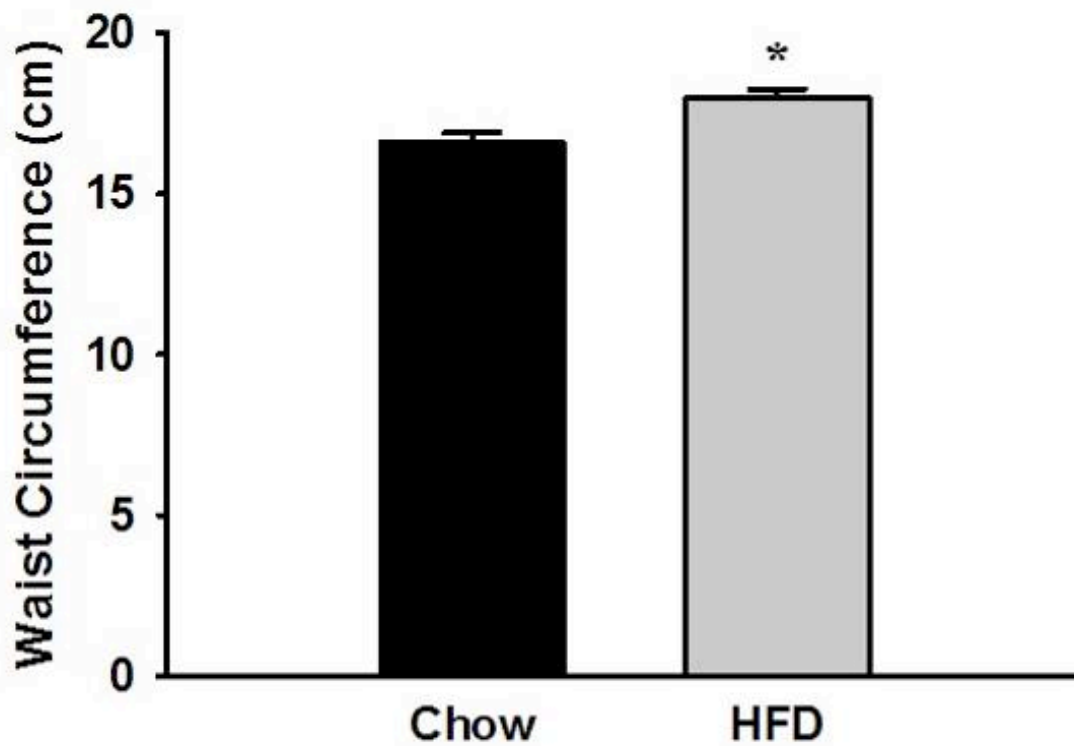


Figure 9 – Waist circumference of chow and HFD-fed rats. The mean differences between the waist circumferences of chow and HFD animals were statistically significant, indicating that the HFD induced increases in abdominal obesity (n = 9 chow and n = 8 HFD animals). Data are expressed as means \pm SEM. *p = 0.004.

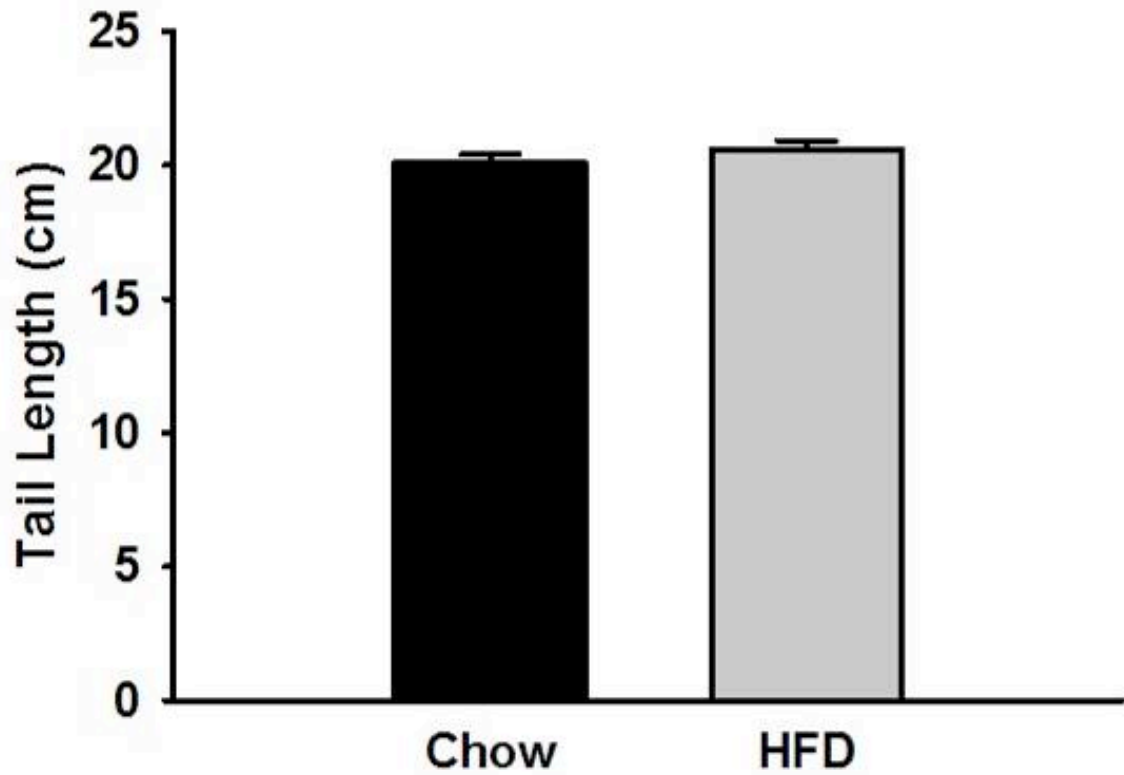


Figure 10 – Tail lengths of chow and HFD animals. There was no difference between the tail lengths of the chow and HFD-fed rats, demonstrating that changes in waist circumference, epididymal fat pad mass, body mass, and renal mass did not result from overall animal growth. (n = 9 chow and n = 8 HFD animals). Data are expressed as means \pm SEM. p = 0.276.

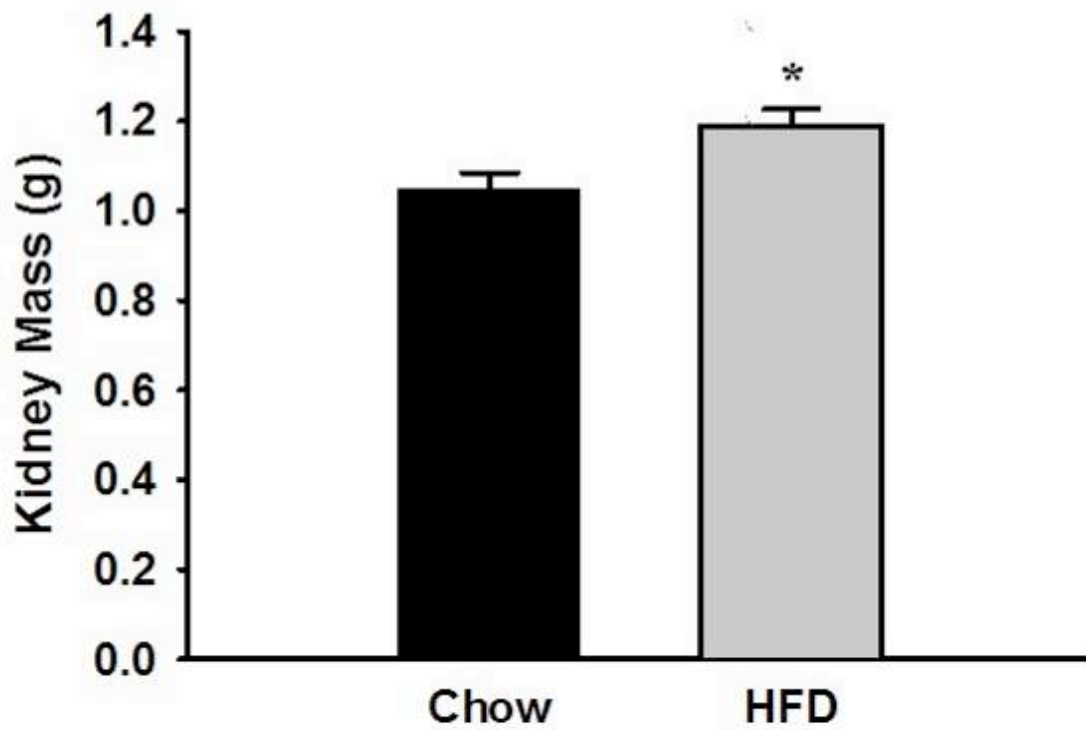


Figure 11 – Renal mass of chow and HFD rats. The HFD-fed rat kidneys were significantly heavier than the chow-fed rat kidneys (n = 9 chow and n = 8 HFD animals). Data are expressed as means \pm SEM. *p = 0.019.

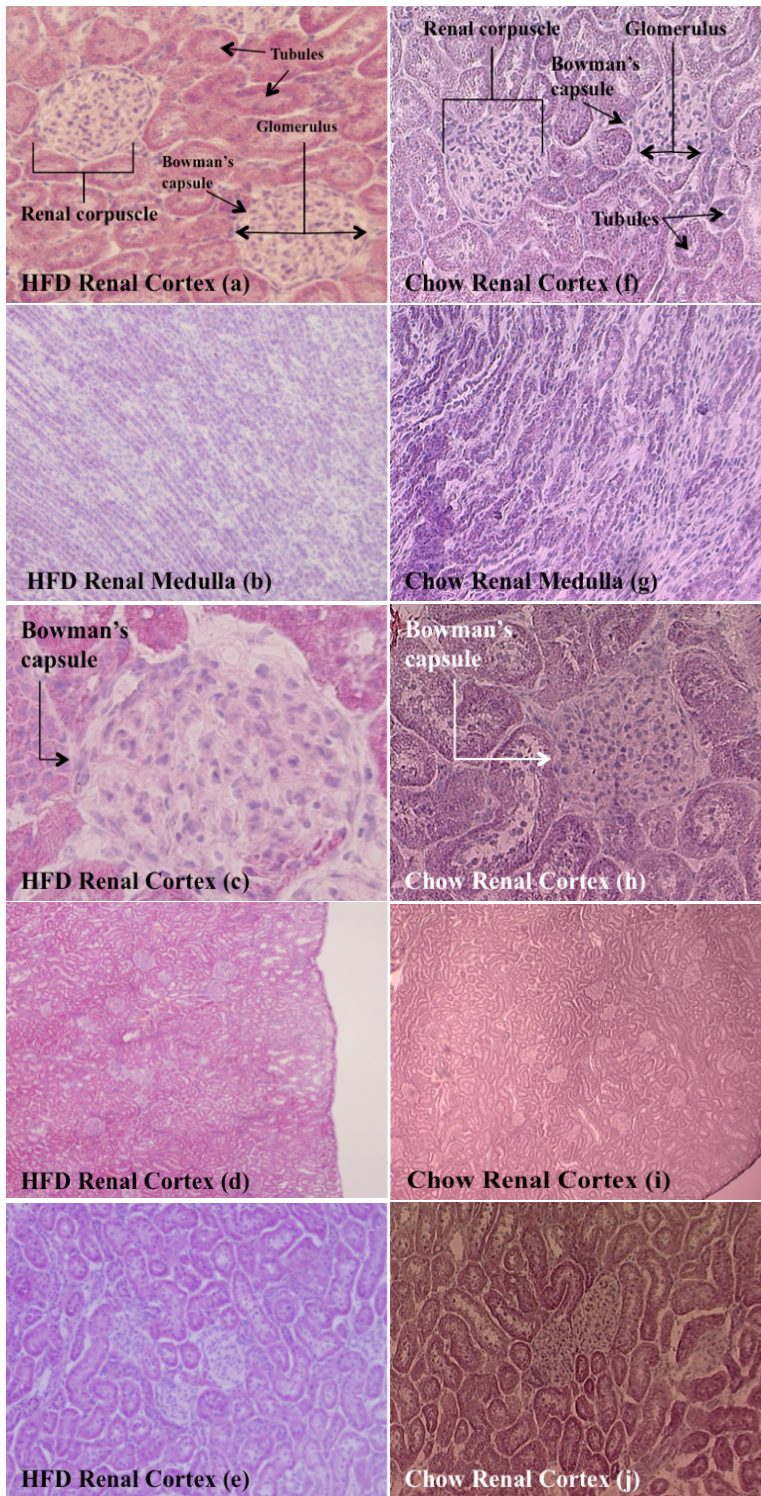


Figure 12 – Hematoxylin and eosin staining of kidneys for morphology.

Hematoxylin and eosin staining shows no signs of morphological damage to the HFD kidneys (n = 4 chow and 5 HFD rats). Magnification: (a) 100x; (b) 40x; (c) 200x; (d) 40x; (e) 100x; (f) 200x; (g) 200x; (h) 200X; (i) 40x; (j) 100x.

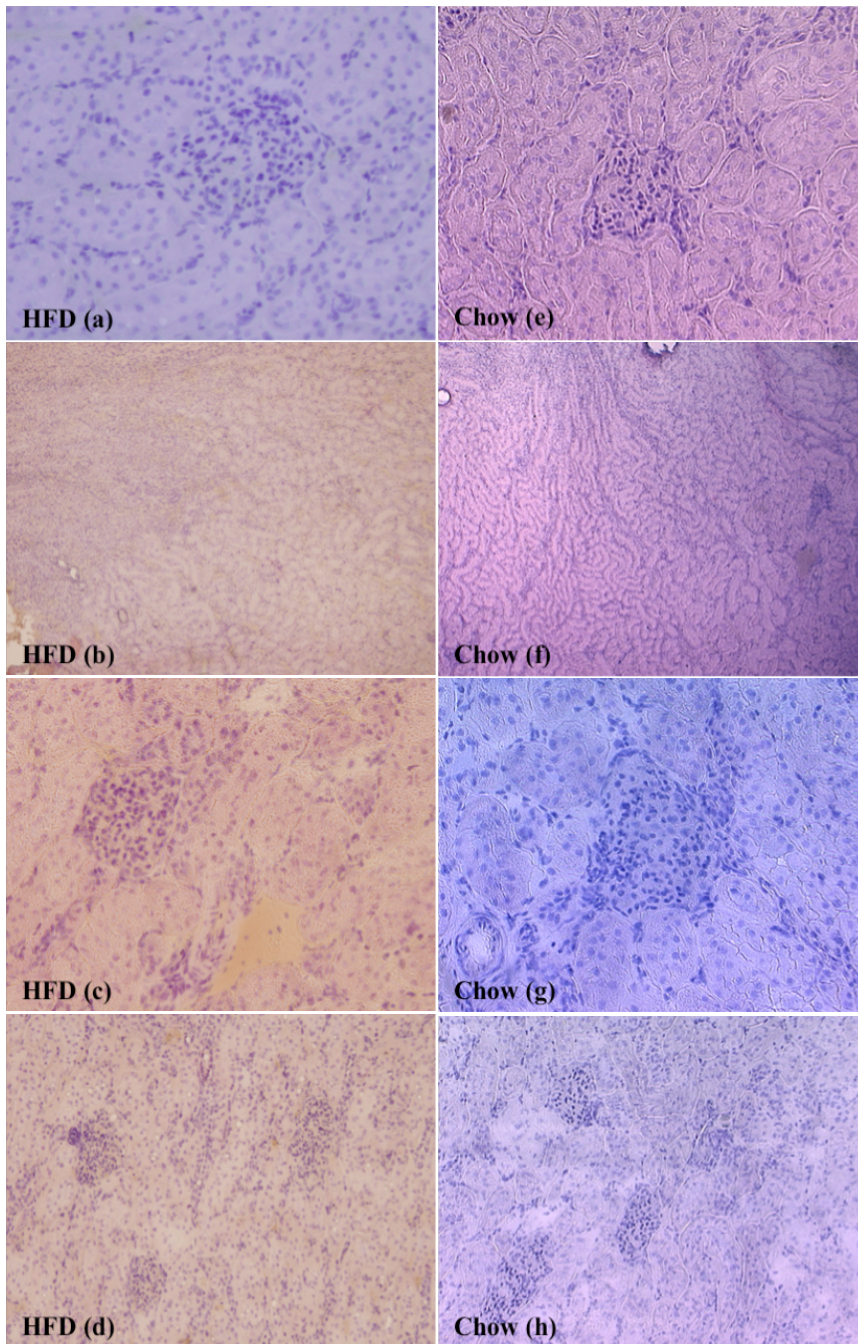


Figure 13 – Oil Red O staining of kidneys. Oil Red O staining of kidneys from HFD-fed rats shows no signs of renal steatosis or fat infiltration (n = 4/group). Magnification: (a) 200x; (b) 40x; (c) 100x; (d) 100x; (e) 200x; (f) 40x; (g) 200x; (h) 100x.

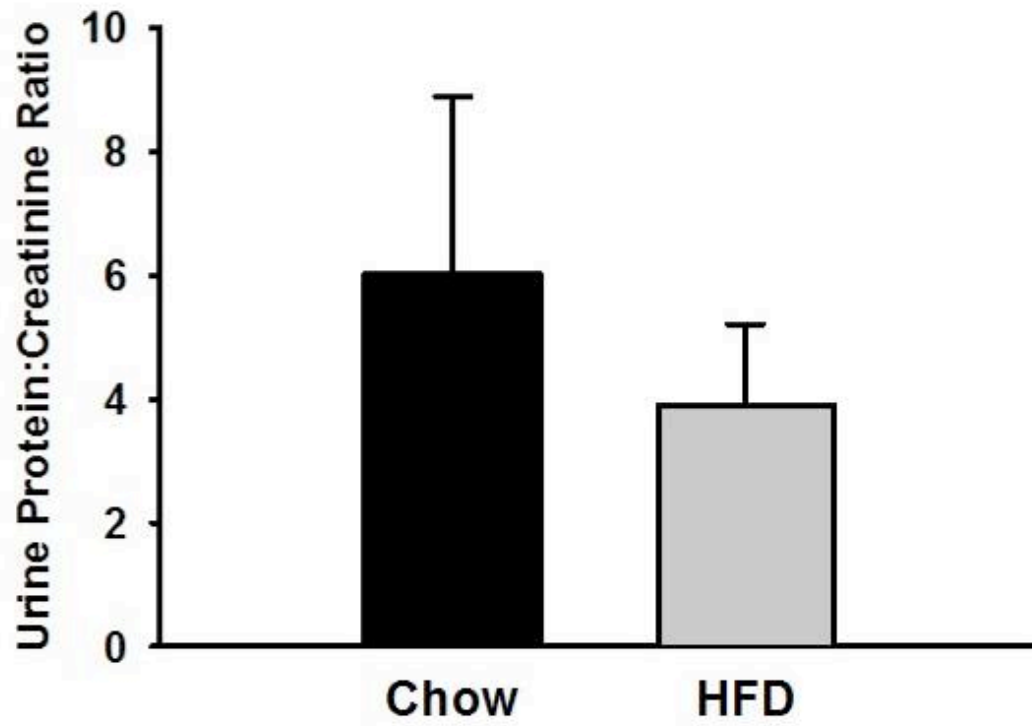


Figure 14 – Urine protein:creatinine ratios of chow-fed and HFD-fed rats. There was no significant difference between the urine protein:creatinine ratios of the two diet groups (n = 8/group). Data are expressed as ratio of means \pm SEM. p = 0.574.

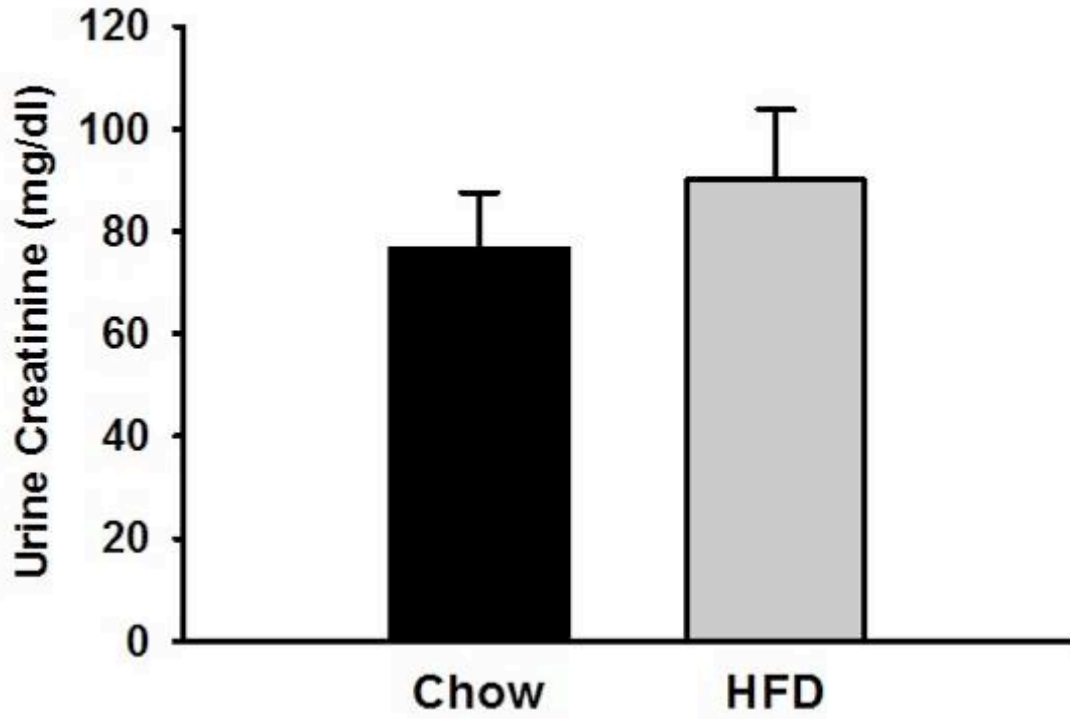


Figure 15 – Urine creatinine in chow-fed and HFD-fed rats. There was no significant difference between the urine creatinine concentrations of the two diet groups (n = 8/group). Data are expressed as ratio of means \pm SEM. p = 0.456.

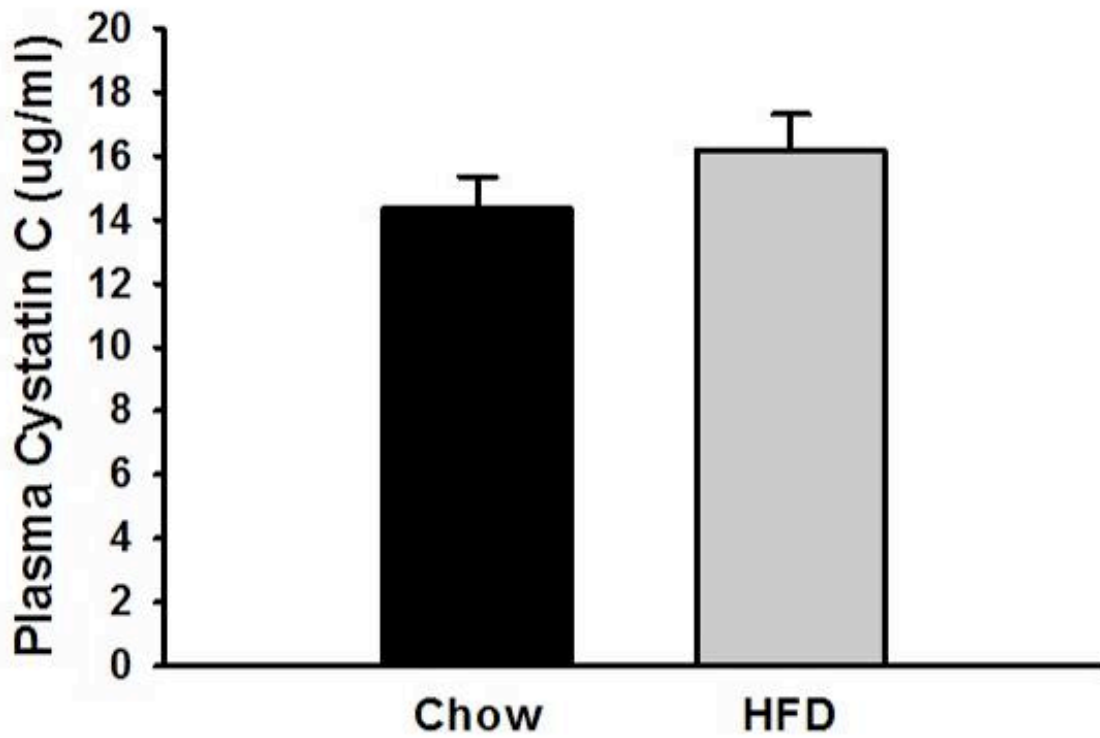


Figure 16 – Plasma cystatin C in chow and HFD rats. Although the average plasma cystatin C concentrations in the HFD rat group were higher than that of the chow fed rats, this difference was not statistically significant (n = 10/group). Data are expressed as means \pm SEM. p = 0.233.

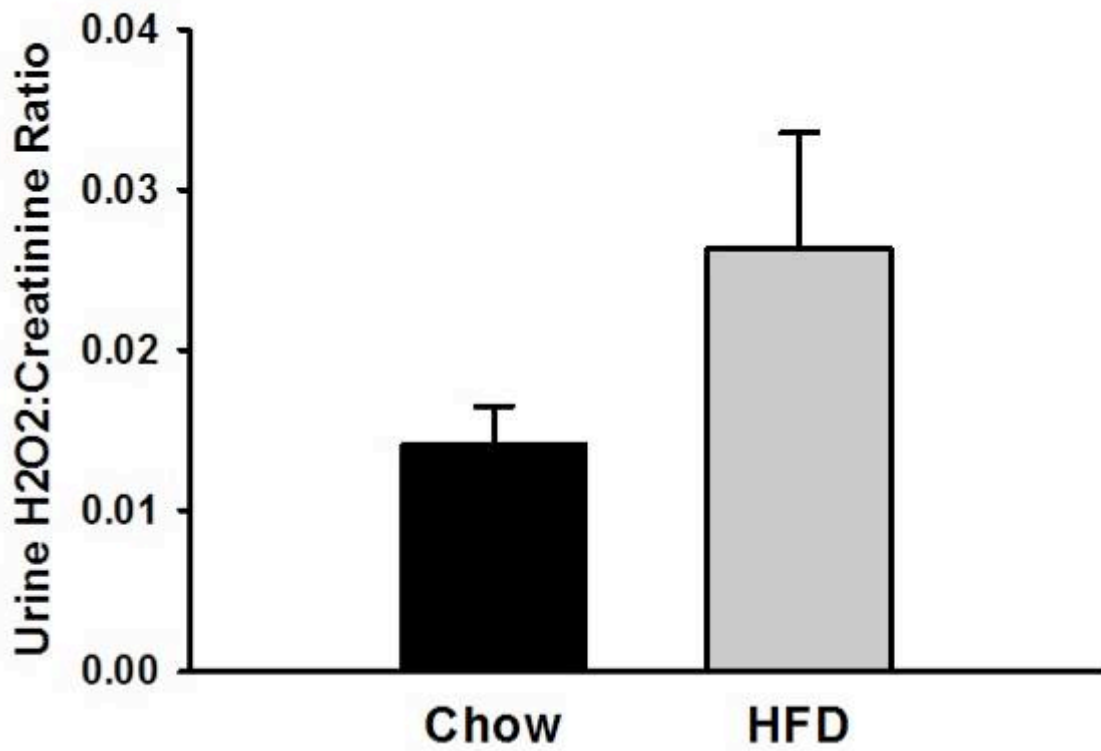


Figure 17 – Urinary hydrogen peroxide:creatinine in chow and HFD rats. Although the HFD rat groups demonstrated higher urinary hydrogen peroxide concentrations than the chow fed rats, this difference was not statistically significant (n = 10/group). Data are expressed as means ± SEM. p = 0.142.

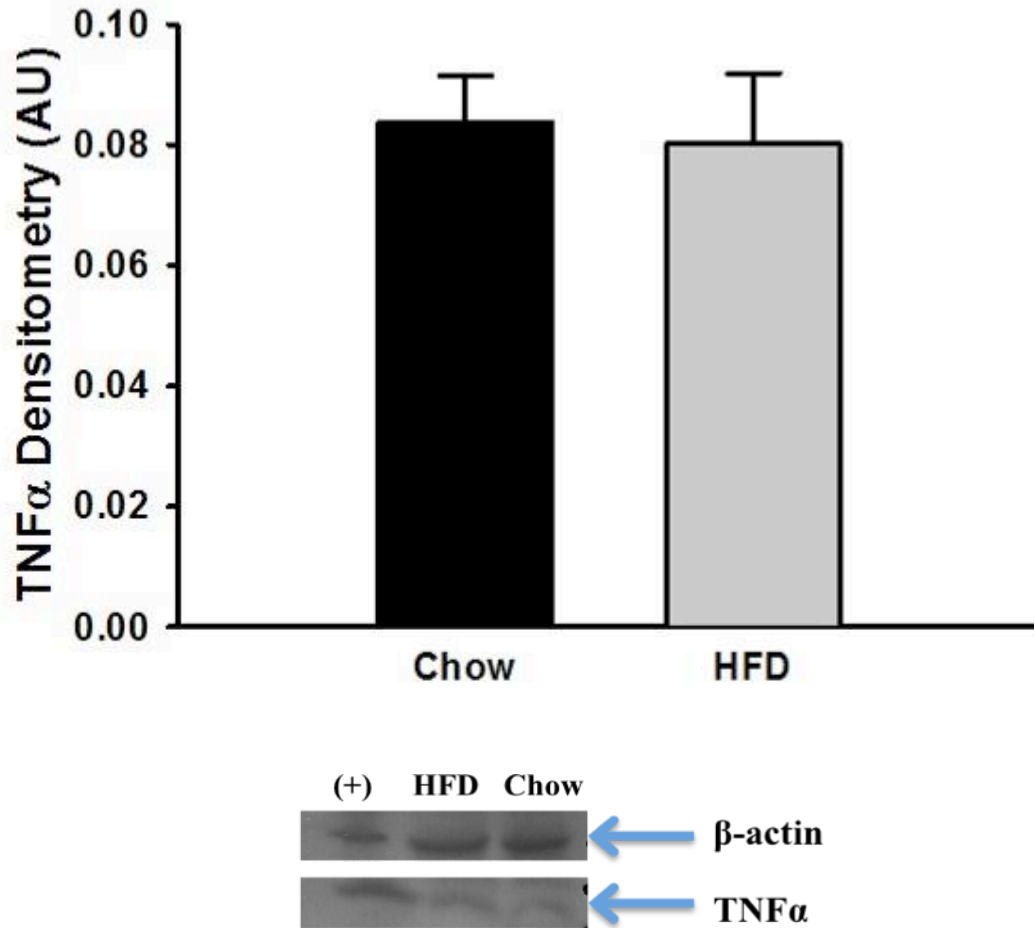


Figure 18 – Renal tissue TNF α protein expression in chow and HFD rats. There was no difference in the TNF α expression of the two diet groups ($n = 8/\text{group}$). A positive control (+) was used to demonstrate the accuracy of antibody detection and is demonstrated in the first column. The HFD and Chow columns indicate the presence of TNF α and show no difference in the darkness of the bands. Data are expressed as means \pm SEM. $p = 0.803$.

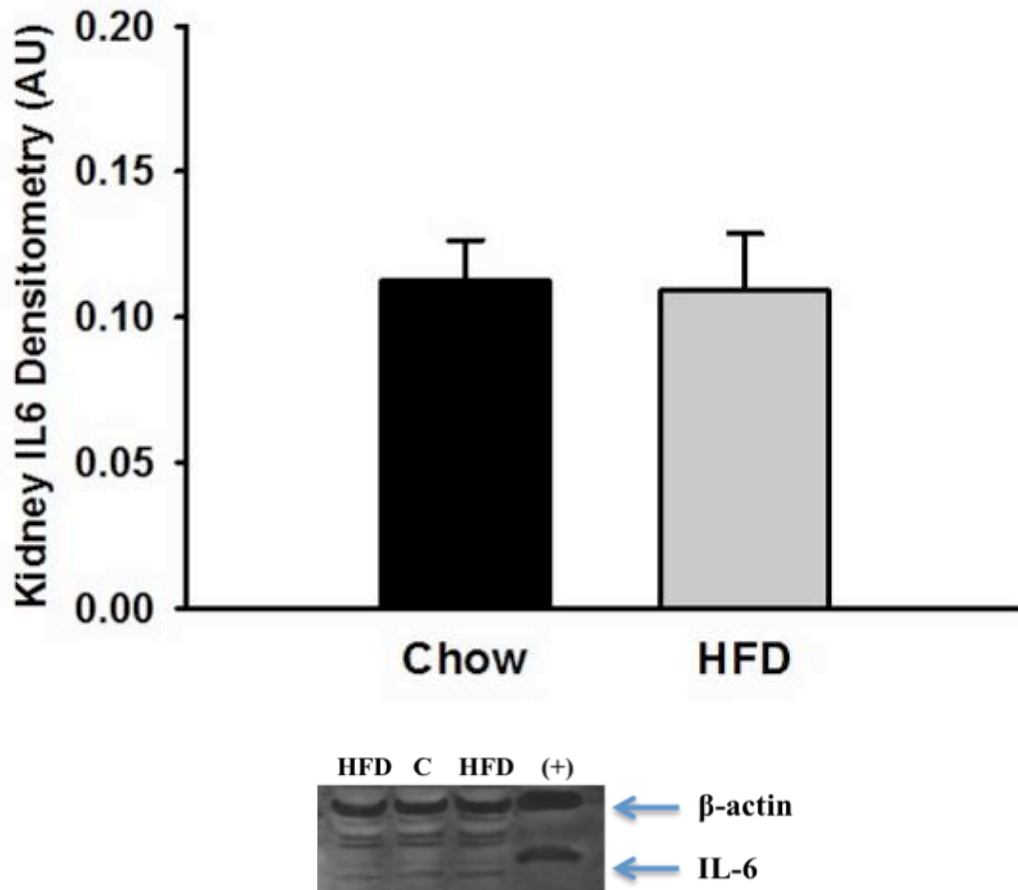


Figure 19 – Renal tissue IL-6 protein expression in chow and HFD rats. There was no difference in the IL-6 expression of the two diet groups (n = 5 chow and 6 HFD rats). A positive control (+) was used to demonstrate the accuracy of antibody detection and is demonstrated in the first column. The HFD and C (Chow) columns indicate the presence of IL-6 and show no difference in the darkness of the bands. Data are expressed as means \pm SEM. p = 0.903.

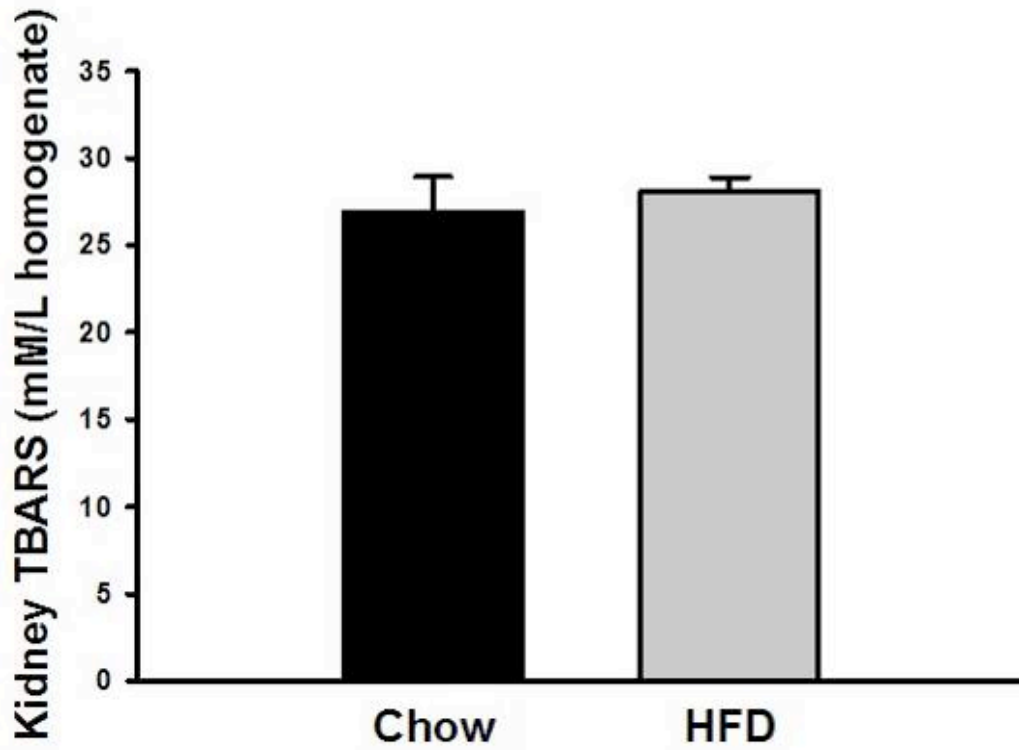


Figure 20 – Renal tissue TBARS in chow and HFD rats. There was no significant difference in the renal TBARS levels between the chow and HFD-fed rats (n = 5/group). Data are expressed as means \pm SEM. p = 0.600.

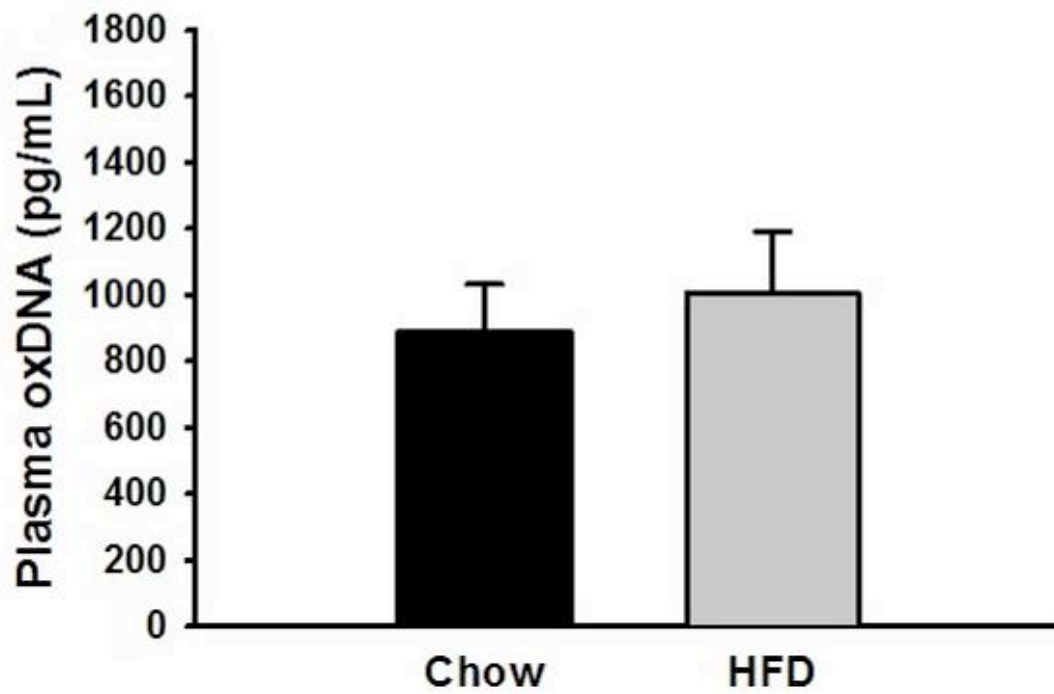


Figure 21 – Oxidative DNA damage in the plasma of chow and HFD-fed rats. Plasma concentrations of chow and HFD-fed rats were statistically equivalent (n = 10 - 11). Data are expressed as means \pm SEM. p = 0.634.

Table 2 – Summary of Descriptive Statistics

Variable	Mean±SEM (SD)	Normality†	Equal Variance†	P-value
Body Mass (g)				
<i>Chow</i> (n=9)	349.8±7.98 (23.9)	0.193 (P)	0.841 (P)	0.056
<i>HFD</i> (n=8)	376.4±10.3 (29.1)			
Tail Length (cm)				
<i>Chow</i> (n=9)	20.1±0.30 (0.91)	0.309 (P)	0.712 (P)	0.276
<i>HFD</i> (n=8)	20.6±0.32 (0.91)			
Waist Circumference (cm)				
<i>Chow</i> (n=9)	16.59±0.30 (0.89)	0.492 (P)	0.463 (P)	0.004*
<i>HFD</i> (n=8)	17.96±0.27 (0.78)			
Epididymal Fat Pad Mass (g)				
<i>Chow</i> (n=9)	3.49±0.18 (0.55)	0.693 (P)	0.308 (P)	<0.001*
<i>HFD</i> (n=8)	5.60±0.38 (1.08)			
Renal Mass (g)				
<i>Chow</i> (n=9)	1.05±0.04 (0.11)	0.608 (P)	0.898 (P)	0.019*
<i>HFD</i> (n=8)	1.19±0.04 (0.11)			
Urine Protein:Creatinine Ratio (AU)				
<i>Chow</i> (n=8)	6.01±2.86 (8.10)	<0.050	NA	0.574‡
<i>HFD</i> (n=8)	3.89±1.31 (3.71)			
Urine Creatinine (mg/L)				
<i>Chow</i> (n=8)	765.0±110.6 (312.8)	0.697 (P)	0.429 (P)	0.456
<i>HFD</i> (n=8)	900.3±137.4 (388.5)			
Urine Hydrogen Peroxide:Creatinine Ratio (AU)				
<i>Chow</i> (n=6)	0.014±0.002 (0.006)	0.192 (P)	0.129 (P)	0.142
<i>HFD</i> (n=6)	0.026±0.007 (0.018)			
Plasma Cystatin C (ug/mL)				
<i>Chow</i> (n=10)	14.35±0.99 (3.13)	0.671 (P)	0.990 (P)	0.233
<i>HFD</i> (n=10)	16.20±1.12 (3.54)			
TNFα Protein Expression (AU)				
<i>Chow</i> (n=8)	0.084±0.008 (0.02)	0.368 (P)	0.230 (P)	0.803
<i>HFD</i> (n=8)	0.080±0.012 (0.03)			
IL-6 Protein Expression (AU)				
<i>Chow</i> (n=5)	0.112±0.014 (0.031)	0.747 (P)	0.372 (P)	0.903
<i>HFD</i> (n=6)	0.109±0.019 (0.048)			
Renal TBARS (mM/L)				
<i>Chow</i> (n=5)	26.90±2.02 (4.52)	0.400 (P)	0.138 (P)	0.600
<i>HFD</i> (n=5)	28.08±0.80 (1.79)			
Plasma oxidative DNA (pg/mL)				
<i>Chow</i> (n=10)	887±145 (456)	0.676 (P)	0.176 (P)	0.634
<i>HFD</i> (n=11)	1003±188 (626)			

†P = passed

‡Mann-Whitney U

* p ≤ 0.05

CHAPTER 5

DISCUSSION

Young male Sprague-Dawley rats (1.5 months old) fed a HFD (60% fat) for six weeks demonstrated significant increases in waist circumference and epididymal fat pad mass along with elevated, though not significant, body mass (Figures 7-9). It is believed that had the sample size included additional animals, a statistically significant difference in body mass may have been found as well. Epididymal fat pad mass was used to determine variations in adiposity between HFD and chow-fed rats because the epididymal fat pad can be easily removed from the animal without introducing bias that could result from attempting to collect visceral or retroperitoneal fat. Tail length is a marker of overall animal growth; there was no difference in the tail lengths of the animals on the HFD and chow diets (Figure 10).

These data also indicate that the rats used for the present study can be classified as a model of increased adiposity. The development of an animal model that mimics the effects of metabolic syndrome and pre-diabetes was crucial to the interpretation of all subsequent results and is consistent with prior studies of HFD intake by both mice and rats [3,4,19,31,32,59,65,77,81]. Previous studies completed on HFD and chow fed rats in the Sweazea laboratory also demonstrated that these rats had high blood glucose concentrations, impaired glucose tolerance, hypertension, endothelial dysfunction, oxidative stress and inflammation, indicating that the HFD rats are also a model of metabolic syndrome [6,7].

The mean renal mass of the HFD rats was significantly higher than the chow-fed rats (Figure 11). The lack of difference in the tail lengths of the same sample of rats

(Figure 10) signifies that the increased mass was not caused by overall growth and instead indicates structural damage to the kidneys. Altunaynak et al. (2008) found similar results in rats fed a HFD (30% fat) for 12 weeks. These rats became overweight and showed increased kidney mass. The damaging effects of hyperglycemia can explain the increases in renal mass with a HFD [4]. The proliferation and hypertrophy of mesangial cells along with the thickening of the glomerular basement membrane would increase the overall mass of the kidney [11,12,39]. Additionally, increased levels of angiotensin II, caused by the inappropriate activation of the RAAS, can cause fibrosis, in addition to the increased secretion of pro-inflammatory cytokines [18,22,41]. Other explanations include vasodilation, inflammation and connective tissue enlargement [4].

Despite the increases in overall kidney mass, and the hypothesis that the kidneys were damaged by the HFD, hematoxylin and eosin staining of the kidneys showed no evidence of morphological damage (Figure 12). HFDs with longer feeding protocols have been found to cause morphological renal changes such as: glomerular capillary dilation, enlarged lumens in the tubules and Bowman's capsule, amassing of extracellular proteins, nephron degradation, glomerular membrane thickening, glomerulosclerosis, renal and tubular interstitial cell necrosis, and shortened tubular epitheliums [3,4,18]. Therefore, a longer feeding protocol may have allowed for observable renal structural damage.

The accumulation of lipids in renal tissue has been associated with the pathogenesis of CKD in animal models [30,37]. There was also no evidence of fat infiltration into the kidneys of animals examined in the present study (Figure 13), indicating that the kidneys of the HFD rats were able to resist fat infiltration despite

increases in visceral adiposity, elevation of plasma TNF α , and hepatic steatosis [6,7]. Kume et al. (2007) fed mice a HFD of 45% fat; after developing insulin resistance at week four, renal steatosis was evident at week eight, two weeks after the six week protocol in this study. Although lipid infiltration caused by HFD feedings are evident in the literature, Stemmer et al. (2012) found that despite significant morphological damage to the kidneys, 2-month-old male Wistar rats fed a HFD (40% fat) for eleven months did not show signs of triglyceride accumulation in the kidney, a finding similar to this study [30]. Stemmer et al. (2012) suggest that factors other than lipotoxicity caused by the high fat feedings may be involved in renal pathology [30].

Proteinuria indicates that the filtering ability of the glomerulus is compromised and is allowing proteins, which normally remain in the blood, to be passed through the filtration membrane and into the urine. In evaluating renal function, the protein albumin is sometimes specifically examined; however, by studying total protein excretion, a wider picture of filtration ability can be ascertained. Proteinuria, specifically, can be used as a marker of endothelial dysfunction as well as a surrogate outcome for renal disease progression. Urinary protein concentrations were normalized to urinary creatinine concentrations in order to account for variations in urine output [82]. Creatinine is also filtered by the kidneys and was therefore evaluated for differences between the HFD and chow-fed groups. Ruggiero et al. (2011) found no significant changes in creatinine levels after C57BL mice consumed a 45% fat diet for sixteen weeks; the authors felt this indicated early stages of renal damage without severe renal functional damage (Figure 15). In the present study, no statistically significant differences were observed between the urinary protein to creatinine ratio for animals ingesting either the chow or HFD

(Figure 14), indication that the filtration abilities of the glomeruli were not damaged by the HFD or at least not to the extent of allowing large proteins to be excreted. With additional feeding time, research suggests that the HFD may have increased blood glucose concentrations that would increase stress on the kidneys.

Plasma cystatin C is considered a marker of early renal dysfunction and the lack of difference between the cystatin C concentrations of the HFD and chow-fed rats indicates that the six week feeding protocol may not have been long enough to initiate functional renal damage (Figure 16). The HFD group did develop higher concentrations of plasma cystatin C, however this difference was not statistically significant (p-value = 0.142). Although cystatin C levels in plasma have been shown to be an early sensitive marker of renal dysfunction, these results indicate that the kidneys of the HFD-fed rats were not damaged enough so as to prevent cystatin C from being filtered normally by the nephrons [54,55,57,83].

H_2O_2 is an early marker of oxidative stress and inflammation. Hypertension associated with obesity has been shown to increase H_2O_2 via RAAS activation and angiotensin II secretion [60,61]. Despite the increased renal perfusion pressure that is associated with hypertension and which elevates H_2O_2 excretion, there was no significant difference in urinary H_2O_2 between the two groups (Figure 17). Urinary H_2O_2 was initially elevated in the HFD-rats but once H_2O_2 levels were normalized to creatinine, the significance was lost. A true elevation in H_2O_2 in the HFD group would have indicated early renal damage, as H_2O_2 has been found to be elevated prior to GFR decline, proteinuria, and more robust inflammatory and fibrotic responses following high fat feedings [59,64,65]. Overall, these results demonstrate that although prior studies indicate

that the HFD rats develop plasma and vascular oxidative stress and inflammation in addition to endothelial dysfunction, they were not sufficient to impair renal function [6,7].

Both ELISA and Western Blot analyses established no difference between the TNF α concentrations of renal tissue (Figure 18). These results corroborate each other and confirm that there was no increase in renal TNF α , a marker of inflammation. Although increased TNF α expression in adipose tissue has been shown to promote insulin resistance in overweight and obese rodent models, there was no indication that the HFD caused either fat infiltration into the kidneys or an increase in renal tissue expression of this inflammatory cytokine [84,85]. There was also no increase in IL-6 expression, another a pro-inflammatory cytokine, which also confirms the lack of observed renal fat infiltration (Figure 19). Adipocyte infiltration would likely have resulted in cytokine expression. Other experimental models of renal injury indicate that increases in IL-6 secretion are not necessarily an integral step in progressive renal failure [86]. Overall, the lack of significant findings in markers of early renal dysfunction, such as proteinuria and urinary H₂O₂, support the lack of increases in cytokine expression.

Previous studies completed in the Sweazea laboratory demonstrated that plasma TBARS, as a measure of whole body oxidative stress, was increased in the HFD-fed rats. Despite the plasma TBARS increases, renal tissue TBARS showed no indication of lipid peroxidation or oxidative stress (Figure 20). These results indicate that although the HFD rats exhibited generalized oxidative stress, oxidative stress within the kidneys is not yet present. Moreover, no significant difference in oxidative DNA/RNA damage between the experimental and control groups was observed (Figure 21). Lipid peroxidation levels,

examined via TBARS, and DNA/RNA oxidation, have been shown to have a strong positive correlation [49,50]. The lack of TNF α and IL-6 expression in renal tissue supports the lack of oxidative stress within the kidneys as inflammation and oxidative stress have been shown to exacerbate each other [48].

In conclusion, aside from morphological data points, the only statistically significant finding in this study was an increase in renal mass following a six week HFD. It is understood that the study protocol may not have been long enough to cause significant renal damage. This study is novel in that it is the first to examine the results of a six week HFD; prior to this study, the shortest feeding protocol that is evident in the literature is eight weeks. The resilience of the kidneys is made evident by the lack of damage after a 60% lard diet. Previous studies conducted in the Sweazea laboratory on rats fed a HFD for six weeks have found evidence of significant vascular damage, endothelial dysfunction, increased blood glucose concentrations, and liver steatosis [6,7]. The infiltration of lipids into the liver but not the kidneys indicates the strength of the kidneys. Since the kidneys are designed to filter wastes from the body, the resilience seen in this study is understandable. The increasing rates of CKD demonstrate how prolonged poorly controlled diabetes must be to cause significant renal damage.

REFERENCES

1. **National diabetes fact sheet: national estimates and general information on diabetes and prediabetes in the United States** [<http://www.cdc.gov/diabetes/pubs/factsheet11.htm>].
2. **National Chronic Kidney Disease Fact Sheet: General Information and National Estimates on Chronic Kidney Disease in the United States** [<http://www.cdc.gov/diabetes/pubs/factsheets/kidney.htm>].
3. Deji N, Kume S, Araki S, Soumura M, Sugimoto T, Isshiki K, Chin-kanasaki M, Sakaguchi M, Koya D, Haneda M, Kashiwagi A, Uzu T, Sakaguchi M, Koya D, Haneda M: **Structural and functional changes in the kidneys of high-fat diet-induced obese mice.** *Am J Physiol Renal Physiol* 2009, **118**:118-126.
4. Altunkaynak ME, Ozbek E, Altunkaynak BZ, Can I, Unal D, Unal B: **The effects of high-fat diet on the renal structure and morphometric parametric of kidneys in rats.** *J Anat* 2008, **212**:845-852.
5. Cao W, Zhou QG, Nie J, Wang GB, Liu Y, Zhou ZM, Hou FF: **Albumin overload activates intrarenal renin-angiotensin system through protein kinase C and NADPH oxidase-dependent pathway.** *J Hypertens* 2011, **29**:1411-1421.
6. Sweazea KL, Lekic M, Walker BR: **Comparison of mechanisms involved in impaired vascular reactivity between high sucrose and high fat diets in rats.** *Nutr Metab (Lond)* 2010, **7**:48-7075-7-48.
7. Sweazea KL, Walker BR: **High fat feeding impairs endothelin-1 mediated vasoconstriction through increased iNOS-derived nitric oxide.** *Horm Metab Res* 2011, **43**:470-476.
8. Reutens A: **Epidemiology of Diabetic Kidney Disease.** *Med Clin North Am* 2013, **97**:1-18.
9. Maahs DM, Bushman L, Kerr B, Ellis SL, Pyle L, McFann K, Bouffard A, Bishop FK, Nguyen N, Anderson PL: **A practical method to measure GFR in people with type 1 diabetes.** *J Diabetes Complications* 2014, **28**:667-673.
10. **Your Kidneys and How They Work** [<http://www.webmd.com/a-to-z-guides/function-kidneys>].
11. Harris RD, Steffes MW, Bilous RW, Sutherland DE, Mauer SM: **Global glomerular sclerosis and glomerular arteriolar hyalinosis in insulin dependent diabetes.** *Kidney Int* 1991, **40**:107-114.

12. Heilig CW, Concepcion LA, Riser BL, Freytag SO, Zhu M, Cortes P: **Overexpression of glucose transporters in rat mesangial cells cultured in a normal glucose milieu mimics the diabetic phenotype.** *J Clin Invest* 1995, **96**:1802-1814.
13. Singh AK, Mo W, Dunea G, Arruda JA: **Effect of glycated proteins on the matrix of glomerular epithelial cells.** *J Am Soc Nephrol* 1998, **9**:802-810.
14. Yamagishi S, Fukami K, Ueda S, Okuda S: **Molecular mechanisms of diabetic nephropathy and its therapeutic intervention.** *Curr Drug Targets* 2007, **8**:952-959.
15. Porte D, Jr, Schwartz MW: **Diabetes complications: why is glucose potentially toxic?** *Science* 1996, **272**:699-700.
16. Keane WF, Eknoyan G: **Proteinuria, albuminuria, risk, assessment, detection, elimination (PARADE): a position paper of the National Kidney Foundation.** *Am J Kidney Dis* 1999, **33**:1004-1010.
17. Levey AS, Cattran D, Friedman A, Miller WG, Sedor J, Tuttle K, Kasiske B, Hostetter T: **Proteinuria as a surrogate outcome in CKD: report of a scientific workshop sponsored by the National Kidney Foundation and the US Food and Drug Administration.** *Am J Kidney Dis* 2009, **54**:205-226.
18. Thethi T, Kamiyama M, Kobori H: **The Link Between the Renin-Angiotensin-Aldosterone System and Renal Injury in Obesity and the Metabolic Syndrome.** *Curr Hypertens Rep* 2012, **14**:160-169.
19. Ozay R, Uzar E, Aktas A, Uyar ME, Gurer B, Evliyaoglu O, Cetinalp NE, Turkey C: **The role of oxidative stress and inflammatory response in high-fat diet induced peripheral neuropathy.** *J Chem Neuroanat* 2014, **55**:51-57.
20. Gluba A, Mikhailidis DP, Lip GY, Hannam S, Rysz J, Banach M: **Metabolic syndrome and renal disease.** *Int J Cardiol* 2013, **164**:141-150.
21. de Castro, Uberdan Guilherme Mendes, Dos Santos, Robson Augusto Souza, Silva ME, de Lima WG, Campagnole-Santos MJ, Alzamora AC: **Age-dependent effect of high-fructose and high-fat diets on lipid metabolism and lipid accumulation in liver and kidney of rats.** *Lipids Health Dis* 2013, **12**:136.
22. Ruster C, Wolf G: **The role of the renin-angiotensin-aldosterone system in obesity-related renal diseases.** *Semin Nephrol* 2013, **33**:44-53.
23. Foster MC, Hwang S, Porter SA, Massaro JM, Hoffmann U, Fox CS: **Fatty kidney, hypertension, and chronic kidney disease: the Framingham Heart Study.** *Hypertension* 2011, **58**:784-790.

24. Tramonti G, Kanwar YS: **Review and discussion of tubular biomarkers in the diagnosis and management of diabetic nephropathy.** *Endocrine* 2013, **43**:494-503.
25. Von Diemen V, Trindade EN, Trindade MR: **Experimental model to induce obesity in rats.** *Acta Cir Bras* 2006, **21**:425-429.
26. Chalmers L, Kaskel F, Bamgbola O: **The role of obesity and its biochemical correlates in the progression of chronic kidney disease.** *Adv Chronic Kidney Dis* 2006, **4**:352-364.
27. Ruster C, Wolf G: **Adipokines promote chronic kidney disease.** *Nephrol Dial Transplant* 2013, **28 Suppl 4**:8-14.
28. Klein S: **The case of visceral fat: argument for the defense.** *J Clin Invest* 2004, **113**:1530-1532.
29. Jensen MD: **Role of body fat distribution and the metabolic complications of obesity.** *J Clin Endocrinol Metab* 2008, **93**:S57-63.
30. Stemmer K, Perez-Tilve D, Ananthakrishnan G, Bort A, Seeley RJ, Tschop MH, Dietrich DR, Pfluger PT: **High-fat-diet-induced obesity causes an inflammatory and tumor-promoting microenvironment in the rat kidney.** *Dis Model Mech* 2012, **5**:627-635.
31. Ruggiero C, Ehrenshaft M, Cleland E, Stadler K: **High-fat diet induces an initial adaptation of mitochondrial bioenergetics in the kidney despite evident oxidative stress and mitochondrial ROS production.** *Am J Physiol Endocrinol Metab* 2011, **300**:E1047-58.
32. Borst SE, Conover CF: **High-fat diet induces increased tissue expression of TNF-alpha.** *Life Sci* 2005, **77**:2156-2165.
33. Tbahriti HF, Meknassi D, Moussaoui R, Messaoudi A, Zemour L, Kaddous A, Bouchenak M, Mekki K: **Inflammatory status in chronic renal failure: The role of homocysteinemia and pro-inflammatory cytokines.** *World J Nephrol* 2013, **2**:31-37.
34. Dwyer TM, Mizelle HL, Cockrell K, Buhner P: **Renal sinus lipomatosis and body composition in hypertensive, obese rabbits.** *Int J Obes Relat Metab Disord* 1995, **19**:869-874.
35. Montani JP, Carroll JF, Dwyer TM, Antic V, Yang Z, Dulloo AG: **Ectopic fat storage in heart, blood vessels and kidneys in the pathogenesis of cardiovascular diseases.** *Int J Obes Relat Metab Disord* 2004, **28 Suppl 4**:S58-65.

36. Chughtai HL, Morgan TM, Rocco M, Stacey B, Brinkley TE, Ding J, Nicklas B, Hamilton C, Hundley WG: **Renal sinus fat and poor blood pressure control in middle-aged and elderly individuals at risk for cardiovascular events.** *Hypertension* 2010, **56**:901-906.
37. Kume S, Uzu T, Araki S, Sugimoto T, Isshiki K, Chin-Kanasaki M, Sakaguchi M, Kubota N, Terauchi Y, Kadowaki T, Haneda M, Kashiwagi A, Koya D: **Role of altered renal lipid metabolism in the development of renal injury induced by a high-fat diet.** *J Am Soc Nephrol* 2007, **18**:2715-2723.
38. Ejerblad E, Fored C, Lindblad P: **Obesity and risk for chronic renal failure.** 2006.
39. Obineche EN, Mensah-Brown E, Chandranath SI, Ahmed I, Naseer O, Adem a: **Morphological changes in the rat kidney following long-term diabetes.** *Arch Physiol Biochem* 2001, **109**:241-245.
40. Tang S, Leung JC, Abe K, Chan KW, Chan LY, Chan TM, Lai KN: **Albumin stimulates interleukin-8 expression in proximal tubular epithelial cells in vitro and in vivo.** *J Clin Invest* 2003, **111**:515-527.
41. Shatanawi A, Romero MJ, Iddings JA, Chandra S, Umopathy NS, Verin AD, Caldwell RB, Caldwell RW: **Angiotensin II-induced vascular endothelial dysfunction through RhoA/Rho kinase/p38 mitogen-activated protein kinase/arginase pathway.** *Am J Physiol Cell Physiol* 2011, **300**:C1181-92.
42. Poulsen HE, Nadal LL, Broedbaek K, Nielsen PE, Weimann A: **Detection and interpretation of 8-oxodG and 8-oxoGua in urine, plasma and cerebrospinal fluid.** *Biochim Biophys Acta* 2013, 4-11.
43. Ozbek E: **Induction of oxidative stress in kidney.** *Int J Nephrol* 2012, **2012**:465897.
44. Ll'yasova D, Scarbrough P, Spasojevic I: **Urinary Biomarkers of Oxidative Status.** *Clin Chim Acta* 2012, **413**:1446-1453.
45. Noeman SA, Hamooda HE, Baalash AA: **Biochemical study of oxidative stress markers in the liver, kidney and heart of high fat diet induced obesity in rats.** *Diabetol Metab Syndr* 2011, **3**:17-5996-3-17.
46. Stoyanova E, Sandoval SB, Zuniga LA, El-Yamani N, Coll E, Pastor S, Reyes J, Andres E, Ballarin J, Xamena N, Marcos R: **Oxidative DNA damage in chronic renal failure patients.** *Nephrol Dial Transplant* 2010, **25**:879-885.
47. Park KS, Kim JH, Kim MS, Kim JM, Kim SK, Choi JY, Chung MH, Han B, Kim SY, Lee HK: **Effects of insulin and antioxidant on plasma 8-hydroxyguanine and**

- tissue 8-hydroxydeoxyguanosine in streptozotocin-induced diabetic rats. *Diabetes* 2001, **50**:2837-2841.
48. Vincent HK, Taylor AG: **Biomarkers and potential mechanisms of obesity-induced oxidant stress in humans.** *Int J Obes (Lond)* 2006, **30**:400-418.
49. Kato A, Odamaki M, Hishida A: **Blood 8-hydroxy-2'-deoxyguanosine is associated with erythropoietin resistance in haemodialysis patients.** *Nephrol Dial Transplant* 2003, **18**:931-936.
50. Kaya Y, Cebi A, Soylemez N, Demir H, Alp HH, Bakan E: **Correlations between oxidative DNA damage, oxidative stress and coenzyme Q10 in patients with coronary artery disease.** *Int J Med Sci* 2012, **9**:621-626.
51. McNamara NV, Chen R, Janu MR, Bwititi P, Car G, Seibel M: **Early renal failure detection by cystatin C in Type 2 diabetes mellitus: varying patterns of renal analyte expression.** *Pathology* 2009, **41**:269-275.
52. Grubb A: **Diagnostic value of analysis of cystatin C and protein HC in biological fluids.** *Clin Nephrol* 1992, **38 Suppl 1**:S20-S27.
53. Sirota JC, Klawitter J, Edelstein CL: **Biomarkers of acute kidney injury.** *J Toxicol* 2011, **2011**:328120.
54. Chew J, Saleem M, Florkowski CM, George PM: **Cystatin C: A Paradigm of Evidence Based Laboratory Medicine.** *Clin Biochem Rev* 2008, **29**:47-62.
55. Chew-Harris J: **The relative effects of fat versus muscle mass on cystatin C and estimates of renal function in healthy young men.** *Ann Clin Biochem* 2013, **50**:39-46.
56. Dharnidharka VR, Kwon C, Stevens G: **Serum cystatin C is superior to serum creatinine as a marker of kidney function: a meta-analysis.** *Am J Kidney Dis* 2002, **40**:221-226.
57. Hojs R, Bevc S, Ekart R, Gorenjak M, Puklavec L: **Serum cystatin C as an endogenous marker of renal function in patients with chronic kidney disease.** *Ren Fail* 2008, **30**:181-186.
58. Schuck O, Teplan V, Stollova M, Skibova J: **Estimation of glomerular filtration rate in obese patients with chronic renal impairment based on serum cystatin C levels.** *Clin Nephrol* 2004, **62**:92-96.
59. Decleves AE, Rychak JJ, Smith DJ, Sharma K: **Effects of high-fat diet and losartan on renal cortical blood flow using contrast ultrasound imaging.** *Am J Physiol Renal Physiol* 2013, **305**:F1343-51.

60. Banerjee D, Madhusoodanan UK, Nayak S, Jacob J: **Urinary hydrogen peroxide: a probable marker of oxidative stress in malignancy.** *Clin Chim Acta* 2003, **334**:205-209.
61. Halliwell B, Clement MV, Long LH: **Hydrogen peroxide in the human body.** *FEBS Lett* 2000, **486**:10-13.
62. Jin C, Hu C, Polichnowski A, Mori T, Skelton M, Ito S, Cowley AW, Jr: **Effects of renal perfusion pressure on renal medullary hydrogen peroxide and nitric oxide production.** *Hypertension* 2009, **53**:1048-1053.
63. Patinha D, Afonso J, Sousa T, Morato M, Albino-Teixeira A: **Diabetes-induced increase of renal medullary hydrogen peroxide and urinary angiotensinogen is similar in normotensive and hypertensive rats.** *Life Sci* 2014, **108**:71-79.
64. Yoshioka T, Ichikawa I, Fogo A: **Reactive oxygen metabolites cause massive, reversible proteinuria and glomerular sieving defect without apparent ultrastructural abnormality.** *J Am Soc Nephrol* 1991, **2**:902-912.
65. Decleves AE, Mathew AV, Cunard R, Sharma K: **AMPK mediates the initiation of kidney disease induced by a high-fat diet.** *J Am Soc Nephrol* 2011, **22**:1846-1855.
66. Ramos EJ, Xu Y, Romanova I, Middleton F, Chen C, Quinn R, Inui A, Das U, Meguid MM: **Is obesity an inflammatory disease?** *Surgery* 2003, **134**:329-335.
67. Warnberg J, Cunningham K, Romeo J, Marcos A: **Physical activity, exercise and low-grade systemic inflammation.** *Proc Nutr Soc* 2010, **69**:400-406.
68. Pedersen BK, Febbraio MA: **Muscle as an endocrine organ: focus on muscle-derived interleukin-6.** *Physiol Rev* 2008, **88**:1379-1406.
69. Petersen AM, Pedersen BK: **The anti-inflammatory effect of exercise.** *J Appl Physiol (1985)* 2005, **98**:1154-1162.
70. Brandt C, Pedersen BK: **The role of exercise-induced myokines in muscle homeostasis and the defense against chronic diseases.** *J Biomed Biotechnol* 2010, **2010**:520258.
71. Ramseyer VD, Garvin JL: **Tumor necrosis factor-alpha: regulation of renal function and blood pressure.** *Am J Physiol Renal Physiol* 2013, **304**:F1231-42.
72. Reungjui S, Roncal Ca, Sato W, Glushakova OY, Croker BP, Suga S, Ouyang X, Tungsanga K, Nakagawa T, Johnson RJ, Mu W: **Hypokalemic nephropathy is associated with impaired angiogenesis.** *J Am Soc Nephrol* 2008, **19**:125-134.

73. Kern PA, Ranganathan S, Li C, Wood L, Ranganathan G: **Adipose tissue tumor necrosis factor and interleukin-6 expression in human obesity and insulin resistance.** *Am J Physiol Endocrinol Metab* 2001, **280**:E745-51.
74. Fenkci S, Rota S, Sabir N, Sermez Y, Guclu A, Akdag B: **Relationship of serum interleukin-6 and tumor necrosis factor alpha levels with abdominal fat distribution evaluated by ultrasonography in overweight or obese postmenopausal women.** *J Investig Med* 2006, **54**:455-460.
75. Lamas O, Martinez JA, Marti A: **Decreased splenic mRNA expression levels of TNF-alpha and IL-6 in diet-induced obese animals.** *J Physiol Biochem* 2004, **60**:279-283.
76. Buettner R, Parhofer KG, Woenckhaus M, Wrede CE, Kunz-Schughart LA, Scholmerich J, Bollheimer LC: **Defining high-fat-diet rat models: metabolic and molecular effects of different fat types.** *J Mol Endocrinol* 2006, **36**:485-501.
77. Stark AH, Timar B, Madar Z: **Adaptation of Sprague Dawley rats to long-term feeding of high fat or high fructose diets.** *Eur J Nutr* 2000, **39**:229-234.
78. Pranprawit A, Wolber FM, Heyes Ja, Molan AL, Kruger MC: **Short-term and long-term effects of excessive consumption of saturated fats and/or sucrose on metabolic variables in Sprague Dawley rats: a pilot study.** *J Sci Food Agric* 2013, **93**:3191-3197.
79. Jiao K, Liu H, Chen J, Tian D, Hou J, Kaye AD: **Roles of plasma interleukin-6 and tumor necrosis factor-alpha and FFA and TG in the development of insulin resistance induced by high-fat diet.** *Cytokine* 2008, **42**:161-169.
80. Gonzalez Bosc L, Kurnjek ML, Muller A, Basso N: **Effect of chronic angiotensin II inhibition on the cardiovascular system of the normal rat.** *Am J Hypertens* 2000, **13**:1301-1307.
81. Cortez M, Carmo LS, Rogero MM, Borelli P, Fock RA: **A high-fat diet increases IL-1, IL-6, and TNF-alpha production by increasing NF-kappaB and attenuating PPAR-gamma expression in bone marrow mesenchymal stem cells.** *Inflammation* 2013, **36**:379-386.
82. Waikar SS, Sabbiseti VS, Bonventre JV: **Normalization of urinary biomarkers to creatinine during changes in glomerular filtration rate.** *Kidney Int* 2010, **78**:486-494.
83. Amin I: **Novel Renal Biomarker Cystatin C for Diagnosis of Impaired Renal Function for Uncontrolled Iraqi Diabetics.** *J Adv Med Research* 2013, **3**:10.

84. Hotamisligil GS, Shargill NS, Spiegelman BM: **Adipose expression of tumor necrosis factor-alpha: direct role in obesity-linked insulin resistance.** *Science* 1993, **259**:87-91.
85. Cawthorn WP, Sethi JK: **TNF-alpha and adipocyte biology.** *FEBS Lett* 2008, **582**:117-131.
86. Jones SA, Fraser DJ, Fielding CA, Jones GW: **Interleukin-6 in renal disease and therapy.** *Nephrol Dial Transplant* 2014.

APPENDIX A

HIGH FAT DIET COMPONENTS – D12492



Product Data - DIO SERIES DIETS

Report ▶ Repeat ▶ Revise

The "Original" High-Fat Diets for Diet Induced Obesity

Formulated by E. A. Ulman, Ph.D., Research Diets, Inc., 8/26/98 and 3/11/99.

Research Diets, Inc. formulated the "original" high-fat diet for diet induced obesity (DIO) studies in 1996. Today, our high-fat diets are the research standard for DIO mice and rats worldwide.



DIO Low-Fat Control Diets

Matched, Purified Ingredient Diet

We recommend that you use a matched, purified ingredient diet and not a grain-based 'chow' diet. There are many, many differences between purified diets and chow diets and these variables make it difficult to interpret your data from a study in which one group was fed a purified ingredient high-fat and the other a low-fat chow diet. Differences between your groups could be due to the level of fat, but could also be due to differences in fiber type and level, source of carbohydrate, and the presence or absence of plant chemicals (such as phytoestrogens), just to name a few.

See next page for low-fat control formulas.

(DIO) Formulas

Product #	D12451		D12492	
	gm%	kcal%	gm%	kcal%
Protein	24	20	26	20
Carbohydrate	41	35	26	20
Fat	24	45	35	60
Total		100		100
kcal/gm	4.73		5.24	
Ingredient	gm	kcal	gm	kcal
Casain, 30 Mesh	200	800	200	800
L-Cystine	3	12	3	12
Corn Starch	72.8	291	0	0
Maltodextrin 10	100	400	125	500
Sucrose	172.8	691	68.8	275
Cellulose, BW200	50	0	50	0
Soybean Oil	25	225	25	225
Lard	177.5	1598	245	2205
Mineral Mix S10026	10	0	10	0
DiCalcium Phosphate	13	0	13	0
Calcium Carbonate	5.5	0	5.5	0
Potassium Citrate, 1 H2O	16.5	0	16.5	0
Vitamin Mix V10001	10	40	10	40
Choline Bitartrate	2	0	2	0
FD&C Red Dye #40	0.05	0		
FD&C Blue Dye #1			0.05	0
Total	858.15	4057	773.85	4057

*Typical analysis of cholesterol in lard = 72 mg per 100 gram.

D12451 -
Cholesterol (mg)/4057 kcal = 167.8
Cholesterol (mg)/kg = 195.5

D12492 -
Cholesterol (mg)/4057 kcal = 216.4
Cholesterol (mg)/kg = 279.6



www.ResearchDiets.com
Where NutriPhenomics Begins





Mineral Mix S10026

Formulated by:
E.A. Ulman, Ph.D.
Research Diets, Inc.
January 18, 1996

***Mineral Mix for DIO Series Diets**

Use at 10 gm/kg diet or 10 gm/ 4000 kcal digestible energy.

Ingredient	gm	Amt in 10 gm	
Sodium Chloride 39.3% Na 60.7% Cl	259	1.0 gm	Na
		1.6 gm	Cl
Magnesium Oxide, Heavy, DC USP 60.3% Mg	41.9	0.5 gm	Mg
Magnesium Sulfate, Heptahydrate 9.87% Mg 13.0% S	257.6	0.33 gm	S
Ammonium Molybdate Tetrahydrate	0.3	1.6 mg	Mo
Chromium Potassium Sulfate 10.4% Cr	1.925	2.0 mg	Cr
Copper Carbonate 57.5% CU	1.05	6.0 mg	Cu
Ferric Citrate 17.4% Fe	21	37 mg	Fe
Manganese Carbonate Hydrate 47.8 Mn	12.25	59 mg	Mn
Potassium Iodate 59.3% I	0.035	0.2 mg	I
Sodium Fluoride 45.2% FI	0.2	0.9 mg	Fl
Sodium Selenite 45.7% Se	0.035	0.16 mg	Se
Zinc Carbonate 52.1% Zn	5.6	29 mg	Zn
Sucrose	399.105	3.9911	

TOTAL **1000**

**For Calcium, Phosphorus and Potassium amounts see DIO formula.*

Research Diets, Inc.
20 Jules Lane
New Brunswick, NJ 08901 USA
info@researchdiets.com

xS10026.xls





Vitamin Mix V10001

Formulated by:
 J. Nutr. 107:1340-1348, 1977
 j. Nutr. 110:1726, 1980

Vitamin Mix for AIN- 76A Rodent Diet
 Use at 10 gm/kg diet or 10 gm/ 4000 kcal digestible energy.

Ingredient	gm	Amt in 10 gm	
Vitamin A Acetate 500,000 IU/gm	0.8	4000 IU	Vit A
Vitamin D3 100,000 IU/gm	1	1000 IU	Vit D3
Vitamin E Acetate 500 IU/gm	10	50 IU	Vit E
Menadione Sodium Bisulfite 62.5% Menadione	0.08	0.5 mg	Menadione
Biotin, 1.0%	2	0.2 mg	Biotin
Cyanocobalamin, 0.1%	1	10 µg	Vit B12
Folic Acid	0.2	2 mg	Folic Acid
Nicotinic Acid	3	30 mg	Niacin
Calcium Pantothenate	1.6	16 mg	Pantothenic Acid
Pyridoxine-HCl	0.7	7 mg	Vit B6
Riboflavin	0.6	6 mg	Vit B2
Thiamin HCl	0.6	6 mg	Vit B1
Sucrose	978.42		
TOTAL	1000		

Research Diets, Inc.
 20 Jules Lane
 New Brunswick, NJ 08901 USA
 info@researchdiets.com

xV10001.xls



APPENDIX B

STANDARD RODENT CHOW DIET COMPONENTS

Teklad Global 18% Protein Rodent Diet

Product Description- 2018 is a fixed formula, non-autoclavable diet manufactured with high quality ingredients and designed to support gestation, lactation, and growth of rodents. 2018 does not contain alfalfa, thus lowering the occurrence of natural phytoestrogens. Typical isoflavone concentrations (daidzein + genistein aglycone equivalents) range from 150 to 250 mg/kg. Exclusion of alfalfa reduces chlorophyll, improving optical imaging clarity. Absence of animal protein and fish meal minimizes the presence of nitrosamines. **Also available certified (2018C) and irradiated (2918). For autoclavable diet, refer to 2018S (Sterilizable) or 2018SX (Extruded & Sterilizable).**

Ingredients (in descending order of inclusion)- Ground wheat, ground corn, wheat middlings, dehulled soybean meal, corn gluten meal, soybean oil, calcium carbonate, dicalcium phosphate, brewers dried yeast, iodized salt, L-lysine, DL-methionine, choline chloride, kaolin, magnesium oxide, vitamin E acetate, menadione sodium bisulfite complex (source of vitamin K activity), manganous oxide, ferrous sulfate, zinc oxide, niacin, calcium pantothenate, copper sulfate, pyridoxine hydrochloride, riboflavin, thiamin mononitrate, vitamin A acetate, calcium iodate, vitamin B₁₂ supplement, folic acid, biotin, vitamin D₃ supplement, cobalt carbonate.

Macronutrients		
Crude Protein	%	18.6
Fat (ether extract) ^a	%	6.2
Carbohydrate (available) ^b	%	44.2
Crude Fiber	%	3.5
Neutral Detergent Fiber ^c	%	14.7
Ash	%	5.3
Energy Density ^d	kcal/g (kJ/g)	3.1 (13.0)
Calories from Protein	%	24
Calories from Fat	%	18
Calories from Carbohydrate	%	58
Minerals		
Calcium	%	1.0
Phosphorus	%	0.7
Non-Phytate Phosphorus	%	0.4
Sodium	%	0.2
Potassium	%	0.6
Chloride	%	0.4
Magnesium	%	0.2
Zinc	mg/kg	70
Manganese	mg/kg	100
Copper	mg/kg	15
Iodine	mg/kg	6
Iron	mg/kg	200
Selenium	mg/kg	0.23
Amino Acids		
Aspartic Acid	%	1.4
Glutamic Acid	%	3.4
Alanine	%	1.1
Glycine	%	0.8
Threonine	%	0.7
Proline	%	1.6
Serine	%	1.1
Leucine	%	1.8
Isoleucine	%	0.8
Valine	%	0.9
Phenylalanine	%	1.0
Tyrosine	%	0.6
Methionine	%	0.4
Cystine	%	0.3
Lysine	%	0.9
Histidine	%	0.4
Arginine	%	1.0
Tryptophan	%	0.2

Standard Product Form: Pellet

Vitamins		
Vitamin A ^{e, f}	IU/g	15.0
Vitamin D ₃ ^{e, g}	IU/g	1.5
Vitamin E	IU/kg	110
Vitamin K ₃ (menadione)	mg/kg	50
Vitamin B ₁ (thiamin)	mg/kg	17
Vitamin B ₂ (riboflavin)	mg/kg	15
Niacin (nicotinic acid)	mg/kg	70
Vitamin B ₆ (pyridoxine)	mg/kg	18
Pantothenic Acid	mg/kg	33
Vitamin B ₁₂ (cyanocobalamin)	mg/kg	0.08
Biotin	mg/kg	0.40
Folate	mg/kg	4
Choline	mg/kg	1200
Fatty Acids		
C16:0 Palmitic	%	0.7
C18:0 Stearic	%	0.2
C18:1ω9 Oleic	%	1.2
C18:2ω6 Linoleic	%	3.1
C18:3ω3 Linolenic	%	0.3
Total Saturated	%	0.9
Total Monounsaturated	%	1.3
Total Polyunsaturated	%	3.4
Other		
Cholesterol	mg/kg	--

^a Ether extract is used to measure fat in pelleted diets, while an acid hydrolysis method is required to recover fat in extruded diets. Compared to ether extract, the fat value for acid hydrolysis will be approximately 1% point higher.

^b Carbohydrate (available) is calculated by subtracting neutral detergent fiber from total carbohydrates.

^c Neutral detergent fiber is an estimate of insoluble fiber, including cellulose, hemicellulose, and lignin. Crude fiber methodology underestimates total fiber.

^d Energy density is a calculated estimate of *metabolizable energy* based on the Atwater factors assigning 4 kcal/g to protein, 9 kcal/g to fat, and 4 kcal/g to available carbohydrate.

^e Indicates added amount but does not account for contribution from other ingredients.

^f 1 IU vitamin A = 0.3 µg retinol

^g 1 IU vitamin D = 25 ng cholecalciferol

For nutrients not listed, insufficient data is available to quantify.

Nutrient data represent the best information available, calculated from published values and direct analytical testing of raw materials and finished product. Nutrient values may vary due to the natural variations in the ingredients, analysis, and effects of processing.

Teklad Diets are designed and manufactured for research purposes only.

Harlan, Harlan Laboratories, Helping you do research better, and the Harlan logo are trademarks and trade names of Harlan Laboratories, Inc. © 2008 Harlan Laboratories, Inc.



APPENDIX C

HEMATOXYLIN AND EOSIN STAIN PROTOCOL

Hematoxylin and Eosin Staining

1. Isolate tissues and embed in OCT
2. Freeze in isopentane cooled by dry ice or liquid nitrogen
3. Cut 10-15 μ m sections on cryostat and collect sections onto poly-lysine coated slides
4. Let sections air-dry for 10 minutes
5. Fix sections with 10% formalin for 10 minutes
6. Wash sections 3-4 times with tap water
7. Stain nuclei with filtered Harris Hematoxylin for 2-3 minutes
8. Wash slides with warm tap water several times until the nuclei turn blue
9. Differentiate: Rinse several dips in acid alcohol (0.5% HCl in 70% Ethanol)
10. Wash in ammonia water (0.25% ammonia hydroxide in deionized water) for 5 minutes until the nuclei turn blue
11. Rinse in deionized water
12. Stain the cytoplasm by dipping slides several times in Eosin, 3-5 minutes
13. Remove the excess Eosin with tap water
14. Coverslip with shurmount (water based mounting medium)

APPENDIX D
OIL RED O STAIN PROTOCOL



Instructions For Use ORK-1-IFU		
Rev. Date: July 5, 2011	Revision: 2	Page 1 of 2

P.O. Box 3286 - Logan, Utah 84323, U.S.A. - Tel. (800) 729-8350 – Tel. (435) 755-9848 - Fax (435) 755-0015 - www.scytek.com

Oil Red O Stain Kit (For Fat)

Description: Oil Red O Stain Kit (For Fat) is intended for use in the histological visualization of fat cells and neutral fat. This kit may be used **ONLY** on frozen tissue sections, fresh smears, or touch preps as xylenes and alcohols will dissolve fat deposits.

Fat Cells:	Red
Neutral Fat:	Red
Nuclei:	Blue

Uses/Limitations: Not to be taken internally.
 For In-Vitro Diagnostic use only.
 Histological applications.
 Do not use past expiration date.
 Use caution when handling reagents.
 Non-Sterile

Control Tissue: Any frozen section containing fat.

Availability/Contents:

<u>Item #</u>	<u>Kit Contents</u>	<u>Volume</u>	<u>Storage</u>
PRG500	Propylene Glycol	500 ml	18-25 °C
ORG125	Oil Red O Solution	125 ml	18-25 °C
HMM125	Hematoxylin, Mayer's (Lillie's Mod.)	125 ml	18-25 °C

Precautions: Keep away from open flame.
 Avoid contact with skin and eyes.
 Harmful if swallowed.
 Follow all Federal, State, and local regulations regarding disposal.
 Use in chemical fume hood whenever possible.

Procedure (Standard):


NOTE: Heat Oil Red O Solution to 60 °C prior to beginning.

1. Prepare fresh or frozen tissue section as usual.
2. Place slide in room temperature Propylene Glycol for 5 minutes.
3. Incubate slide in heated (60 °C) Oil Red O Solution for 6-10 minutes or overnight at room temperature.

Note: Prepare mixture of 85% Propylene Glycol in distilled water.

4. Differentiate tissue section in 85% Propylene Glycol for 1 minute.
5. Rinse slide in 2 changes of distilled water.
6. Stain tissue section with Hematoxylin, Mayer's (Lillie's Modification) for 1-2 minutes.
7. Rinse slide thoroughly in tap water.
8. Rinse slide in 2 changes of distilled water.
9. Coverslip using an aqueous mounting medium (cat# AML060).

Storage: 18° C  25° C

 ScyTek Laboratories, Inc.
 205 South 600 West
 Logan, UT 84321
 U.S.A.



 EmergoEurope (31)(0) 70 345-8570
 Molsstraat 15
 2513 BH Hague, The Netherlands

Doc: IFU-Template18-25rev2

APPENDIX E
CREATININE PROTOCOL

Microplate Assay for Creatinine

For Research Use Only

INTRODUCTION

Creatine (Cr) is produced in the kidney, liver and pancreas, phosphorylated, and transported to the brain and muscle tissue. However, a small proportion of free Cr is converted irreversibly to creatinine (Crn) in the muscular tissue in proportion to the muscle mass. The amount of Crn excreted daily by an individual is relatively constant. Thus, urinary creatinine levels may be used as an index of standardization. 24-h urinary Crn excretion is used to estimate total muscle mass because the rate of non-enzymatic production of Crn from Cr is nearly constant and >90% of the total body Cr is found in muscle tissue. Normal urinary creatinine values for men and women range from 9.7 – 24.7 and 7.9 – 14.2 mmol/24h respectively. Changes in excretion rate may be indicative of impaired renal metabolism.

PRINCIPLES OF PROCEDURE

This is a colorimetric assay for the quantitative analysis of creatinine levels in urine. Urinary creatinine reacts with picric acid under alkaline conditions to produce an orange color, which can be quantified by absorption spectroscopy near the 500 nm wavelength. This reaction, known as the Jaffe reaction, also occurs non-specifically with other components in biological fluids. However, the specific color produced with creatine in this reaction is known to degrade rapidly under acidic conditions (Slot et al.). Heinegard and Tiderstrom showed that the difference in color intensity determined before and after the addition of acid is a direct estimate of creatinine concentration in the sample.

MATERIALS PROVIDED

Component	Description	Volume	Storage	Cat no.
S1: Creatinine Standard 1	Creatinine Standard Solution (10 mg/dL)	110 μ L	4°C	CR01a
S2: Creatinine Standard 2	Creatinine Standard Solution (3 mg/dL)	110 μ L	4°C	CR01b
S3: Creatinine Standard 3	Creatinine Standard Solution (1 mg/dL)	110 μ L	4°C	CR01c
R1: Picrate Reagent	Picric Acid Solution	20 mL	25°C	CR01d
R2: Alkali Solution	NaOH and Sodium Borate Solution	4 mL	25°C	CR01e
R3: Acid Reagent	Acetic Acid Solution	2 mL	25°C	CR01f
Microplate	96-well Microplate	1 plate	25°C	CR01g

MATERIALS NEEDED BUT NOT PROVIDED

1. Microplate reader with 490 or 500 nm filter
2. Adjustable micropipettes (10 – 1000 μ L) and tips
3. Deionized water
4. Plate shaker
5. Plate cover or plastic film

STORAGE

1. Store the components of this kit at the temperatures specified on the labels.
2. Unopened reagents are stable until the indicated kit expiration date.

WARNINGS AND PRECAUTIONS

1. Use aseptic technique when opening and dispensing reagents.
2. This kit is designed to work properly as provided and instructed. Additions, deletions or substitutions to the procedure or reagents are not recommended, as they may be detrimental to the assay.
3. Picric acid can be explosive when dry, and can irritate the eyes, skin and respiratory system. Wear suitable protective clothing, gloves, and eye protection.

PROCEDURAL NOTES

1. Turbidity may develop in the Picrate Reagent at lower temperatures and may be removed by warming. The reagent is still usable.
2. To minimize errors in absorbance measurements due to handling, wipe the exterior bottom of the microplate wells with a lint-free paper towel prior to inserting into the plate reader.

REAGENT PREPARATION

1. **Alkaline Picrate Reagent:** Add R2: Alkali Solution to R1: Picrate Reagent in a one part to five parts ratio. If the entire plate is being used, add the entire contents of R2 to R1.

STANDARD CURVE PREPARATION

The Creatinine Standards are provided ready to use. A null Standard (0 mg/dL) is made with deionized water.

Table 1: Standard Curve Preparation

Standard	Creatinine Concentration (mg/dL)	Volume of Water (µL)	Volume of Creatinine Standard (µL)
S1	10.0	-	110
S2	3.0	-	110
S3	1.0	-	110
S4	0	110	-

ASSAY PROCEDURE

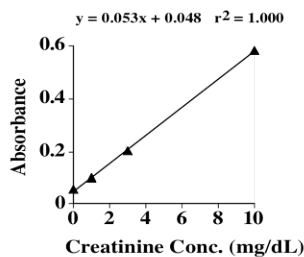
1. Add 25 µL of Standards or Samples (may require diluting 1:4 or 1:8) to the corresponding wells on the microplate in duplicate. See **Scheme I** for a sample plate layout.
2. Add 180 µL of the Alkaline Picrate Reagent to each well.
3. Mix by shaking or placing the plate on a shaker and incubate at room temperature for 10 minutes.
4. Read the plate at 490 nm. (First Reading)
5. Add 15 µL of R3: Acid Reagent to each well.
6. Mix thoroughly by tapping or shaking and allow to stand at room temperature for 5 minutes.
7. Read the plate again at 490 nm. (Second Reading)

Scheme I: Sample Plate Layout

	1	2	3	4	5	6	7	8	9	10	11	12
A	S4	S4	U5	U5	U13	U13	U21	U21	U29	U29	U37	U37
B	S3	S3	U6	U6	U14	U14	U22	U22	U30	U30	U38	U38
C	S2	S2	U7	U7	U15	U15	U23	U23	U31	U31	U39	U39
D	S1	S1	U8	U8	U16	U16	U24	U24	U32	U32	U40	U40
E	U1	U1	U9	U9	U17	U17	U25	U25	U33	U33	U41	U41
F	U2	U2	U10	U10	U18	U18	U26	U26	U34	U34	U42	U42
G	U3	U3	U11	U11	U19	U19	U27	U27	U35	U35	U43	U43
H	U4	U4	U12	U12	U20	U20	U28	U28	U36	U36	U44	U44

CALCULATIONS

- Subtract the values of the Second Reading from those of the First Reading.
NOTE: Some microplate readers can be programmed to do these subtractions automatically when reading the plate. Consult your instrument manual.
- The difference in absorbance [ΔA] is directly proportional to Creatinine concentration.
- Construct a Standard Curve with ΔA on the y-axis versus Creatinine Conc. (mg/dL) on the x-axis.
- Determine the creatinine concentration (mg/dL) in the samples.
NOTE: Normally a 5-10 fold urine dilution yields results in the linear range of the standard curve. If the samples are diluted, the concentration determined from the standard curve must be multiplied by the dilution factor.
- Multiply the creatinine concentration in mg/dL by 88.4 to convert into $\mu\text{mol/L}$ (SI unit).

Figure 1: Typical Standard Curve**INTERFERING SUBSTANCES**

- Samples containing bilirubin will give elevated results.
- The measurement is not useful in samples containing sulfonphthalein dyes such as phenolsulfonphthalein.
- Certain drugs are known to interfere with circulating creatinine levels and hence will not provide consistent results. (Young, 1990).

REFERENCES

- Slot, C.; (1965) *Scand J. Clin. Lab. Invest.* **17**:381
- Heinegard, D. and Tiderstrom, G.; (1973) *Clin. Chim. Acta* **43**:305
- Cook, J.G.H.; (1975) *Ann Clin. Biochem.* **43**:305
- Young, D.S., Editor; (1990) *Effects of drugs on clinical laboratory tests.* AACC Press, Washington
- Wyss, M. and Kaddurah-Daouk, R.; (2000) *Phys. Rev.* **80**:1107

DISCLAIMER

This information is believed to be correct but does not purport to be all-inclusive and shall be used only as a guide. Oxford Biomedical Research, Inc. shall not be held liable for any damage resulting from handling or from contact with the above product. See catalog for additional terms and conditions of sale.

ORDERING INFORMATION

For additional kits or a complete catalog please call 800-692-4633.

TECHNICAL SUPPORT

If you need technical information or assistance with assay procedures, call our Technical Support Department at 800-692-4633 or 248-852-8815. Our staff will be happy to answer your questions about this or any other product in the Oxford Biomedical line.

GUARANTEE AND LIMITATION OF REMEDY

Oxford Biomedical Research, Inc. makes no guarantee of any kind, expressed or implied, which extends beyond the description of the materials in this kit, except that these materials and this kit will meet our specifications at the time of delivery. Buyer's remedy and Oxford Biomedical Research, Inc.'s sole liability hereunder is limited to, at Oxford Biomedical Research, Inc.'s option, refund of the purchase price of, or the replacement of, material that does not meet our specification. By acceptance of our products, Buyer indemnifies and holds Oxford Biomedical Research, Inc. harmless against, assumes all liability for the consequence of its use or misuse by the Buyer, its employees, or others. Said refund or replacement is conditioned on Buyer notifying Oxford Biomedical Research, Inc. within thirty (30) days of the receipt of product. Failure of Buyer to give said notice within thirty (30) days of receipt of product shall constitute a waiver by the Buyer of all claims hereunder with respect to said material(s).

Oxford Biomedical Research, Inc.
P.O. Box 522
Oxford, MI 48371 U.S.A.

Orders: 800-692-4633
Technical Service: 248-852-8815
Fax: 248-852-4466
E-mail: info@oxfordbiomed.com

Made in the U.S.A.

APPENDIX F
CYSTATIN C PROTOCOL

Quantikine® ELISA

Mouse/Rat Cystatin C Immunoassay

Catalog Number MSCTC0

For the quantitative determination of mouse/rat Cystatin C concentrations in cell culture supernates, cell lysates, serum, plasma, and urine.

This package insert must be read in its entirety before using this product.
For research use only. Not for use in diagnostic procedures.

PRECAUTIONS

Cystatin C is detectable in saliva. Take precautionary measures to prevent contamination of kit reagents while running this assay.

The Stop Solution provided with this kit is an acid solution.

Some components in this kit contain ProClin® which may cause an allergic skin reaction. Avoid breathing mist.

Color Reagent B may cause skin, eye, and respiratory irritation. Avoid breathing fumes.

Wear protective gloves, clothing, eye, and face protection. Wash hands thoroughly after handling. Please refer to the MSDS on our website prior to use.

SAMPLE COLLECTION & STORAGE

The sample collection and storage conditions listed below are intended as general guidelines. Sample stability has not been evaluated.

Cell Culture Supernates - Remove particulates by centrifugation. Assay immediately or aliquot and store samples at ≤ -20 °C. Avoid repeated freeze-thaw cycles.

Cell Lysates - Cells must be lysed prior to assay. See Sample Values section.

Serum - Allow blood samples to clot for 2 hours at room temperature before centrifuging for 20 minutes at 2000 x g. Remove serum and assay immediately or aliquot and store samples at ≤ -20 °C. Avoid repeated freeze-thaw cycles.

Plasma - Collect plasma using EDTA or heparin as an anticoagulant. Centrifuge for 20 minutes at 2000 x g within 30 minutes of collection. Assay immediately or aliquot and store samples at ≤ -20 °C. Avoid repeated freeze-thaw cycles.

Note: Citrate plasma has not been validated for use in this assay. Grossly lipemic samples are not suitable for use in this assay.

Urine - Collect urine using a metabolic cage. Remove any particulates by centrifugation and assay immediately or aliquot and store samples at ≤ -20 °C. Avoid repeated freeze-thaw cycles. Centrifuge again before assaying to remove any additional precipitates that may appear after storage.

SAMPLE PREPARATION

Mouse serum and plasma, and rat urine samples require a 200-fold dilution. A suggested 200-fold dilution can be achieved by adding 10 μ L of sample to 90 μ L of Calibrator Diluent RD5-26 (1X). Complete the 200-fold dilution by adding 10 μ L of the diluted sample to 190 μ L of Calibrator Diluent RD5-26 (1X).

Rat serum and plasma samples require a 400-fold dilution. A suggested 400-fold dilution can be achieved by adding 10 μ L of sample to 90 μ L of Calibrator Diluent RD5-26 (1X). Complete the 400-fold dilution by adding 10 μ L of the diluted sample to 390 μ L of Calibrator Diluent RD5-26 (1X).

Mouse urine samples require a 40-fold dilution. A suggested 40-fold dilution can be achieved by adding 10 μ L of sample to 390 μ L of Calibrator Diluent RD5-26 (1X).

REAGENT PREPARATION

Bring all reagents to room temperature before use.

Note: *Cystatin C is detectable in saliva. It is recommended that a face mask and gloves be used to protect kit reagents from contamination.*

Mouse/Rat Cystatin C Control - Reconstitute the Control with 1.0 mL of deionized or distilled water. Mix thoroughly. Assay the Control undiluted.

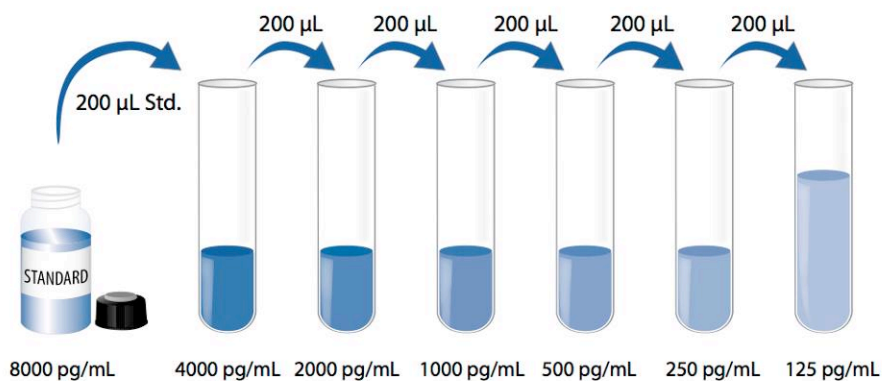
Wash Buffer - If crystals have formed in the concentrate, warm to room temperature and mix gently until the crystals have completely dissolved. Add 20 mL of Wash Buffer Concentrate to deionized or distilled water to prepare 500 mL of Wash Buffer.

Substrate Solution - Color Reagents A and B should be mixed together in equal volumes within 15 minutes of use. Protect from light. 100 μ L of the resultant mixture is required per well.

Calibrator Diluent RD5-26 (1X) - Add 20 mL of Calibrator Diluent RD5-26 Concentrate to 60 mL of deionized or distilled water to prepare 80 mL of Calibrator Diluent RD5-26 (1X).

Mouse/Rat Cystatin C Standard - Reconstitute the Mouse/Rat Cystatin C Standard with 5.0 mL of Calibrator Diluent RD5-26 (1X). This reconstitution produces a stock solution of 8000 pg/mL. Allow the standard to sit for a minimum of 5 minutes with gentle mixing prior to making dilutions.

Pipette 200 μ L of Calibrator Diluent RD5-26 (1X) into each of six tubes. Use the stock solution to produce a 2-fold dilution series (below). Mix each tube thoroughly before the next transfer. The undiluted Mouse/Rat Cystatin C Standard serves as the high standard (8000 pg/mL). Calibrator Diluent RD5-26 (1X) serves as the zero standard (0 pg/mL).



ASSAY PROCEDURE

Bring all reagents and samples to room temperature before use. It is recommended that all samples, Control, and standards be assayed in duplicate.

Note: *Cystatin C is detectable in saliva. It is recommended that a face mask and gloves be used to protect kit reagents from contamination.*

1. Prepare all reagents, working standards, Control, and samples as directed in the previous sections.
2. Remove excess microplate strips from the plate frame, return them to the foil pouch containing the desiccant pack, and reseal.
3. Add 50 μL of Assay Diluent RD1W to each well.
4. Add 50 μL of Standard, Control, or sample* per well. Cover with the adhesive strip provided. Incubate for 2 hours at room temperature. A plate layout is provided to record standards and samples assayed.
5. Aspirate each well and wash, repeating the process four times for a total of five washes. Wash by filling each well with Wash Buffer (400 μL) using a squirt bottle, manifold dispenser, or autowasher. Complete removal of liquid at each step is essential to good performance. After the last wash, remove any remaining Wash Buffer by aspirating or decanting. Invert the plate and blot it against clean paper towels.
6. Add 100 μL of Mouse/Rat Cystatin C Conjugate to each well. Cover with a new adhesive strip. Incubate for 2 hours at room temperature.
7. Repeat the aspiration/wash as in step 5.
8. Add 100 μL of Substrate Solution to each well. Incubate for 30 minutes at room temperature. **Protect from light.**
9. Add 100 μL of Stop Solution to each well. Gently tap the plate to ensure thorough mixing.
10. Determine the optical density of each well within 30 minutes, using a microplate reader set to 450 nm. If wavelength correction is available, set to 540 nm or 570 nm. If wavelength correction is not available, subtract readings at 540 nm or 570 nm from the readings at 450 nm. This subtraction will correct for optical imperfections in the plate. Readings made directly at 450 nm without correction may be higher and less accurate.

*Samples may require dilution. See Sample Preparation section.

CALCULATION OF RESULTS

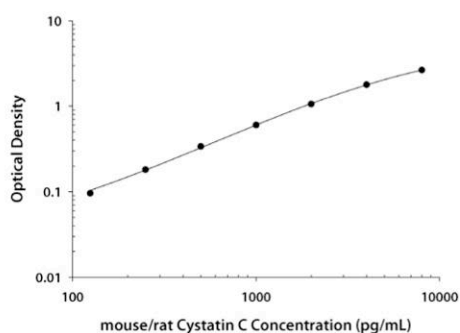
Average the duplicate readings for each standard, control, and sample and subtract the average zero standard optical density (O.D.).

Create a standard curve by reducing the data using computer software capable of generating a four parameter logistic (4-PL) curve-fit. As an alternative, construct a standard curve by plotting the mean absorbance for each standard on the y-axis against the concentration on the x-axis and draw a best fit curve through the points on the graph. The data may be linearized by plotting the log of the mouse/rat Cystatin C concentrations versus the log of the O.D. and the best fit line can be determined by regression analysis. This procedure will produce an adequate but less precise fit of the data.

If samples have been diluted, the concentration read from the standard curve must be multiplied by the dilution factor.

TYPICAL DATA

This standard curve is provided for demonstration only. A standard curve should be generated for each set of samples assayed.



(pg/mL)	O.D.	Average	Corrected
0	0.013 0.013	0.013	—
125	0.106 0.111	0.109	0.096
250	0.189 0.198	0.194	0.181
500	0.341 0.360	0.351	0.338
1000	0.603 0.625	0.614	0.601
2000	1.047 1.093	1.070	1.057
4000	1.802 1.804	1.803	1.790
8000	2.653 2.675	2.664	2.651

APPENDIX G
HYDROGEN PEROXIDE PROTOCOL



ab102500

**Hydrogen Peroxide
Assay Kit**

Instructions for Use

For the rapid, sensitive and accurate measurement of Hydrogen Peroxide in various samples

This product is for research use only and is not intended for diagnostic use.

4. Assay Protocol

1. Sample Preparation:

- a) Collect cell culture supernatant, serum, plasma, urine and other biological fluids (contains 0.8-6 μM H_2O_2).
- b) Centrifuge for 15 minutes at 1000 x g within 30 minutes of collection. Remove particulate pellet.
- c) Samples, especially those such as culture medium, tissue lysate or plasma should be filtered through a 10 kDa MW spin filter to remove all proteins then kept at -80°C for storage.
- d) It is recommended with all sample types to assay immediately or aliquot and store the samples at -80°C . Avoid repeated freeze-thaw cycles
- e) Add 2-50 μl samples into each well; bring the volume to 50 μl with assay buffer.

2. Standard Curve Preparation:

a. For the colorimetric assay:

Dilute 10 μl 0.88M H_2O_2 standard into 870 μl dH_2O to generate 10 mM H_2O_2 standard, then dilute 10 μl 10 mM H_2O_2 standard into 990 μl dH_2O to generate 0.1 mM H_2O_2 standard.

Add 0, 10, 20, 30, 40, 50 μl of the 0.1 mM H_2O_2 standard into 96-well plate in duplicate to generate 0, 1, 2, 3, 4, 5 nmol/well H_2O_2 standard.

b. For the fluorometric assay:

Dilute 100 μl of the 0.1 mM H_2O_2 standard into 900 μl dH_2O to generate 10 μM H_2O_2 Standard.

Add 0, 10, 20, 30, 40, 50 μl of the 10 μM H_2O_2 standard into 96-well plate in duplicate to generate 0, 0.1, 0.2, 0.3, 0.4, 0.5 nmol/well H_2O_2 standard.

3. Reaction Mix: Mix enough reagents for the number of assays to be performed. For each well, prepare a total 50 μl Reaction Mix:

	Colorimetric Assay	Fluorometric Assay
Assay Buffer	46 μl	48 μl
OxiRed Probe	2 μl	1 μl
HRP	2 μl	1 μl

Add 50 μl of the Reaction Mix to each test sample and H_2O_2 standards. Mix well. Incubate at room temperature for 10 min.

Note:

For a more sensitive assay, you can dilute the standard 10 fold further by decreasing OxiRed amount to 0.2 μl and HRP amount to 0.4 μl per well. This will decrease the fluorescence background, detecting as low as 2 pmol/well (or 40 μM concentration) H_2O_2 .

4. Measure: Read $\text{OD}_{570\text{nm}}$ or fluorescence (Ex/Em = 535/587 nm) in a micro-plate reader.

5. Data Analysis

Correct background by subtracting the value derived from the zero nmol H_2O_2 control from all sample and standard readings.

The background reading can be significant and must be subtracted from sample readings.

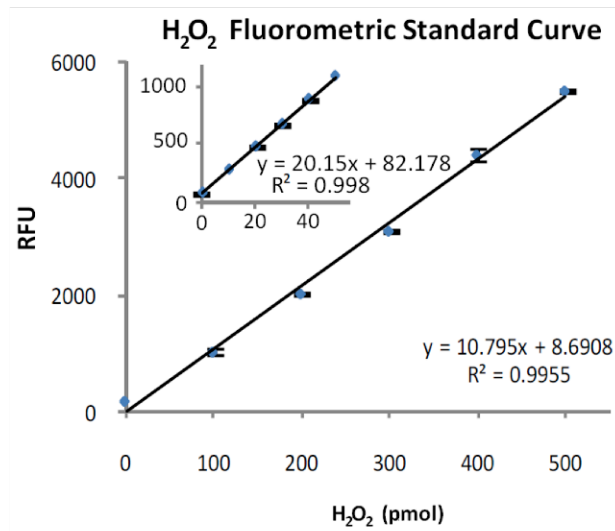
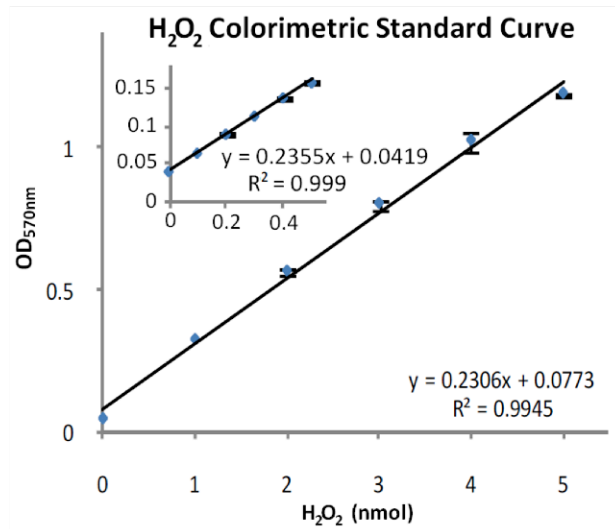
Plot the H_2O_2 standard curve. Apply your sample readings to the standard curve. H_2O_2 concentrations of the test samples can then be calculated:

$$\text{Concentration} = \text{Sa} / \text{Sv} \text{ (pmol/}\mu\text{l or } \mu\text{M)}$$

Where:

Sa is the sample amount from your standard curve (in pmol),

Sv is sample volume (μl).



H₂O₂ Standard Curves performed according to Assay Protocol.

APPENDIX H
IL-6 ANTIBODY

Anti-IL6 antibody ab6672

★★★★★ 24 Abreviews | 59 References | 9 Images



Overview

Product name	Anti-IL6 antibody
Description	Rabbit polyclonal to IL6
Tested applications	WB, ELISA, IHC-P, RIA, IP, IHC-Fr, Neutralising, ICC/IF
Species reactivity	Reacts with: Mouse, Rat, Human, Pig
Immunogen	recombinant human IL-6 produced in <i>E.coli</i> .
Positive control	<p>Purchase matching WB positive control: Human IL6 full length protein ></p> <p>WB: lysate of 2 x 10⁶ endotoxin-stimulated human peripheral blood mononuclear cells (PBMC)(PBMC are stimulated for 24 hours with 1% (v/v) human serum plus 10 ng/mL E.coli LPS)</p>
General notes	<p>The recent lot GR58964 is red in color due to hemolysis of blood during processing of the serum and did not affect the function of this rabbit antiserum during testing. We normally avoid hemolysis as much as possible, but it is sometimes unavoidable, and it does not affect the function of this primary antibody.</p> <p>IL-6 synonyms: plasmacytoma growth factor (PCT-GF),interferon-a-2 (IFN-a2), monocyte derived human B cellgrowth factor, B cell stimulating factor (BSF-2),hepatocyte stimulating factor (HSF), and interleukinhybridoma/plasmacytoma-1 (IL-HP1).</p>

Properties

Form	Liquid
Storage instructions	Store at +4°C short term (1-2 weeks). Aliquot and store at -20°C or -80°C. Avoid repeated freeze / thaw cycles.
Storage buffer	pH: 7.20 Constituents: 0.42% Potassium phosphate, 0.87% Sodium chloride
Purity	Whole antiserum
Purification notes	This antiserum has been heated to 56°C for 30 minutes.
Clonality	Polyclonal
Isotype	IgG

Applications

Our [Abpromise guarantee](#) covers the use of **ab6672** in the following tested applications.

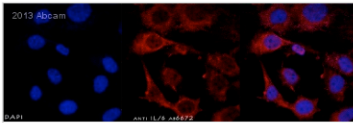
The application notes include recommended starting dilutions; optimal dilutions/concentrations should be determined by the end user.

Application	Abreviews	Notes
WB	★★★★★	1/500 - 1/2000. Can be blocked with IL6 peptide (ab133194) .
ELISA		1/1000 - 1/5000.
IHC-P	★★★★★	1/400 - 1/800.
RIA		1/4000 - 1/8000.
IP		1/400 - 1/800.
IHC-Fr	★★★★★	1/400 - 1/800.
Neutralising		1/400.

Target

Function	Cytokine with a wide variety of biological functions. It is a potent inducer of the acute phase response. Plays an essential role in the final differentiation of B-cells into Ig-secreting cells. Involved in lymphocyte and monocyte differentiation. It induces myeloma and plasmacytoma growth and induces nerve cells differentiation. Acts on B-cells, T-cells, hepatocytes, hematopoietic progenitor cells and cells of the CNS. Also acts as a myokine. It is discharged into the bloodstream after muscle contraction and acts to increase the breakdown of fats and to improve insulin resistance.
Involvement in disease	Genetic variations in IL6 are associated with susceptibility to rheumatoid arthritis systemic juvenile (RASJ) [MIM:604302]. An inflammatory articular disorder with systemic-onset beginning before the age of 16. It represents a subgroup of juvenile arthritis associated with severe extraarticular features and occasionally fatal complications. During active phases of the disorder, patients display a typical daily spiking fever, an evanescent macular rash, lymphadenopathy, hepatosplenomegaly, serositis, myalgia and arthritis. Note=A IL6 promoter polymorphism is associated with a lifetime risk of development of Kaposi sarcoma in HIV-infected men.
Sequence similarities	Belongs to the IL-6 superfamily.
Post-translational modifications	N- and O-glycosylated.
Cellular localization	Secreted.

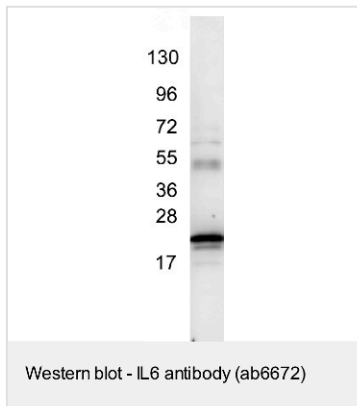
Anti-IL6 antibody images



Immunocytochemistry/
Immunofluorescence - Anti-IL6 antibody
(ab6672)

This image is courtesy of an anonymous Abreview

ab6672 staining IL6 (red) in Mouse mesenchymal SC cells by ICC/IF (Immunocytochemistry/immunofluorescence). Cells were fixed with formaldehyde, permeabilized with 0.5% Tween-20 and blocked with 3% BSA for 1 hour at room temperature. Samples were incubated with primary antibody (1/500 in 3% BSA) for 1 hour. An Alexa Fluor® 555-conjugated Donkey anti-rabbit IgG polyclonal (1:500) was used as the secondary antibody. Blue (DAPI) - nuclei.



Western blot - IL6 antibody (ab6672)

Anti-IL6 antibody (ab6672) at 1/500 dilution + Endotoxin-stimulated human peripheral blood mononuclear cells

APPENDIX I
TNF α ANTIBODY

Store at
-20°C
#11948

TNF- α (D2D4) XP[®] Rabbit mAb (Rodent Specific)

Small 100 μ l (10 western blots)
Petite 40 μ l (4 western blots)

www.cellsignal.com

Support: 877-678-TECH (8324)
info@cellsignal.com

Orders: 877-616-CELL (2355)
orders@cellsignal.com

Entrez-Gene ID #21926
UniProt ID #P06804

rev. 06/16/14

For Research Use Only. Not For Use In Diagnostic Procedures.

Applications W, IP, IF-IC, F Endogenous	Species Cross-Reactivity* M, R	Molecular Wt. 17,25,28 kDa	Isotype Rabbit IgG**
---	-----------------------------------	-------------------------------	-------------------------

Background: TNF- α , the prototypical member of the TNF protein superfamily, is a homotrimeric type-II membrane protein (1,2). Membrane-bound TNF- α is cleaved by the metalloprotease TACE/ADAM17 to generate a soluble homotrimer (2). Both membrane and soluble forms of TNF- α are biologically active. TNF- α is produced by a variety of immune cells including T cells, B cells, NK cells, and macrophages (1). Cellular response to TNF- α is mediated through interaction with receptors TNF-R1 and TNF-R2 and results in activation of pathways that favor both cell survival and apoptosis depending on the cell type and biological context. Activation of kinase pathways (including JNK, Erk1/2, p38 MAPK, and NF- κ B) promotes the survival of cells, while TNF- α -mediated activation of caspase-8 leads to programmed cell death (1,2). TNF- α plays a key regulatory role in inflammation and host defense against bacterial infection, notably *Mycobacterium tuberculosis* (3).

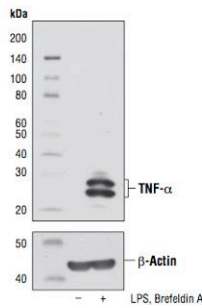
Mouse and rat TNF- α are predicted to be glycosylated, while human TNF- α is not (4).

Specificity/Sensitivity: TNF- α (D2D4) XP[®] Rabbit mAb (Rodent Specific) recognizes endogenous levels of total TNF- α protein.

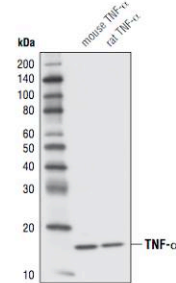
Source/Purification: Monoclonal antibody is produced by immunizing animals with a recombinant mouse TNF- α protein.

Background References:

- (1) Aggarwal, B.B. (2003) *Nat Rev Immunol* 3, 745-56.
- (2) Hehligans, T. and Pfeffer, K. (2005) *Immunology* 115, 1-20.
- (3) Lin, P.L. et al. (2007) *J Invest Dermatol Symp Proc* 12, 22-5.
- (4) Pennica, D. et al. (1985) *Proc Natl Acad Sci USA* 82, 6060-4.



Western blot analysis of extracts from Raw 264.7 cells, untreated (-) or treated (+) with LPS (100 ng/mL, 6 hr) and Brefeldin A #9972 (300 ng/mL, last 3 hr of stimulation), using TNF- α (D2D4) XP[®] Rabbit mAb (Rodent Specific) (upper) or β -Actin (D6A8) Rabbit mAb #8457 (lower).



Western blot analysis of 1 ng recombinant mTNF- α #5178 and 1 ng recombinant rat TNF- α using TNF- α (D2D4) XP[®] Rabbit mAb (Rodent Specific).

Storage: Supplied in 10 mM sodium HEPES (pH 7.5), 150 mM NaCl, 100 μ g/ml BSA, 50% glycerol and less than 0.02% sodium azide. Store at -20°C. Do not aliquot the antibody.

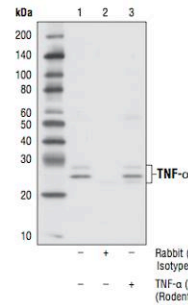
*Species cross-reactivity is determined by western blot.

**Anti-rabbit secondary antibodies must be used to detect this antibody.

Recommended Antibody Dilutions:

Western blotting	1:1000
Immunoprecipitation	1:50
Immunofluorescence (IF-IC)	1:200
Flow Cytometry	1:100

DRAQ5[®] is a registered trademark of Biostatus Limited.
Tween[®] is a registered trademark of ICI Americas, Inc.



Immunoprecipitation of TNF- α from Raw 264.7 cell extracts, treated with LPS (100 ng/mL, 6 hr) and Brefeldin A #9972 (300 ng/mL, last 3 hr of stimulation), using Rabbit (DA1E) mAb IgG XP[®] Isotype Control #3900 (lane 2) or TNF- α (D2D4) XP[®] Rabbit mAb (Rodent Specific) (lane 3). Lane 1 is 10% input. Western blot analysis was performed using TNF- α (D2D4) XP[®] Rabbit mAb (Rodent Specific), Mouse Anti-rabbit IgG (Conformation Specific) (L27A9) #3678 and Anti-mouse IgG, HRP-linked Antibody #7076 were used as secondary antibodies.

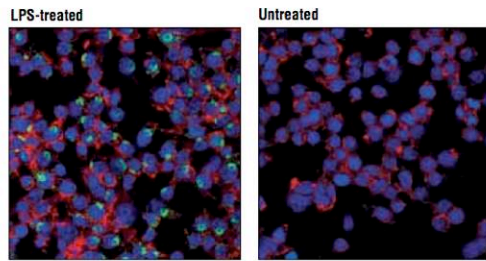
IMPORTANT: For western blots, incubate membrane with diluted antibody in 5% w/v BSA, 1X TBS, 0.1% Tween[®]20 at 4°C with gentle shaking, overnight.

© 2014 Cell Signaling Technology, Inc.
XP[®] and Cell Signaling Technology[®] are trademarks of Cell Signaling Technology, Inc.

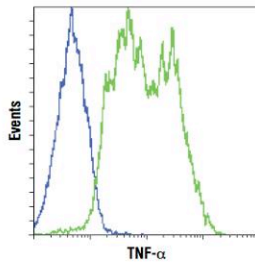
Applications: W—Western; IP—Immunoprecipitation; IHC—Immunohistochemistry; ChIP—Chromatin Immunoprecipitation; IF—Immunofluorescence; F—Flow cytometry; E-P—ELISA; Peptide; Species Cross-Reactivity: H—human; M—mouse; R—rat; Hm—hamster; Mk—monkey; Mi—mink; C—chicken; Dm—D. melanogaster; X—Xenopus; Z—zebrafish; B—bovine; Dg—dog; Pg—pig; Sc—S. cerevisiae; Ce—C. elegans; Hr—Horse; All—all species expected. Species enclosed in parentheses are predicted to react based on 100% homology.

Thank you for your recent purchase. If you would like to provide a review visit www.cellsignal.com/comments.

Cell Signaling
TECHNOLOGY[®]



Confocal immunofluorescent analysis of Raw 264.7 cells, treated with LPS (100 ng/mL, 6 hr; left) or untreated (right), using TNF- α (D2D4) XP[®] Rabbit mAb (Rodent Specific) (green). Actin filaments were labeled with DY-554 phalloidin (red). Blue pseudocolor = DRAQS[®] #4084 (fluorescent DNA dye).



Flow cytometric analysis of Raw 264.7 cells, untreated (blue) or treated with LPS (100 ng/ml, 6 hr) and Brefeldin A #9972 (300 ng/ml, last 3 hr of treatment) (green), using TNF- α (D2D4) XP[®] Rabbit mAb (Rodent Specific), Anti-rabbit IgG (H+L), F(ab)₂ Fragment (Alexa Fluor[®] 647 Conjugate) #4414 was used as a secondary antibody.

APPENDIX J
BETA-ACTIN ANTIBODY

Anti-beta Actin antibody ab8227

★★★★★ 78 Abreviews | 📄 252 References | 🖼️ 12 Images

Overview

Product name	Anti-beta Actin antibody
Description	Rabbit polyclonal to beta Actin
Tested applications	IHC-Fr, IP, WB, ICC, Flow Cyt, IHC-FrFI, IHC-P, ICC/IF, ELISA
Species reactivity	<p>Reacts with: Mouse, Rat, Sheep, Rabbit, Chicken, Guinea pig, Cow, Dog, Human, Pig, Xenopus laevis, Fruit fly (<i>Drosophila melanogaster</i>), Fish, Monkey, Rhesus monkey, Chinese Hamster</p> <p>Does not react with</p> <p>Zebrafish</p>
Immunogen	Synthetic peptide derived from within residues 1 - 100 of Human beta Actin. Read Abcam's proprietary immunogen policy (Peptide available as ab13772 .)
Positive control	This antibody gave a positive signal in Mouse Brain tissue lysate as well as the following whole cell lysates: HeLa; A431; HEK293; NIH3T3; PC12; Yeast Extract. In IHC, this antibody gave a positive signal in normal human colon and normal human liver.

Properties

Form	Liquid
Storage instructions	Store at +4°C short term (1-2 weeks). Aliquot and store at -20°C or -80°C. Avoid repeated freeze / thaw cycles.
Storage buffer	Preservative: 0.02% Sodium Azide Constituents: 1% BSA, PBS, pH 7.4
Purity	Immunogen affinity purified
Clonality	Polyclonal
Isotype	IgG

Applications

Our [Abpromise guarantee](#) covers the use of **ab8227** in the following tested applications.

The application notes include recommended starting dilutions; optimal dilutions/concentrations should be determined by the end user.

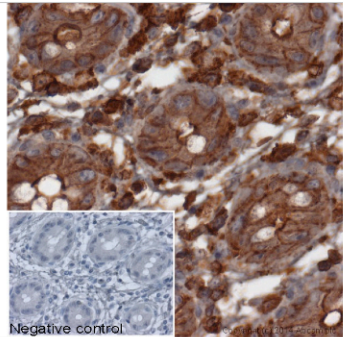
Application	Abreviews	Notes
IHC-Fr	★★★★★	Use at an assay dependent concentration.
IP	★★★★★	Use at an assay dependent concentration.
WB	★★★★★	1/1000 - 1/5000. Can be blocked with Human beta Actin peptide (ab13772) .
ICC	★★★★★	Use at an assay dependent concentration.
Flow Cyt	★★★★★	Use at an assay dependent concentration.
IHC-FrFI	★★★★★	Use at an assay dependent concentration.
IHC-P	★★★★★	Use a concentration of 1 µg/ml. Perform heat mediated antigen retrieval before commencing with IHC staining protocol.
ICC/IF	★★★★★	Use a concentration of 1 µg/ml.
ELISA	★★★★★	1/1000.

Target

Product Datasheet

Function	Actins are highly conserved proteins that are involved in various types of cell motility and are ubiquitously expressed in all eukaryotic cells.
Involvement in disease	Defects in ACTB are a cause of dystonia juvenile-onset (DYTJ) [MIM:607371]. DYTJ is a form of dystonia with juvenile onset. Dystonia is defined by the presence of sustained involuntary muscle contraction, often leading to abnormal postures. DYTJ patients manifest progressive, generalized, dopa-unresponsive dystonia, developmental malformations and sensory hearing loss.
Sequence similarities	Belongs to the actin family.
Post-translational modifications	ISGylated.
Cellular localization	Cytoplasm > cytoskeleton. Localized in cytoplasmic mRNP granules containing untranslated mRNAs.

Anti-beta Actin antibody images

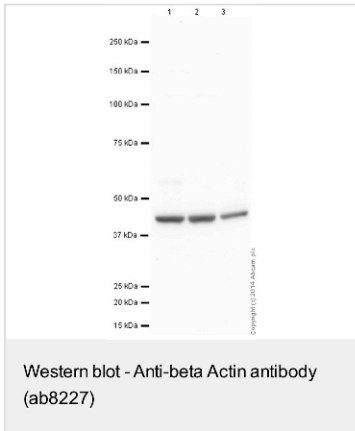


Immunohistochemistry (Formalin/PFA-fixed paraffin-embedded sections) - Anti-beta Actin antibody (ab8227)

IHC image of beta Actin staining in normal human colon, formalin-fixed and paraffin-embedded tissue*. The section was pre-treated using pressure cooker heat mediated antigen retrieval with sodium citrate buffer (pH6) for 30mins. The section was incubated with ab8227, 3µg/ml overnight at +4°C. An HRP-conjugated secondary (Ab97200, 1/200 dilution) was used for 1hr at room temperature. The section was counterstained with haematoxylin and mounted with DPX.

*Tissue obtained from the Human Research Tissue Bank, supported by the NIHR Cambridge Biomedical Research Centre

Product Datasheet



All lanes : Anti-beta Actin antibody (ab8227) at 0.1 µg/ml

Lane 1 : HeLa (Human epithelial carcinoma cell line) Whole Cell Lysate

Lane 2 : NIH 3T3 (Mouse embryonic fibroblast cell line) Whole Cell Lysate

Lane 3 : Liver (Rat) Tissue Lysate

Lysates/proteins at 10 µg per lane.

Secondary

Goat Anti-Rabbit IgG H&L (HRP) ([ab97051](#)) at 1/50000 dilution

Performed under reducing conditions.

Observed band size : 42 kDa

Exposure time :

 1 minute

This blot was produced using a 4-12% Bis-tris gel under the MOPS buffer system. The gel was run at 200V for 50 minutes before being transferred onto a Nitrocellulose membrane at 30V for 70 minutes. The membrane was then blocked for an hour using 2% Bovine Serum Albumin before being incubated with ab8227 overnight at 4°C. Antibody binding was detected using an anti-rabbit antibody conjugated to HRP, and visualised using ECL development solution [ab133406](#)

APPENDIX K
TNF α ELISA PROTOCOL

INSTRUCTIONS



Rat TNF α ELISA Kit

ER3TNFA ER3TNFA2 ER3TNFA5

1482.5

Number	Description
ER3TNFA	Rat Tumor Necrosis Factor Alpha (TNF α) ELISA, sufficient reagents for 96 determinations
ER3TNFA2	Rat Tumor Necrosis Factor Alpha (TNF α) ELISA, sufficient reagents for 2 \times 96 determinations
ER3TNFA5	Rat Tumor Necrosis Factor Alpha (TNF α) ELISA, sufficient reagents for 5 \times 96 determinations

Kit Contents	ER3TNFA	ER3TNFA2	ER3TNFA5
Anti-Rat TNF α Pre-coated 96-well Strip Plate	1 each	2 each	5 each
Lyophilized Recombinant Rat TNF α Standard	2 vials	4 vials	10 vials
Standard Diluent	25mL	2 \times 25mL	5 \times 25mL
Pre-Treatment Buffer	6mL	2 \times 6mL	5 \times 6mL
Biotinylated Antibody Reagent	6mL	2 \times 6mL	5 \times 6mL
Streptavidin-HRP Reagent	14mL	2 \times 14mL	5 \times 14mL
30X Wash Buffer	50mL	2 \times 50mL	5 \times 50mL
TMB Substrate	13mL	2 \times 13mL	5 \times 13mL
Stop Solution, contains 0.16M sulfuric acid	13mL	2 \times 13mL	5 \times 13mL
Adhesive plate sealers	6 each	12 each	30 each

For research use only – not for use in diagnostic procedures.

Storage: For maximum stability, store in a non-defrosting -20°C freezer and refer to the expiration date for frozen storage on the label. Alternatively, store at 2-8°C and refer to the expiration date for refrigerated storage. Once thawed, store at 4°C until the expiration date for refrigerated storage. Kit is shipped on dry ice.


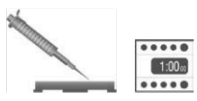




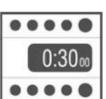





Table of Contents

Introduction	1
Procedure Summary.....	2
Additional Materials Required.....	2
Precautions.....	2
Sample Preparation.....	3
Reagent Preparation.....	4
Assay Procedure	5
Performance Characteristics	6
Cited Reference	7
Data Templates	8

Introduction

The Thermo Scientific Rat TNF α ELISA Kit is for measuring rat TNF α in serum, EDTA plasma and culture supernatant.

Procedure Summary

- | | | | |
|---|--|--|---|
| 
1. Add 50µL of Pre-Treatment Buffer to each well. | 
2. Add 50µL of Standards or samples to each well in duplicate.* Cover plate and incubate at room temperature (20-25°C) for 1 hour. | 
3. Wash plate THREE times. | 
4. Add 50µL of Biotinylated Antibody Reagent to each well. Cover plate and incubate at room temperature for 1 hour. |
| 
5. Wash plate THREE times. | 
6. Add 100µL of Streptavidin-HRP Reagent to each well. | 
7. Cover and incubate plate at room temperature for 30 minutes. | 
8. Wash plate THREE times. |
| 
9. Add 100µL of TMB Substrate to each well. | 
10. Develop plate in the dark at room temperature for 10 minutes. | 
11. Stop reaction by adding 100µL of Stop Solution to each well. | 
12. Measure the absorbance on a plate reader at 450nm minus 550nm. Calculate results. |

* Always dilute serum and EDTA plasma samples 1:1 before testing.

Additional Materials Required

- Precision pipettors with disposable plastic tips to deliver 5-1000µL and plastic pipettes to deliver 5-15mL
- A glass or plastic 2L container to prepare Wash Buffer
- A squirt wash bottle or an automated 96-well plate washer
- 1.5mL polypropylene or polyethylene tubes to prepare standards – do not use polystyrene, polycarbonate or glass tubes
- Disposable reagent reservoirs
- A standard ELISA reader for measuring absorbance at 450nm and 550nm. If a 550nm filter is not available, the absorbance can be measured at 450nm only. Refer to the instruction manual supplied with the instrument being used.
- Graph paper or a computerized curve-fitting statistical software package

Precautions

- **All samples and reagents must be at room temperature (20-25°C) before use in the assay.**
- Review these instructions carefully and verify all components against the Kit Contents list (page 1) before beginning.
- Do not use a water bath to thaw samples. Thaw samples at room temperature.
- When assaying culture medium, prepare the standard curve and sample dilutions using the same medium used to culture cells. For example, if RPMI with 10% fetal calf serum (FCS) was used to culture cells, then use RPMI with 10% FCS to dilute standard and samples. For best results, use a culture medium that contains a carrier protein such as FCS. Lack of a carrier protein in the media or addition of other compounds may compromise assay results. If alternative media must be

Reagent Preparation

For procedural differences when using partial plates, look for **(PP)** throughout this instruction booklet.

Wash Buffer

- **(PP)** When using partial plates, store the Wash Buffer at 2-8°C.
 - **Note:** Wash Buffer must be at room temperature before use in the assay. Do not use Wash Buffer that has become visibly contaminated during storage.
1. Label a clean glass or plastic 2L container "Wash Buffer." The 30X Wash Buffer may have a cloudy appearance.
 2. Add the entire contents of the 30X Wash Buffer (50mL) bottle to the 2L container and dilute to a final volume of 1.5L with ultrapure water. Mix thoroughly.

Standards

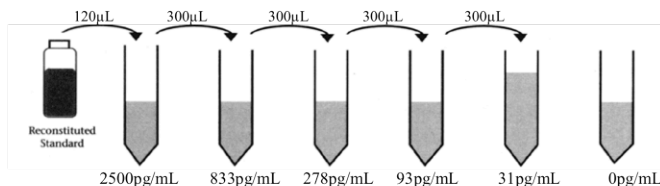
- **(PP)** Reconstitute and use one vial of the lyophilized Standard per partial plate.
 - Prepare Standards just before use and use within one hour of reconstitution. Do not store reconstituted standards.
1. For **culture supernatant** samples, reconstitute standard with ultrapure water to the volume indicated on the standard vial label. The standard will dissolve in approximately 1 minute. Mix by gently inverting vial. Use the sample culture medium to prepare Standard Curve dilutions (see Precautions Section).

For **serum** or **plasma** samples, reconstitute standard with ultrapure water to the volume indicated on the standard vial label. The standard will dissolve in approximately 1 minute. Mix by gently inverting vial. Use the Standard Diluent provided to prepare standard curve serial dilutions.

When testing **serum** or **plasma** and **cell culture supernatant** samples on the same plate, validate the media to establish if the same standard curve can be used for both sample types. Prepare a standard curve (including a zero) using culture medium to dilute the standard. Use medium containing serum or other protein to maximize stability of the rat TNF α . Perform this curve in parallel with a standard curve prepared with Standard Diluent. If the OD values of the two curves are within 10% of the mean for both curves, then perform the assay with Standard Diluent, whether testing culture supernatant, plasma or serum samples.

2. Label six tubes, one for each standard curve point: 2500, 833, 278, 93, 31, and 0pg/mL. Prepare an initial 1:6 dilution followed by 1:3 serial dilutions for the standard curve as follows:
3. Pipette 600 μ L of appropriate diluent into each tube.
4. Pipette 120 μ L of the reconstituted standard into the first tube (i.e., 2500pg/mL) and mix.
5. Pipette 300 μ L of this dilution into the second tube (i.e., 833pg/mL) and mix.
6. Repeat serial dilutions (using 300 μ L) three more times to complete the standard curve points.

Standard Dilutions Schematic



Assay Procedure

A. Sample Incubation

- **(PP)** Determine the number of strips required. Leave these strips in the plate frame. Tightly seal the remaining unused strips in the foil pouch with the desiccant provided and store at 2-8°C. After completing the assay, retain the plate frame for the second partial plate. When using the second partial plate, place the reserved strips securely in the plate frame.
- Use the Data Template provided to record locations of the zero standard, rat TNF α standards and test samples. Perform five standard points and one blank in duplicate with each series of unknown samples.

1. Add 50 μ L of the Pre-Treatment buffer to each well.
2. Add 50 μ L of the reconstituted standard or diluted sample to each well in duplicate. Mix by gently tapping the plate several times.

Note: All serum and EDTA plasma samples must be diluted 1:1 before testing (see the Sample Dilution Section). If the TNF α concentration in any test sample is expected to exceed the highest point on the standard curve (i.e., 2500pg/mL) refer to the Sample Dilution section.

3. Add 50 μ L of Standard Diluent to all wells that do not contain standards or samples.
4. Carefully cover plate with an adhesive plate cover. Ensure that all edges and strips are sealed tightly by running your thumb over the edges and down each strip. Incubate for one (1) hour at room temperature (i.e., 20-25°C).
5. Carefully remove the adhesive plate cover. Wash plate THREE times with Wash Buffer using the procedure described in the Plate Washing Section (Section B).

B. Plate Washing

Note: Automated plate washers may produce sub-optimal results. For best results, perform a manual wash the first time the assay is performed. Automated plate washing may require validation to determine the number of washes necessary to achieve optimal results; typically, 3-5 washes are sufficient.

1. Gently squeeze the long sides of plate frame before washing to ensure all strips securely remain in the frame.
2. Empty plate contents. Use a squirt wash bottle to vigorously fill each well completely with Wash Buffer, then empty plate contents. Repeat procedure two additional times for a total of THREE washes. Blot plate onto paper towels or other absorbent material.

Note: For automated washing, aspirate all wells and wash with Wash Buffer, overfilling wells with Wash Buffer. Blot plate onto paper towels or other absorbent material. The number of washes necessary may require optimization.

C. Biotinylated Antibody Reagent Incubation

- If using a multichannel pipettor, **use new reagent reservoir and pipette tips** when adding the Biotinylated Antibody Reagent.
1. Add 50 μ L of Biotinylated Antibody Reagent to each well.
 2. Carefully attach a new adhesive plate cover, ensuring all edges and strips are tightly sealed. Incubate plate for 1 hour at room temperature.
 3. Carefully remove the adhesive plate cover, discard plate contents and wash THREE times as described in the Plate Washing Section.

D. Streptavidin-HRP Reagent Incubation

- If using a multichannel pipettor, **use new reagent reservoir and pipette tips** when adding the Streptavidin-HRP Reagent.
1. Add 100 μ L of Streptavidin-HRP Reagent to each well.
 2. Carefully attach a new adhesive plate cover, ensuring all edges and strips are tightly sealed. Incubate plate for 30 minutes at room temperature.

- Carefully remove the adhesive plate cover, discard plate contents and wash THREE times as described in the Plate Washing Section (section B).

E. Substrate Incubation and Stop Step

- Use new disposable reagent reservoirs when adding TMB Substrate Solution and Stop Solution.
 - Dispense from bottle ONLY the amount required, 100µL per well, for the number of wells being used. Do not use a glass pipette to measure the TMB Substrate Solution.
 - (PP)** Do not combine leftover substrate with that reserved for the second partial plate. Take care not to contaminate remaining TMB Substrate Solution.
 - If using a multichannel pipettor, use new reagent reservoir and pipette tips when adding the TMB Substrate Solution and when adding the Stop Solution.
- Pipette 100µL of TMB Substrate Solution into each well.
 - Allow the color reaction to develop at room temperature in the dark for 10 minutes. Do not cover plate with a plate sealer. The substrate reaction yields a blue solution that turns yellow when Stop Solution is added.
 - After 10 minutes, stop the reaction by adding 100µL of Stop Solution to each well.

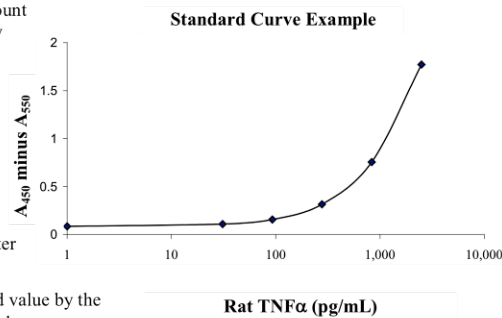
F. Absorbance Measurement

Note: Evaluate the plate within 30 minutes of stopping the reaction.

Measure absorbance on an ELISA plate reader set at 450nm and 550nm. Subtract 550nm values from 450nm values to correct for optical imperfections in the microplate. If an absorbance at 550nm is not available, measure the absorbance at 450nm only. When the 550nm measurement is omitted, absorbance values will be higher.

G. Calculation of Results

- The standard curve is used to determine rat TNFα amount in an unknown sample. Generate the standard curve by plotting the average absorbance obtained for each Standard concentration on the vertical (Y) axis vs. the corresponding TNFα concentration (pg/mL) on the horizontal (X) axis.
- Calculate results using graph paper or curve-fitting statistical software. Determine the TNFα amount in each sample by interpolating from the absorbance value (Y-axis) to TNFα concentration (X-axis) using the standard curve. For best results, use a four-parameter curve fit.
- If the test sample was diluted, multiply the interpolated value by the dilution factor to calculate pg/mL of TNFα in the sample.
- Absorbance values obtained for duplicates should be within 10% of the mean value. Carefully consider duplicate values that differ from the mean by greater than 10%.



Performance Characteristics

Sensitivity: < 15pg/mL

The sensitivity or lower limit of detection (LLD)¹ was determined by assaying 24 replicates of zero and the standard curve. The mean signal of zero + 2 standard deviations read in dose from the standard curve is the LLD.

Assay Range: 31-2500pg/mL

Suggested standard curve points are 2500, 833, 278, 93, 31, and 0pg/mL.

Specificity: The antibodies utilized in this ELISA are specific for the measurement of natural and recombinant rat TNF α . They do not cross-react with human TNF α , human TNF β or porcine TNF α . Mouse TNF α cross-reacted weakly (< 3%).

Calibration: The standard in this ELISA is calibrated to an internal rat TNF α reference standard.

Precision/Reproducibility:

Intra-assay CV: < 10%
(Table 1)

Inter-assay CV: < 10%
(Table 2)

Table 1. Intra-assay results using the rat TNF α ELISA kit.

Mean (pg/mL)	%CV	n
2022	3.2	24
912	4.2	24
148	4.0	24

Table 2. Inter-assay results using the rat TNF α ELISA kit.

Mean (pg/mL)	%CV	n
2021	2.9	4
898	3.8	4
142	4.7	4

Recovery: Cytokine recovery was determined by spiking recombinant rat TNF α into serum and plasma samples collected from apparently healthy rats and a Standard Diluent control buffer (Table 3).

Table 3. Spike and recovery results using the rat TNF α ELISA Kit.

Spike Level	Mean Percent Recovery	
	Serum	Plasma
High	102	118
Medium	78	95
Low	75	84
Mean	85	99
Range	73-105	68-119

Cited Reference

1. *Immunoassay: A Practical Guide*, ed. Chan and Perlstein, Eds. (1987). Academic Press: New York, p.71.

Products are warranted to operate or perform substantially in conformance with published Product specifications in effect at the time of sale, as set forth in the Product documentation, specifications and/or accompanying package inserts ("Documentation"). No claim of suitability for use in applications regulated by FDA is made. The warranty provided herein is valid only when used by properly trained individuals. Unless otherwise stated in the Documentation, this warranty is limited to one year from date of shipment when the Product is subjected to normal, proper and intended usage. This warranty does not extend to anyone other than Buyer. Any model or sample furnished to Buyer is merely illustrative of the general type and quality of goods and does not represent that any Product will conform to such model or sample.

NO OTHER WARRANTIES, EXPRESS OR IMPLIED, ARE GRANTED, INCLUDING WITHOUT LIMITATION, IMPLIED WARRANTIES OF MERCHANTABILITY, FITNESS FOR ANY PARTICULAR PURPOSE, OR NON INFRINGEMENT. BUYER'S EXCLUSIVE REMEDY FOR NON-CONFORMING PRODUCTS DURING THE WARRANTY PERIOD IS LIMITED TO REPAIR, REPLACEMENT OF OR REFUND FOR THE NON-CONFORMING PRODUCT(S) AT SELLER'S SOLE OPTION. THERE IS NO OBLIGATION TO REPAIR, REPLACE OR REFUND FOR PRODUCTS AS THE RESULT OF (I) ACCIDENT, DISASTER OR EVENT OF FORCE MAJEURE, (II) MISUSE, FAULT OR NEGLIGENCE OF OR BY BUYER, (III) USE OF THE PRODUCTS IN A MANNER FOR WHICH THEY WERE NOT DESIGNED, OR (IV) IMPROPER STORAGE AND HANDLING OF THE PRODUCTS.

Unless otherwise expressly stated on the Product or in the documentation accompanying the Product, the Product is intended for research only and is not to be used for any other purpose, including without limitation, unauthorized commercial uses, in vitro diagnostic uses, ex vivo or in vivo therapeutic uses, or any type of consumption by or application to humans or animals.

Current product instructions are available at www.thermoscientific.com/pierce. For a faxed copy, call 800-874-3723 or contact your local distributor.

© 2014 Thermo Fisher Scientific Inc. All rights reserved. Unless otherwise indicated, all trademarks are property of Thermo Fisher Scientific Inc. and its subsidiaries. Printed in the USA.

APPENDIX L
TBARS PROTOCOL

TBARS Assay-Tissues

NB. All solutions must warm up to RT before use (at least 1 hour)

Tissue Samples:

- Can use frozen tissue.
- Place 50mg/mL tissue in saline or PBS (i.e., 50mg tissue with 0.5 mL PBS; 100mg tissue in 1mL PBS).
- Grind in Potter-Elvehjem glass homogenizer on ice until homogenized

Use homogenate as a "sample" (see below)

TBARS assay:

1. Set heat block to 95°C.
2. Mix TBA Buffer:
 - a) Mix 106mg TBA powder with 10mL diluent 1 (cover with parafilm)
 - b) Mix on hot plate (on low setting ~ 30) until dissolved
 - c) Add 10mL diluent 2
 - d) Mix on hot plate (turned off) for 10 minutes

Mixture is sufficient for up to 25 reactions (including standards: 5 standards + 20 unknown samples). For additional samples make up additional buffer.

TBA buffer is stable at 2-4 °C for 24 hours.

3. Prepare MDA Standards:
 - a) Label eppendorf tubes 0 through 4
 - b) Adding MDA diluent first, make up the following MDA standard concentrations
 - c) Vortex.
 - d) Keep standards on ice

<u>Standard</u>	<u>MDA concentration (nM/mL)</u>	<u>MDA standard</u>	<u>MDA Diluent</u>
0	0	0	100
1	12.5	12.5	87.5
2	25	25	75
3	50	50	50
4	100	100	0

Each standard can now be treated as a "sample"

4. Label eppendorf tubes
 - a) Label tubes with standard number (0-4) or animal ID
 - b) Pierce hole in top of tube with 18-20G needle

5. Prepare samples
 - a) Mix samples for duplicate runs
 - b) Add 30uL of sample (or standard "sample") to labeled eppendorf tubes
 - c) Add 30uL SDS solution
 - d) Add 750uL TBA buffer
 - e) Vortex tubes
 - f) Place in heat block @ 95 °C for 60 minutes
 - g) Place on ice for 10 minutes
 - h) Centrifuge at 3000 rpm for 15 minutes
 - i) Remove supernatant and add to new labeled eppendorf tube
 - j) Centrifuge supernatant at 3000 rpm for 15 minutes

6. Load 96-well plate
 - a) Add 200uL of supernatant to plate well x 2 (in duplicate)

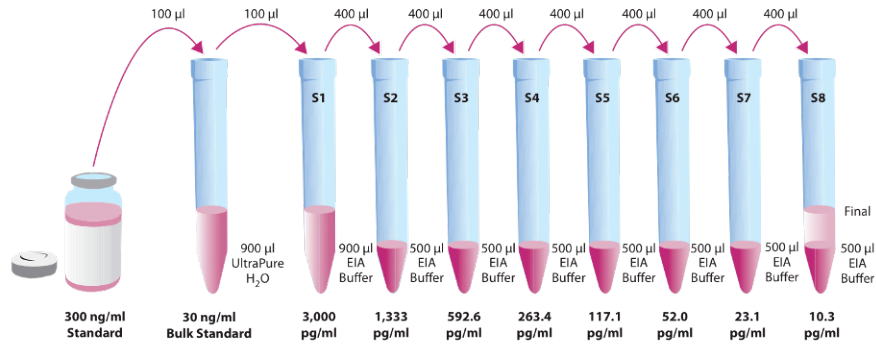
7. Absorbance reading
 - a) Read supernatants on plate reader @ 540nm.

APPENDIX M

OXIDATIVE DNA/RNA PROTOCOL

DNA/RNA Oxidative Damage EIA Short Protocol

- EIA Buffer** - Dilute with 90 ml of UltraPure water.
- Wash Buffer** - Dilute the 5 ml vial to 2 L and add 1 ml Polysorbate 20 or dilute the 12.5 ml vial to 5 L and add 2.5 ml Polysorbate 20.
- Tracer** - Reconstitute the 100 dtn vial with 6 ml of EIA Buffer or the 500 dtn vial with 30 ml EIA Buffer.
- Antibody** - Reconstitute the 100 dtn vial with 6 ml of EIA Buffer or the 500 dtn vial with 30 ml EIA Buffer.
- Standard** - Prepare as described in the figure below.



Steps	Reagent	Blank	TA	NSB	B ₀	Std/Sample
1. Add Reagents	EIA Buffer	--	--	100 µl	50 µl	--
	Standard/Sample	--	--	--	--	50 µl
	Tracer	--	--	50 µl	50 µl	50 µl
	Antibody	--	--	--	50 µl	50 µl
2. Incubate	Cover plate and incubate 18 hours at 4°C					
3. Wash	Wash all wells five times					
4. Add Reagents	Tracer	--	5 µl	--	--	--
	Ellman's	200 µl	200 µl	200 µl	200 µl	200 µl
5. Incubate	Cover plate and incubate 90-120 minutes RT with gentle shaking					
6. Read	Read plate at a wavelength between 405-420 nm					